UNIVERSITY OF OKLAHOMA

GRADUATE COLLEGE

SOUTHEAST U.S. COLD SEASON SEVERE THUNDERSTORM ENVIRONMENTS AND THEIR DEPICTIONS USING MULTIPLE PLANETARY BOUNDARY LAYER PARAMETERIZATION SCHEMES

A DISSERTATION

SUBMITTED TO THE GRADUATE FACULTY

in partial fulfillment of the requirements for the

Degree of

DOCTOR OF PHILOSOPHY

By

ARIEL ELMAR COHEN
Norman, Oklahoma
2015

Downloaded from SHAREOK. Persistent Handle URL: https://hdl.handle.net/11244/23328

SOUTHEAST U.S. COLD SEASON SEVERE THUNDERSTORM ENVIRONMENTS AND THEIR DEPICTIONS USING MULTIPLE PLANETARY BOUNDARY LAYER PARAMETERIZATION SCHEMES

A DISSERTATION APPROVED FOR THE
SCHOOL OF METEOROLOGY

BY

Dr. Steven Cavallo, Chair

Dr. Harold Brooks, Co-Chair

Dr. Frederick Carr

Dr. Kevin Kloesel

Dr. Scott Greene

©Copyright by ARIEL ELMAR COHEN 2015
All Rights Reserved.

Dedication

I dedicate this dissertation to my father, Joel Barry Cohen, who has been my constant source of support and encouragement for me to pursue all of my academic and career dreams; to my mother, Hallie Bernice Cohen, whose liveliness and sociability have become well instilled within my personality; and to my sister, Ariana Allegra Cohen, for whom I am proud to call myself big brother. My family is my world.

Acknowledgments

As I finish over a decade of being a college student, I reflect on absolutely irreplaceable, deep relationships I have made with students, professors, researchers, and operational meteorologists along my path through school. I am so grateful to have shared tremendous life experiences with a great number of people. These life experiences are what enrich the educational process and professional work. So many people have had an immeasurable influence on my life, permitting me to reach the goals that I have worked so hard to accomplish to this day. It would be impossible to list them all here, but all of the people with whom I have shared life over the years have ultimately contributed to the path that brought me to where I am today. Subsequently provided names in this Acknowledgments section are not listed in any particular order.

Firstly, I want to acknowledge my Ph.D. committee: Steven Cavallo, Harold Brooks, Frederick Carr, Kevin Kloesel, and Scott Greene. I am incredibly fortunate to have had a committee dedicated to providing encouragement for me to develop as a scientist, a writer, and a speaker. Their awareness of my strengths and weaknesses, and the care that they expressed in terms of positively building upon those elements, have definitively made me into a better meteorologist, from both research and operational perspectives. The challenging questions that they posed, their balanced encouragement, and their oversight helped me in accomplishing my dreams of performing and presenting meaningful research.

Going back in time, Steve and Sarah Corfidi, along with Mike Coniglio, took me on as their Research Experiences for Undergraduates student at the Storm Prediction Center and the National Severe Storms Laboratory when I was only 19 years old, and have remained loyal mentors ever since. Mike has provided considerable time working with me and assisting me with a multitude of dimensions of my research throughout my academic career, allowing me to be able to achieve what I have to this day. Steve and Sarah Corfidi have become what are known as my "adopted parents," and have taught me so much about forecasting. I also recognize Patrick Marsh who has become not only a true friend and emotional support over the years, but also a mentor. His assistance in teaching me computer programming opened doors for me to complete research independently. Likewise, Ryan Sobash dedicated substantial time to helping me learn to use the WRF, teaching me various aspects of modeling, which served as a springboard for me to independently investigate my research area from a modeling perspective.

Throughout my time in school, including my time working at the National Weather Service offices in Tulsa, Oklahoma; Great Falls, Montana; and Jackson, Mississippi; and at the National Hurricane Center in Miami, Florida and the Storm Prediction Center in Norman, Oklahoma, I have made some amazing friends, many of whom have become family to me. All of them have shared wonderful life experiences with me, making life so much more enjoyable. Barbara Armitage, Carol Landis, and Mark Maley, who are some of my former

high school teachers, and Jeff Rogers and Jay Hobgood, who are two of my former undergraduate professors, have become positive influences on me over the years. From early in my time at The Ohio State University, Andrew Annunzio has been a loyal friend who has stuck with me since the beginning of college. Kim Klockow, Angelyn Kolodjiez, Chris Schwartz, Alan and Lisa Gerard, Jared Guyer, Joanne Culin, Daniel Lamb, Derek Stratman, Jennifer Newman, Tim Bonin, Chris Birchfield, Carly Kovacik, Kristen Cassady, Landon Klein, Eric Jacobsen, John Banghoff, Matt Flournoy, Matt Campbell, Brandon Centeno, Andrew Dzambo, Gladys Rubio, Jessica Schauer, Eric Christensen, Steve Piltz, Christopher Juckins, Hugh Cobb, Jaret Rogers, Chantelli Fulst, Jeremy Bower, Tina Stall, Michael Mercer, Dan Brown, Jared Allen, Megan VanDenHeuvel, Bryan Smith, and I all met at various points around my time in college, and all have become solid friends through the years. Steve Amburn, retired Science and Operations Officer at the National Weather Service in Tulsa, has been a dedicated mentor and friend of mine since I was 13 years old growing up in Worthington, Ohio, and effectively opened the door to my career as a meteorologist. Rich Thompson, from the Storm Prediction Center, has effectively become a big brother to me during my time in Norman, successfully challenging me to become a better meteorologist and get in better physical shape, and has invested substantial care into being there for me. Many others at the Storm Prediction Center have provided meaningful support over the years, including Russ Schneider, Greg Carbin, John Hart, Steve Goss, Corey Mead, Jeremy Grams, Roger

Edwards, Greg Dial, Jeff Peters, Ashton Robinson Cook, Joey Picca, and James Correia Jr., along with David Imy and many others. Israel Jirak has especially demonstrated tremendous care and patience in providing meaningful feedback with respect to my work. The tremendous care and attention that Steve Weiss has provided me over many years have been a huge part of my personal and professional growth. Bill Bunting has dedicated honest and deep professional and personal encouragement that have truly positively influenced my growth over the years.

Finally, I want to thank my family, whose love is unending. My dad, Joel Cohen; my mom, Hallie Cohen; and my sister, Ariana Cohen have been my support since the very beginning; along with my grandparents who have all passed away – Norman and Lilly Cohen and Alexander and Ethel Horowitz. My professional abilities are a direct reflection of my dad's persistent dedication to strengthening my academic development through the decades. In recent years, I have been incredibly fortunate to know Lee Carlaw, who has become family. The life experiences that Lee and I shared as graduate students in Norman – from lifting weights to stadium sprints to school activities to being there for each other no matter what day after day – have shaped me personally, physically, and professionally. I am proud to call Lee not only my best friend, but also my brother. I can honestly say that graduate school, to me, is not only school and work, but it is life. I am honored to have lived it, and the relationships that flourished during this time are permanent.

Table of Contents

Acknowledgments **iv**

List of Tables **x**

List of Figures **xi**

Abstract **xix**

1 Introduction **1**
- 1.1 Background 1
- 1.2 Dissertation structure 7

2 The Southeast United States Cold Season Tornado Environment **12**
- 2.1 Dataset for Analysis of the Southeast United States Cold Season Tornado Environment 12
- 2.2 Testing the Distinguishability of the Southeast United States Cold Season Tornado Environment 17
- 2.3 Convective Mode in the Southeast United States Cold Season Tornado Environment 40
- 2.4 Daytime versus Nighttime Variability in the Southeast United States Cold Season Tornado Environment 52

3 Planetary Boundary Layer Parameterization Schemes **61**
- 3.1 Purpose of Planetary Boundary Layer Parameterization Schemes 61
- 3.2 Theoretical Underpinnings of Planetary Boundary Layer Parameterization Schemes 63
- 3.3 Performance by Planetary Boundary Layer Parameterization Schemes 65

4 Application of Planetary Boundary Layer Parameterization Schemes to Southeast United States Cold Season Tornado Environments **69**

4.1 Experiment Motivation 69
4.2 Experiment Design 71
4.3 Testing the Sensitivity of the ACM2 Scheme 84
4.4 Evaluation Process 86
4.5 Statistical Analysis Introduction 91
4.6 Statistical Analysis of 0-3-km Lapse Rate 96
4.7 Statistical Analysis of Mixing Ratio 102
4.8 Statistical Analysis of PBL Depth 108
4.9 Statistical Analysis of MLCAPE 116
4.10 Statistical Analysis of 0-3-km SRH 122
4.11 Statistical Analysis of 0-1-km SRH 129

5 Final Remarks and Future Work **135**

References **140**

List of Tables

2.1 P-values corresponding to the Kolmogorov-Smirnov statistical test of the difference in parameter values between the "SEC-OLD" and "NONSECOLD" regimes. 20
2.2 P-values corresponding to the Kolmogorov-Smirnov statistical test of the difference in parameter values between the right-moving supercell and QLCS convective modes for the "SEC-OLD" regime. 52

List of Figures

1.1 Reproduction of Fig. 6 of C15 representing mesoanalysis data from Storm Prediction Center (2015a) based on Bothwell et al. (2002) for two severe-weather events in the lower Mississippi Valley region at (top) 0400 UTC 1 Jan 2011 and (bottom) 0600 UTC 23 Jan 2012. Plotted variables are mean sea level pressure (mb) in black contours provided in 4-mb intervals, surface isotherms (°F) denoted by red contours plotted at 5°F interval, isodrosotherms (°F) denoted by dashed contours at 4°F interval and color fill indicating dewpoint values at or above 56°F, and surface winds with full wind barbs corresponding to 5 m s^{-1} (10 kt) and half barbs to 2.5 m s^{-1}. 4

1.2 Reproduction of Fig. 5 of C15 representing tornado paths marked as black segments from (a) 1200 UTC 31 Dec 2010 to 1200 UTC 1 Jan 2011 and (b) 1200 UTC 22 Jan to 1200 UTC 23 Jan 2012 (Storm Prediction Center 2015b). Black ovals indicate locations of sounding analyses that C15 investigate in detail, with city identifiers listed beside the ovals [Jackson (JAN), Brookhaven (BVN), Raleigh (RLG), Meridian (MEI), Greenville (GLH), Tunica (UTA), Tuscaloosa (TCL), and Birmingham (BMX)]. These tornado reports correspond to the surface patterns provided in Fig. 1. 5

2.1 Tornado events associated with the "SECOLD" regime. 15

2.2 As in Fig. 2.1, except for the "NONSECOLD" regime. 15

2.3 As in Fig. 2.1, except for the "SEWARM" regime. 16

2.4 As in Fig. 2.1, except for the "WARMER" regime. 16

2.5 Cumulative density functions corresponding to SBCAPE during the "SECOLD" regime (solid black curve) and "NONSECOLD" regime (dashed red curve). 18

2.6 Box-and-whiskers plots corresponding to the distribution of SBCAPE for tornadoes occurring in the "SECOLD," "SEWARM," "NONSECOLD," and "WARMER" regimes, from left to right, with sample sizes listed below x-axis labels. The blue-outline box corresponds to the interquartile range, the red horizontal line corresponds to the median value, the dot marker corresponds to the mean value, and whiskers extend up to 1.5 times the interquartile range beyond the first and third quartiles. The p-value corresponding to the Kolmogorov-Smirnov statistical test of the difference in parameter values between the "SECOLD" and "NONSECOLD" regimes is listed within the title. 23
2.7 As in Fig. 2.6, except for MLCAPE. 24
2.8 As in Fig. 2.6, except for 0-3-km MLCAPE. 25
2.9 As in Fig. 2.6, except for the ratio of 0-3-km MLCAPE to total MLCAPE. 26
2.10 As in Fig. 2.6, except for 700-500-mb lapse rate. 27
2.11 As in Fig. 2.6, except for surface dewpoint. 28
2.12 As in Fig. 2.6, except for 0-1-km SRH. 29
2.13 As in Fig. 2.6, except for the ratio of 0-3-km SRH. 30
2.14 As in Fig. 2.6, except for 0-1-km bulk shear. 31
2.15 As in Fig. 2.6, except for 0-6-km bulk shear. 32
2.16 Average shifted histograms displaying MLCAPE for tornadoes occurring in the "SECOLD" regime (top left), "NONSECOLD" regime (bottom left), "SEWARM" regime (top right), and "WARMER" regime (bottom right) for the plotted ranges of parameter values. Y-axis ranges of MLCAPE vary from panel to panel to provide focus on the details of each individual distribution. 35
2.17 As in Fig. 2.16, except for 700-500-mb lapse rate. 36
2.18 As in Fig. 2.16, except for surface dewpoint. 37
2.19 As in Fig. 2.16, except for 0-1-km SRH. 38
2.20 As in Fig. 2.16, except for 0-1-km bulk shear. 39
2.21 As in Fig. 2.16, except for 0-6-km bulk shear. 40

2.22 Box-and-whiskers plots corresponding to the distribution of SBCAPE for tornadoes occurring during the "SECOLD" regime for right-moving supercell (RM) tornadoes and for QLCS tornadoes. The sample sizes corresponding to each of these convective modes are listed below the x-axis. The blue-outline box corresponds to the interquartile range, the red horizontal line corresponds to the median value, the dot marker corresponds to the mean value, and whiskers extend up to 1.5 times the interquartile range beyond the first and third quartiles. The p-value corresponding to the Kolmogorov-Smirnov statistical test of the difference in parameter values between the right-moving supercell (RM) and QLCS modes is listed within the title. 43
2.23 As in Fig. 2.22, except for MLCAPE. 44
2.24 As in Fig. 2.22, except for 0-3-km MLCAPE. 45
2.25 As in Fig. 2.22, except for 700-500-mb lapse rate. 46
2.26 As in Fig. 2.22, except for surface dewpoint. 47
2.27 As in Fig. 2.22, except for 0-1-km SRH. 48
2.28 As in Fig. 2.22, except for 0-3-km SRH. 49
2.29 As in Fig. 2.22, except for 0-1-km bulk shear. 50
2.30 As in Fig. 2.22, except for 0-6-km bulk shear. 51
2.31 Time series of box-and-whiskers plots corresponding to the distribution of SBCAPE for tornadoes occurring in the "SECOLD" (top left), "NONSECOLD" (bottom left), "SEWARM" (top right), and "WARMER" (bottom right) regimes grouped within time periods identified along the x-axis. Time periods are listed from start time to end time in UTC (e.g., "0-3" corresponds to the three-hour period beginning at 0000 UTC), with sample sizes listed below the labeled time periods. The blue-outline box corresponds to the interquartile range, the red horizontal line corresponds to the median value, the dot marker corresponds to the mean value, and whiskers extend up to 1.5 times the interquartile range beyond the first and third quartiles. 54
2.32 As in Fig. 2.31, except for MLCAPE. 55
2.33 As in Fig. 2.31, except for surface dewpoint. 56
2.34 As in Fig. 2.31, except for 0-1-km SRH. 58

2.35 As in Fig. 2.31, except for 0-1-km bulk shear. 59

3.1 Reproduction of Fig. 1 of Pleim (2007a) that illustrates the structural development of the ACM, with arrows indicating which model layers are engaged in mixing processes within the simulation of the PBL. 65

4.1 The domain used for WRF simulations. The horizontal grid length is 4 km for the simulations. 72
4.2 Severe thunderstorm reports (tornadoes in red, wind in blue, and hail in green) for 1200 UTC 13 Jan 2005 to 1200 UTC 14 Jan 2005 using Storm Prediction Center (2015b) overlaid with gray-shaded-star markers denoting the four locations used for forecast sounding evaluation for this event. 74
4.3 As in Fig. 4.2, except for 1200 UTC 28 Dec 2005 to 1200 UTC 29 Dec 2005. 74
4.4 As in Fig. 4.2, except for 1200 UTC 13 Jan 2006 to 1200 UTC 14 Jan 2006. 75
4.5 As in Fig. 4.2, except for 1200 UTC 4 Jan 2007 to 1200 UTC 5 Jan 2007. 75
4.6 As in Fig. 4.2, except for 1200 UTC 7 Jan 2007 to 1200 UTC 8 Jan 2007. 76
4.7 As in Fig. 4.2, except for 1200 UTC 12 Feb 2007 to 1200 UTC 13 Feb 2007. 76
4.8 As in Fig. 4.2, except for 1200 UTC 13 Feb 2007 to 1200 UTC 14 Feb 2007. 77
4.9 As in Fig. 4.2, except for 1200 UTC 24 Feb 2007 to 1200 UTC 25 Feb 2007. 77
4.10 As in Fig. 4.2, except for 1200 UTC 12 Feb 2008 to 1200 UTC 13 Feb 2008. 78
4.11 As in Fig. 4.2, except for 1200 UTC 16 Feb 2008 to 1200 UTC 17 Feb 2008. 78
4.12 As in Fig. 4.2, except for 1200 UTC 17 Feb 2008 to 1200 UTC 18 Feb 2008. 79
4.13 As in Fig. 4.2, except for 1200 UTC 25 Feb 2008 to 1200 UTC 26 Feb 2008. 79

4.14 As in Fig. 4.2, except for 1200 UTC 9 Dec 2008 to 1200 UTC 10 Dec 2008. 80
4.15 As in Fig. 4.2, except for 1200 UTC 18 Feb 2009 to 1200 UTC 19 Feb 2009. 80
4.16 As in Fig. 4.2, except for 1200 UTC 24 Dec 2009 to 1200 UTC 25 Dec 2009. 81
4.17 As in Fig. 4.2, except for 1200 UTC 20 Jan 2010 to 1200 UTC 21 Jan 2010. 81
4.18 As in Fig. 4.2, except for 1200 UTC 31 Dec 2010 to 1200 UTC 1 Jan 2011. 82
4.19 As in Fig. 4.2, except for 1200 UTC 28 Feb 2011 to 1200 UTC 1 Mar 2011. 82
4.20 As in Fig. 4.2, except for 1200 UTC 22 Dec 2011 to 1200 UTC 23 Dec 2011. 83
4.21 As in Fig. 4.2, except for 1200 UTC 22 Jan 2012 to 1200 UTC 23 Jan 2012. 83
4.22 As in Fig. 4.2, except for 1200 UTC 25 Jan 2012 to 1200 UTC 26 Jan 2012. 84
4.23 Reproduction of Fig. 16 of C15 representing overlays of soundings from WRF simulations at 0400 UTC 1 Jan 2011 corresponding to Jackson, Mississippi using (a) the nonlocal YSU and MRF PBL schemes and the hybrid nonlocal/local ACM2 PBL scheme around and below the 600-mb level, and using (b) the local MYJ and QNSE PBL schemes and the hybrid nonlocal/local ACM2 PBL scheme around and below the 600-mb level. In both of these panels containing WRF soundings, the observed sounding (OBS) and the RUC/SFCOA sounding corresponding to Jackson, Mississippi at the same time are also overlaid. Profiles in each panel correspond to the color-coded format identified above the plotted wind profile in each panel. The temperature profiles are plotted using the thick solid traces, the dewpoint profiles are plotted using thick dashed traces, and the wind profiles are plotted to the right of these traces. 90

4.24 Box-and-whiskers plots corresponding to the distributions of simulated 0-3-km lapse rate within fixed ranges of RUC/SFCOA ("observed" or "actual") 0-3-km lapse rates for all PBL parameterization schemes. These fixed ranges are denoted by the tan rectangles that span various ranges of actual 0-3-km lapse rate, whose magnitudes correspond to the y-axis. The different schemes are identified based on the color of the interquartile range, as depicted on the legend listed at the rightmost part of the figure. Whiskers extend up to 1.5 times the interquartile range beyond the first and third quartiles, and small stars depict the mean values of the simulated distributions. Sample sizes for each distribution are listed below the x-axis. 97
4.25 Plots of lines resulting from regression of simulated 0-3-km lapse rate on actual 0-3-km lapse rate for the PBL parameterization schemes. Lines are color-coded and correspond to the legend in the bottom-right part of the diagram. The equation corresponding to each line is listed within this legend, along with the r^2 regression coefficient. Overlaid on this plot includes the line characterized by the equation $y = x$, which corresponds to a perfect forecast. 98
4.26 Scatterplot of y-intercept versus slope corresponding to each PBL scheme regression line for 0-3-km lapse rate. Markers depict slope-y-intercept pairs that are color-coded based on the legend in the bottom-right part of the diagram, which also lists the r^2 regression coefficient associated with each PBL scheme linear regression. 99
4.27 For each PBL scheme, comparison of average 0-3-km lapse rate averaged from RUC/SFCOA soundings (shaded circle) and simulations (shaded star). Depictions of mean values are color-coded based on the PBL scheme used, with selected colors corresponding to those displayed in Figs. 4.24-4.26. Sample size for each PBL scheme is provided below the x-axis. 100

4.28 Scatterplot of Theil's inequality coefficient (U) versus bias component of error (U_m) for 0-3-km lapse rate. Each marker corresponds to each PBL parameterization scheme, with markers color-coded based on PBL scheme type and identified in the legend in the bottom-right part of the figure. Vertical and horizontal axes are scaled equivalently for this and all subsequent scatterplots of U versus U_m to permit relative comparisons of error and its bias component (i.e., U and U_m values closer to 0 indicating less error and less bias component, respectively). 101
4.29 As in Fig. 4.24, except for mean mixing ratio in the lowest 100 mb. 103
4.30 As in Fig. 4.25, except for mean mixing ratio in the lowest 100 mb. 104
4.31 As in Fig. 4.26, except for mean mixing ratio in the lowest 100 mb. 105
4.32 As in Fig. 4.27, except for mean mixing ratio in the lowest 100 mb. 106
4.33 As in Fig. 4.28, except for mean mixing ratio in the lowest 100 mb. 107
4.34 As in Fig. 4.24, except for PBL depth. 110
4.35 As in Fig. 4.25, except for PBL depth. 111
4.36 As in Fig. 4.26, except for PBL depth. 112
4.37 As in Fig. 4.27, except for PBL depth. 114
4.38 As in Fig. 4.28, except for PBL depth. 115
4.39 As in Fig. 4.24, except for MLCAPE. 117
4.40 As in Fig. 4.25, except for MLCAPE. 118
4.41 As in Fig. 4.26, except for MLCAPE. 119
4.42 As in Fig. 4.27, except for MLCAPE. 120
4.43 As in Fig. 4.28, except for MLCAPE. 121
4.44 As in Fig. 4.24, except for 0-3-km SRH. 123
4.45 As in Fig. 4.25, except for 0-3-km SRH. 124
4.46 As in Fig. 4.26, except for 0-3-km SRH. 125
4.47 As in Fig. 4.27, except for 0-3-km SRH. 126
4.48 As in Fig. 4.28, except for 0-3-km SRH. 128
4.49 As in Fig. 4.24, except for 0-1-km SRH. 130

4.50 As in Fig. 4.25, except for 0-1-km SRH. 131
4.51 As in Fig. 4.26, except for 0-1-km SRH. 132
4.52 As in Fig. 4.27, except for 0-1-km SRH. 133
4.53 As in Fig. 4.28, except for 0-1-km SRH. 134

Abstract

The primary motivations of this dissertation are to identify meteorological characteristics of the southeastern United States cold season tornado environment and to improve numerical modeling of such environments focused on the parameterization of the planetary boundary layer (PBL). This environment is particularly challenging for forecasters owing to the inherent marginality of one of the necessary conditions supporting thunderstorms: instability. Throughout the first portions of this work, both thermodynamic and kinematic parameters characteristic of the near-storm environment for southeast U.S. cold season tornadoes are found to be different relative to other environments. Numerous thermodynamic and kinematic parameters are found to be statistically significant in this regime, with relatively limited buoyancy and offsetting strong vertical wind shear. As such, this regime is sensitive to small variations in the assessment of buoyancy, of which a relatively greater proportion is concentrated in the low levels compared to other regimes. These findings, along with distinguishable behaviors of kinematic and thermodynamic parameters throughout the daytime heating and nighttime cooling cycles, motivate the need for more thorough investigation of PBL parameterization schemes in this particular regime.

This work then proceeds with a discussion of PBL parameterization schemes and a focused investigation of the performance of nine different PBL schemes

in the Southeast cold season severe weather environment by comparing simulated thermodynamic and kinematic profiles to observationally influenced ones. It is demonstrated that simultaneous representation of both nonlocal and local mixing is most appropriate for the southeast U.S. cold season tornado regime. For storm-relative helicity, strictly nonlocal schemes provide the greatest overall differences from observations (underforecast) in a mean sense. Meanwhile, strictly local schemes yield the most extreme differences from observations (underforecast) in a mean sense for low-level lapse rate and depth of the PBL. A hybrid local/nonlocal scheme is found to mitigate these mean difference extremes, while often minimizing conditional bias inherent to strictly local and nonlocal schemes.

Chapter 1

Introduction

1.1 Background

Severe thunderstorms are responsible for a wide array of impacts to society and are defined by the hazards that they produce: wind gusts exceeding 50 knots, hail with diameter of at least 1 inch, and/or tornadoes. The meteorological conditions that favor these phenomena (e.g., Schaefer 1986) associated with deep, moist convection must simultaneously be met in time and space, and include instability, moisture, and lift. An additional condition of vertical wind shear is required for organized severe thunderstorms to occur.

While these four necessary conditions are simultaneously met at various times each year across portions of the United States, the relative magnitudes of variables characterizing each condition can vary considerably from event to event (e.g., Rasmussen and Blanchard 1998; Thompson et al. 2003; Craven and Brooks 2004; Schneider and Dean 2008). In the spring, steep mid-level lapse rates and related instability developing over the western United States can yield an elevated mixed layer that overspreads rich low-level moisture originating from the Gulf of Mexico farther east to promote severe-thunderstorm potential,

a process that is described by Farrell and Carlson (1989). Alternatively, wintertime severe-weather events in the southeast United States are characterized by weaker instability but stronger vertical wind shear (e.g., Guyer et al. 2006; Guyer and Dean 2010). The juxtaposition of these two regime examples (warm season versus cold season) highlights the seasonal variability that is manifest in the relative magnitudes of the variables that characterize necessary conditions for severe thunderstorms. Specifically, relatively warmer times of the year in the United States are typically associated with warmer and more moist conditions near the surface compared to conditions aloft, yielding greater convective available potential energy (CAPE; Glickman 2000), a measure of atmospheric buoyancy. On the other hand, cooler conditions during the wintertime provide the background for lower CAPE in the United States.

CAPE is one example of a meteorological parameter that forecasters often use for the assessment of severe-weather potential, and is specifically an example of a thermodynamic parameter, which measures the degree of atmospheric buoyancy. Vertical differences in the temperature profile, known as lapse rates, as well as surface dewpoints and mean mixing ratios in the lowest 100 mb are other examples of thermodynamic parameters. Parameters that measure vertical flow variability in the environmental wind profile include storm-relative helicity (Davies-Jones et al. 1990) and vertical differences in the velocity, known as bulk shear, which are examples of kinematic parameters. References to many meteorological parameters used in severe thunderstorm forecasting and their related

climatology are provided by Rasmussen and Blanchard (1998) and references therein, while analysis maps of many parameters can be viewed at Storm Prediction Center (2015a). The Storm Prediction Center, for which references are made throughout this work, is an agency responsible for severe thunderstorm forecasting across the United States. The Storm Prediction Center is within the broader National Oceanic and Atmospheric Administration (NOAA) agency. The acronym "SPC" is used to represent the Storm Prediction Center.

This work focuses on the specific regime of severe thunderstorms that occurs in the southeast United States during the wintertime. Cohen et al. (2015, hereafter C15) illustrate some examples of surface meteorological patterns associated with tornado events evolving within these regimes, corresponding to Figs. 1.1 and 1.2. The societal impact offered by such events is particularly substantial owing to characteristics of the Southeast that inherently make this area more vulnerable to severe weather causalities. As addressed by Ashley (2007), this vulnerability is derived from coincidence of several factors, including climatological considerations and socioeconomic patterns, along with properties of the terrain, which amplify the relative impacts of such severe weather events that can yield fatalities. The higher population density and occurrence of tornadoes at night are associated with the vulnerability across the Southeast.

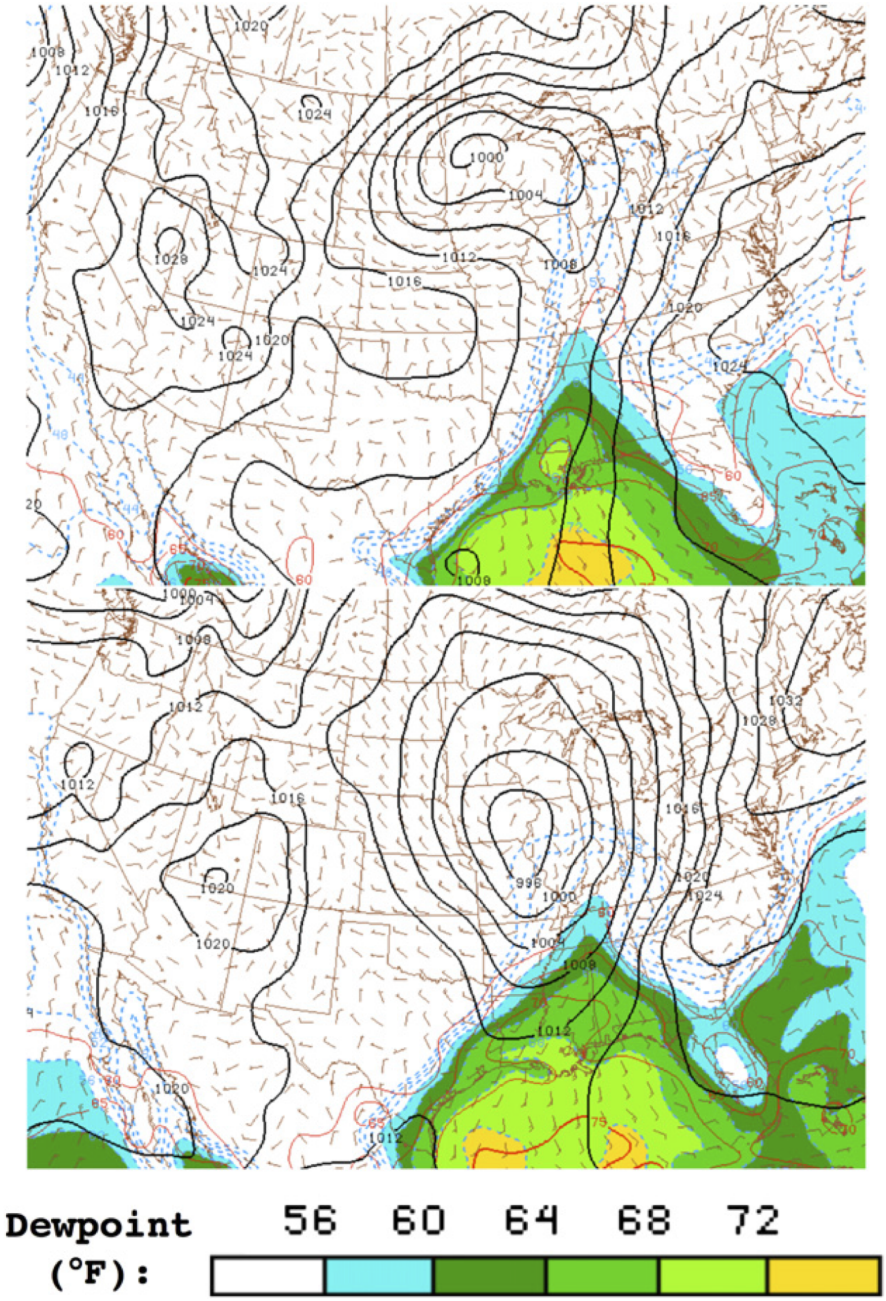

Figure 1.1: Reproduction of Fig. 6 of C15 representing mesoanalysis data from Storm Prediction Center (2015a) based on Bothwell et al. (2002) for two severe-weather events in the lower Mississippi Valley region at (top) 0400 UTC 1 Jan 2011 and (bottom) 0600 UTC 23 Jan 2012. Plotted variables are mean sea level pressure (mb) in black contours provided in 4-mb intervals, surface isotherms (°F) denoted by red contours plotted at 5°F interval, isodrosotherms (°F) denoted by dashed contours at 4°F interval and color fill indicating dewpoint values at or above 56°F, and surface winds with full wind barbs corresponding to 5 m s^{-1} (10 kt) and half barbs to 2.5 m s^{-1}.

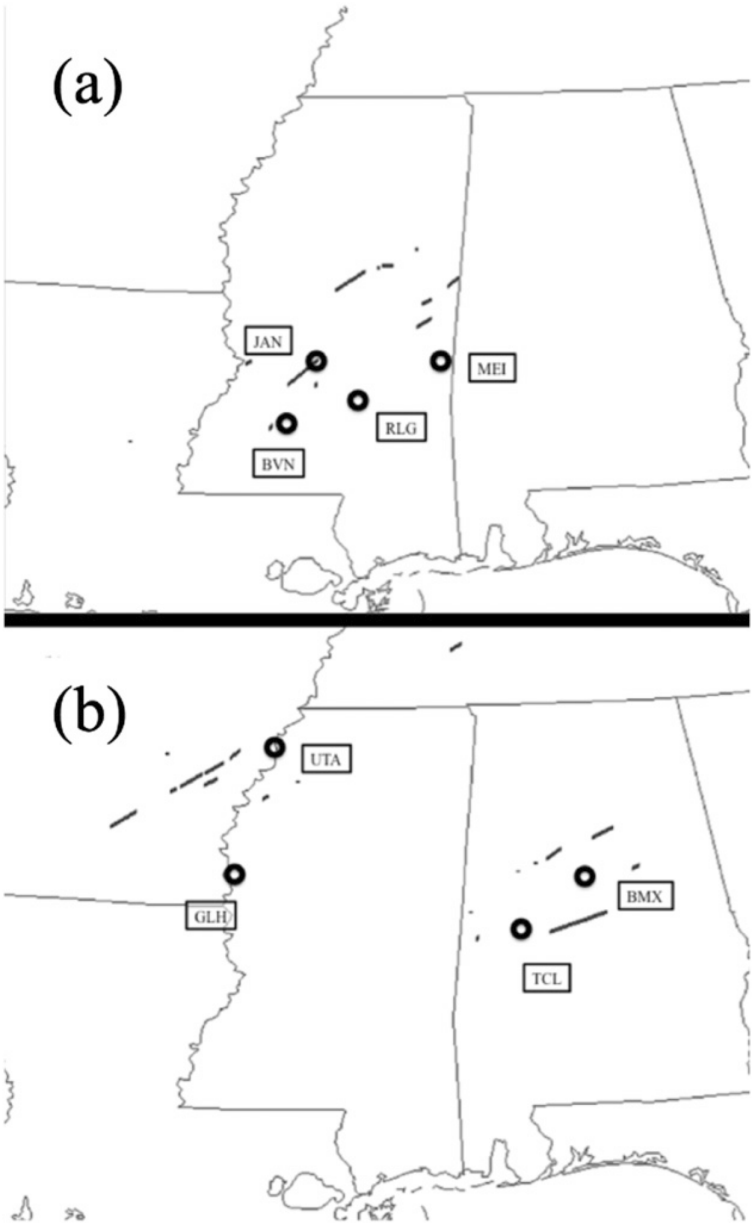

Figure 1.2: Reproduction of Fig. 5 of C15 representing tornado paths marked as black segments from (a) 1200 UTC 31 Dec 2010 to 1200 UTC 1 Jan 2011 and (b) 1200 UTC 22 Jan to 1200 UTC 23 Jan 2012 (Storm Prediction Center 2015b). Black ovals indicate locations of sounding analyses that C15 investigate in detail, with city identifiers listed beside the ovals [Jackson (JAN), Brookhaven (BVN), Raleigh (RLG), Meridian (MEI), Greenville (GLH), Tunica (UTA), Tuscaloosa (TCL), and Birmingham (BMX)]. These tornado reports correspond to the surface patterns provided in Fig. 1.

Furthermore, the cold season severe weather regime of the Southeast offers a substantial challenge to forecasters owing to the marginality of instability that is characteristic of this regime. In fact, in an analysis of weak-CAPE environments supporting tornadoes through the use of SPC mesoanalysis data (Bothwell et al. 2002), it is found that during the months of December, January, and February from 2003 to 2009, tornado occurrences are mostly confined to the southeast United States, with the majority of these tornadoes occurring in association with mixed-layer CAPE (MLCAPE) of 500 J kg^{-1} or less owing to relatively cooler surface temperatures and weaker mid-level lapse rates (Guyer and Dean 2010). MLCAPE represents CAPE associated with the mean thermodynamic conditions in the lowest 100 mb of the atmosphere. Guyer et al. (2006) also reiterate this limiting factor for F2 and stronger tornadoes occurring in the southeast United States from October 15 to February 15 between 1984 and 2004 through application of North American Regional Reanalysis data (Mesinger et al. 2006). This is at a time of the year when strong vertical wind shear associated with high-amplitude, large-scale wave patterns, and a southward-displaced and relatively strong jet stream can offset the limited buoyancy in support of severe weather, such that vertical shear is an important ingredient in support of supercell storms (e.g., Miller 1972; Guyer et al. 2006). The combination of these factors provides the motivation for detailed investigation.

1.2 Dissertation structure

Following the introduction of the general meteorological problem addressed in this chapter, Chapter 2 provides a parameter-based analysis of often-referenced meteorological variables for the southeast United States cold season severe weather regime. Smith et al. (2012), Thompson et al. (2012), and Edwards et al. (2012) introduce, document, and apply the process of merging severe storm reports with near-storm environmental characteristics based on the Storm Prediction Center mesoanalysis data (Bothwell et al. 2002), which are used as the foundation for this analysis. This work then formulates distributions of parameter values characterizing the near-storm environment associated exclusively with southeast U.S. cold season tornadoes, while simultaneously investigating their differences from other regimes supporting severe weather in the United States. Differences between the southeast U.S. cold season tornado regime and other tornado-supporting regimes are statistically distinguished.

Furthermore, Chapter 2 uses results from work featured in the three-part series of Smith et al. (2012), Thompson et al. (2012), and Edwards et al. (2012) that involves the documentation of convective mode – i.e., principal archetypes of morphological features – associated with the tornadoes. This lends opportunities for comparisons of parameters between predominant convective modes supporting tornadoes, specifically in the particular regime of southeast U.S. cold season tornadoes in this second chapter. Convective mode is inherently linked

to the severe-storm intensity, and this work provides specific parameter comparisons amongst the two predominant convective modes characterizing southeast United States cold-season tornadoes: right-moving supercells and quasi-linear convective systems (QLCSs).

The findings presented in Chapter 2 highlight the notion that the particular regime of southeast U.S. cold season tornadoes is associated with different characteristics relative to other regions of the U.S. and at other times of the year. In addition to providing analyses across a vast set of meteorological parameters, the present work reinforces already-suggested notions presented by Guyer et al. (2006) and Guyer and Dean (2010) who highlight defining characteristics of the southeast U.S. cold season tornado environments. Collectively, these characteristics are marked by relatively cooler surface conditions, weaker buoyancy, higher low-level relative humidity, lower lifting condensation level heights, and strong vertical wind shear. However, a contribution of this work is provided by specifically focusing on near-storm environmental characteristics exclusively associated with individual tornado events for southeast United States cold season tornadoes and comparisons with other tornado-supporting regimes.

Ultimately, the assessments of the lower-tropospheric thermodynamic and kinematic structures are important components of the forecast process for accurately identifying these characteristics. Chapter 2 motivates the idea that the defining characteristics of southeast U.S. cold season tornado environment are

directly related to properties very near to the surface, whose behavior is governed by exchanges of mass, heat, and momentum via mixing processes occurring in association with turbulence in what is known as the planetary boundary layer (PBL). The process of mixing is accomplished through turbulent eddies, which directly influence the behavior of thermodynamic and kinematic profiles in the low levels of the atmosphere. Eddies evolve at time and space scales that are not able to be explicitly represented in most mesoscale models, thus requiring expression of their effects using PBL parameterization schemes (e.g., Stull 1988; Holton 2004; Stensrud 2007). Following C15, the term "mesoscale models" herein refers to those with small enough grid length (horizontal distance between adjacent model points within the simulation domain) to explicitly represent convection, while larger grid lengths necessitate convective parameterization schemes (e.g., Kain et al. 2006; Stensrud 2007).

Given the marginality of the necessary condition of instability supporting these wintertime tornado environments and their societal impact, it is important that greater attention be placed on improving numerical simulations of such environments in an era when operational meteorologists place substantial emphasis on considering high-resolution model guidance in the forecast process, which better resolve processes at the meso- and storm-scale (Weiss et al. 2008). Provided the importance of resolving properties of the PBL, it follows that thorough investigation of the PBL in this particular regime is necessary. This investigation is the focus of Chapter 3 and Chapter 4. Chapter 3 provides an overview of

the way in which PBL schemes have traditionally been developed and applied, along with their known biases. Chapter 4 begins with an overview of the experimental design and associated motivation for this design when investigating PBL schemes for the southeast U.S. cold season severe-weather regime, which is a novel regime of focus for evaluation of PBL schemes. Subsequently, Chapter 4 provides the evaluation of PBL schemes for this particular regime, including results corresponding to adjusted schemes that have never been previously investigated. This chapter is then followed by Chapter 5, which provides a review of findings.

Throughout this work, there are three primary, focused questions addressed as a means of improving scientific knowledge of southeast U.S. cold season tornado environments:

1. What are distinguishing characteristics of southeast U.S. cold season tornado regimes relative to other regimes?

2. How well do already developed methods of representing turbulent processes within the PBL perform in reproducing thermodynamic and kinematic structures for these regimes via numerically modeled simulations?

3. How can improvements be made to these methods to improve their viability in such simulations?

Regarding the first question, it is hypothesized that this regime contains distinguishable distributions of thermodynamic and kinematic variables when compared to other regimes in which tornadoes occur. Ultimately, upon identifying this distinguishability, additional analysis in this regime may be worthwhile, covering concepts such as convective mode and daytime versus nighttime variability of related variables. Regarding the second and third questions, it is hypothesized that, following the methods of C15 but for a larger sample size, certain PBL schemes will perform better than other PBL schemes, providing guidance to the numerical modeling community and forecasters in selecting the best PBL parameterization schemes for this environment. PBL-influenced parameter tendencies associated with the larger sample size will be evaluated. This will permit the investigation of whether these tendencies mimic those of C15, whereby the engagement of relatively more model levels throughout the PBL in the mixing process is necessary for better simulated thermodynamic structures.

Chapter 2

The Southeast United States Cold Season Tornado Environment

2.1 Dataset for Analysis of the Southeast United States Cold Season Tornado Environment

The first hypothesis regarding the distinguishable thermodynamic and kinematic characteristics of the southeast United States cold season severe weather environment is investigated by using a large severe-weather environment database, which is subsequently described. Smith et al. (2012), Thompson et al. (2012), and Edwards et al. (2012) document the assignment of environmental characteristics and modes associated with certain severe-weather producing convection across the United States, serving as the foundation for this work. The resulting dataset is a nine-year sample of tornado, significant hail (hail of at least 2 inches in diameter or greater), and significant wind (wind gusts of at least 65 knots) events based on the National Climatic Data Center *Storm Data* publication that is paired with SPC mesoanalysis data (Bothwell et al. 2002) during the period from 2003 through 2011. This involves the documentation of the highest-magnitude report per hour and per report type on the 40-km grid-length

Rapid Update Cycle (RUC) model grid (Benjamin et al. 2004). This process permits the pairing of the severe report database with the mesoanalysis data that correspond to the immediately prior analysis hour. This process amounts to the collection of 22901 total severe-thunderstorm grid-hour events, with 10753 of them corresponding to tornadoes, with the 10753 grid-hour tornado events being the focus of this work.

The 10753 grid-hour tornado events are stratified into four groups:

1. Events occurring within roughly the southeast quarter of the United States – hereafter referred to as the southeast United States encompassing the states of Arkansas, Louisiana, Tennessee, Mississippi, Alabama, Georgia, North Carolina, South Carolina, and Florida – during the cold season (December, January, and February) – referred to as "SECOLD" (503 events),

2. Events occurring outside of the "SECOLD" spatiotemporal regime (i.e., outside of southeast United States any time of year and within the Southeast outside of the December-February period) – referred to as "NONSECOLD" (10250 events),

3. Events occurring within the southeast United States outside of the December-February period – referred to as "SEWARM" (3013 events),

4. Events occurring anywhere in the United States outside of the December-February period – referred to as "WARMER" (9973 events).

Both "SEWARM" and "WARMER" are subsets of "NONSECOLD." The motivation for the aforementioned stratification process is to permit the opportunity to investigate the difference of meteorological variables associated with "SECOLD" tornadoes from those associated with other tornadoes occurring across the country and during warmer times of year. Subsequent discussion focuses on these differences. Tornado events corresponding to tornadoes in each of the aforementioned classes are plotted in Fig. 2.1, Fig. 2.2, Fig. 2.3, and Fig. 2.4, which illustrate the robust nature of the sample of reports following the methodology applied to work featured by Smith et al. (2012), Thompson et al. (2012), and Edwards et al. (2012). While the final section of this chapter addresses daytime versus nighttime variability of parameters associated with the tornado events, these plots and subsequent discussion prior to the final section of this chapter do not make a distinction between events that occurred during the day versus the night.

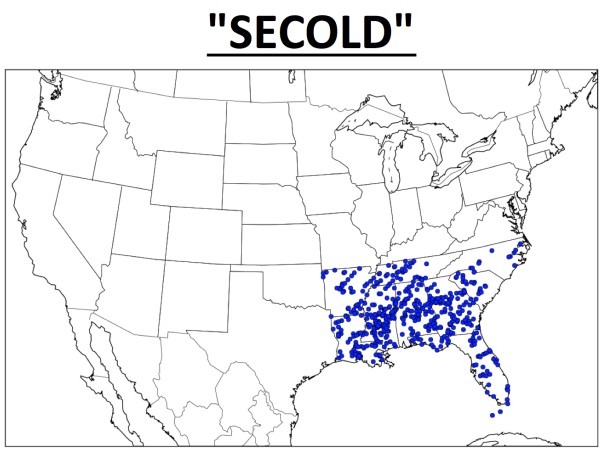

Figure 2.1: Tornado events associated with the "SECOLD" regime.

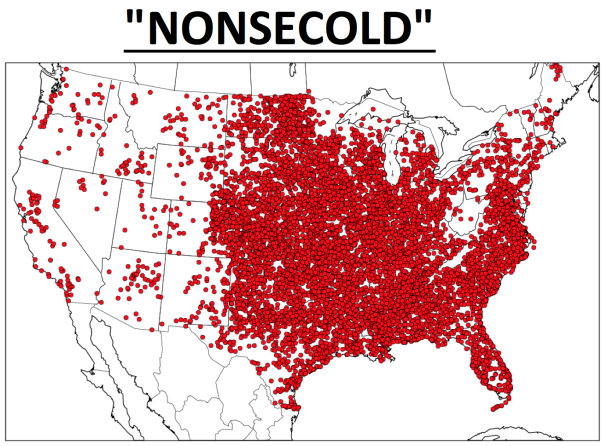

Figure 2.2: As in Fig. 2.1, except for the "NONSECOLD" regime.

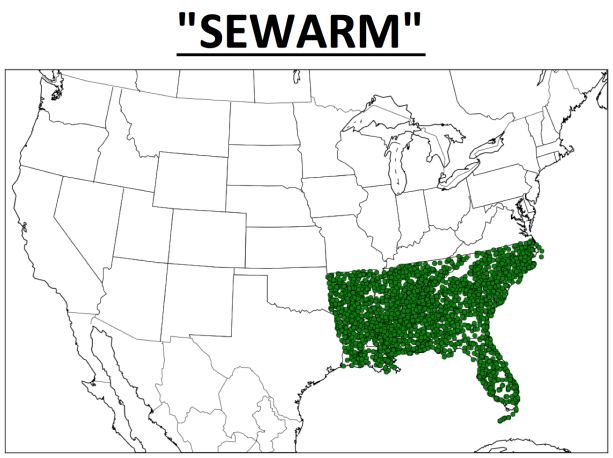

Figure 2.3: As in Fig. 2.1, except for the "SEWARM" regime.

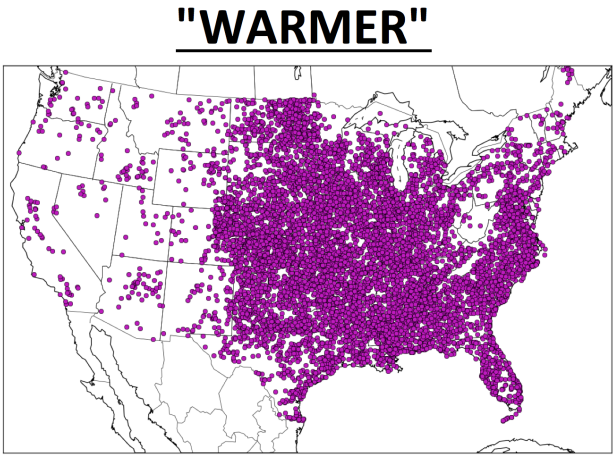

Figure 2.4: As in Fig. 2.1, except for the "WARMER" regime.

2.2 Testing the Distinguishability of the Southeast United States Cold Season Tornado Environment

Tests of statistical significance can be used to identify the "SECOLD" regime as being associated with a distinguishable set of environmental parameters relative to other regimes. In the present work, this is performed by using the Kolmogorov-Smirnov test (Massey 1951). This test compares the differences between the cumulative density functions corresponding to two samples, comparing the "SECOLD" regime to the "NONSECOLD" regime, though no additional seasonal comparison is included. Larger differences of cumulative density function with increasing parameter values correspond to greater likelihood that the two samples are from different populations. This is illustrated in Fig. 2.5 that compares surface-based CAPE (SBCAPE) for "SECOLD" with SBCAPE for "NONSECOLD," with a corresponding p-value of less than 0.0001 suggesting statistically significantly different SBCAPE between "SECOLD" and "NONSECOLD" regimes.

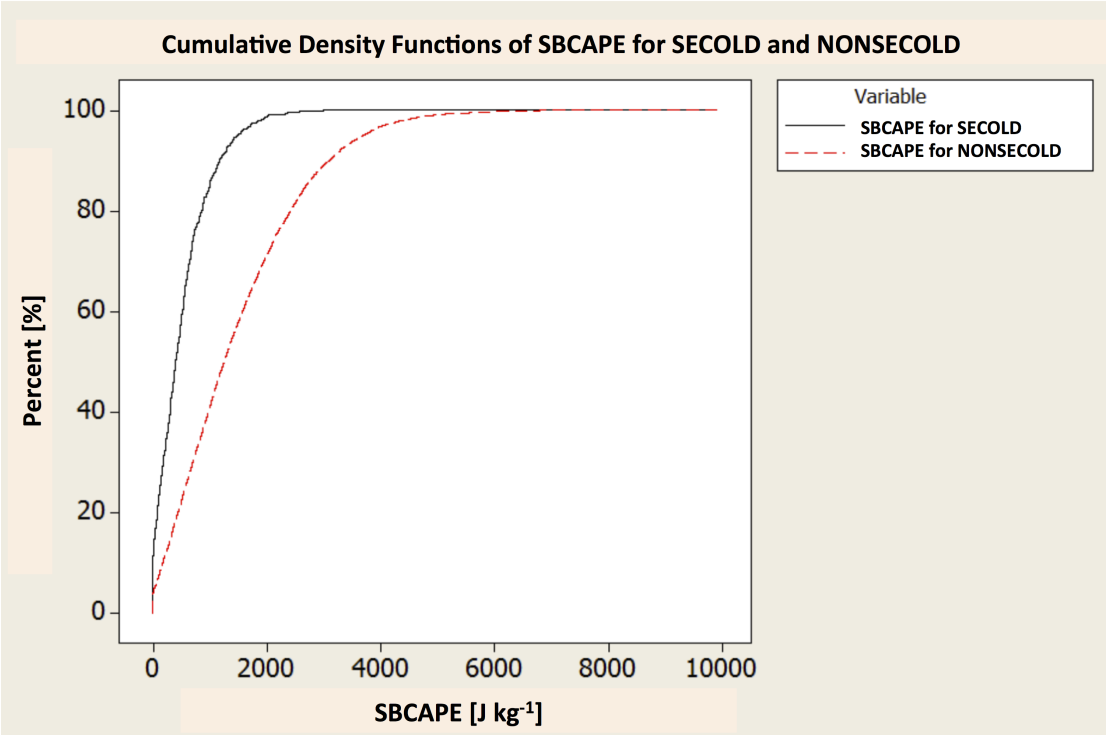

Figure 2.5: Cumulative density functions corresponding to SBCAPE during the "SECOLD" regime (solid black curve) and "NONSECOLD" regime (dashed red curve).

This procedure is extended to many other parameters provided in Table 2.1, which indicates low p-values associated with many often-referenced thermodynamic and kinematic parameters in severe-weather forecasting representing distinguishability of the "SECOLD" regime. The Kolmogorov-Smirnov test is a non-parametetric test, which is a strength of this statistical test owing to its lack of distribution assumption. However, results from this test can be sensitive to both large sample sizes and differences between cumulative density functions that may only occupy relatively small portions of the full ranges of the distribution values, rendering limitations of this test. For example, very large sample sizes could result in determining statistically significant differences that are not

necessarily practically significant. Also, if there were to exist a large difference in the cumulative density functions between two samples over a very small interval of the parameter values, the Kolmogorov-Smirnov test may imply statistically significant differences between the two samples whereas much of the remaining portions of the two samples could be similar, yielding a contradiction. These notions are important to consider when interpreting the results of this statistical test. Also, regarding the specific formulations of meteorological parameters subsequently studied, particular choices involving these formulations (e.g., bounds of layers used to compute lapse rate), are somewhat arbitrary but are accepted by the convective community as representing the severe thunderstorm environment.

Table 2.1: P-values corresponding to the Kolmogorov-Smirnov statistical test of the difference in parameter values between the "SECOLD" and "NONSECOLD" regimes.

Variable	*P-Value*
mixed-layer convective available potential energy	<0.0001
mixed-layer convective inhibition	0.0747
mixed-layer lifting condensation level	<0.0001
mixed-layer level of free convection	0.0003
most-unstable convective available potential energy	<0.0001
most-unstable convective inhibition	<0.0001
most-unstable lifting condensation level	<0.0001
most-unstable level of free convection	0.0162
surface-based convective available potential energy	<0.0001
surface-based convective inhibition	0.0370
0-3-km mixed-layer convective available potential energy	<0.0001
downdraft convective available potential energy	<0.0001
700-500-mb lapse rate	<0.0001
850-500-mb lapse rate	<0.0001
0-3-km lapse rate	<0.0001
surface temperature	<0.0001
surface dewpoint temperature	<0.0001
0-8-km bulk shear	<0.0001
0-6-km bulk shear	<0.0001
0-3-km bulk shear	<0.0001
0-1-km bulk shear	<0.0001
0-3-km storm-relative helicity	<0.0001
0-1-km storm-relative helicity	<0.0001

Box-and-whiskers plots of SBCAPE and MLCAPE (Figs. 2.6 and 2.7, respectively) clearly show the downward-shifted, compressed nature of buoyancy for the "SECOLD" regime compared to other regimes influenced by warmer and more moist conditions in the lower atmosphere that can support greater buoyancy. These box-and-whiskers plots, and all subsequently provided box-and-whiskers plots, indicate the interquartile range, median, and mean values for distributions, with whiskers extending up to 1.5 times the interquartile range beyond the first and third quartiles. However, outlier values are not included to ensure primary focus on the details of the bulk of the distributions. The box-and-whiskers plots of SBCAPE and MLCAPE (Figs. 2.6 and 2.7, respectively) highlight the notion that small variability in "SECOLD" buoyancy is relatively large compared to the overall limited total buoyancy in this regime, compared to other regimes.

Graphically, it is evident that the portion of MLCAPE confined to the lowest 3 km of the atmosphere (Fig. 2.8) during "SECOLD" is associated with smaller separation from the other regimes than MLCAPE derived from the entire freely convective layer (Fig. 2.7). This is further explored by computing the ratio of 0-3-km MLCAPE to total MLCAPE in Fig. 2.9, which explicitly shows larger proportions of MLCAPE confined to the lowest 3 km above ground during "SECOLD" compared to other regimes. This highlights the relative importance of lower-atmospheric thermodynamic structures in explaining the buoyancy in

the "SECOLD" regime. With such structures being directly influenced by turbulent exchanges in the PBL, this provides substantial motivation for further exploration of the PBL in more detail for the "SECOLD" regime, with even further motivation provided by the distinguishability of other thermodynamic parameters (e.g., total MLCAPE and SBCAPE). Relatively lower magnitudes of mid-level lapse rates and surface moisture (Figs. 2.10 and 2.11, respectively) characterize the box-and-whiskers plots for "SECOLD" versus "NONSECOLD" distributions.

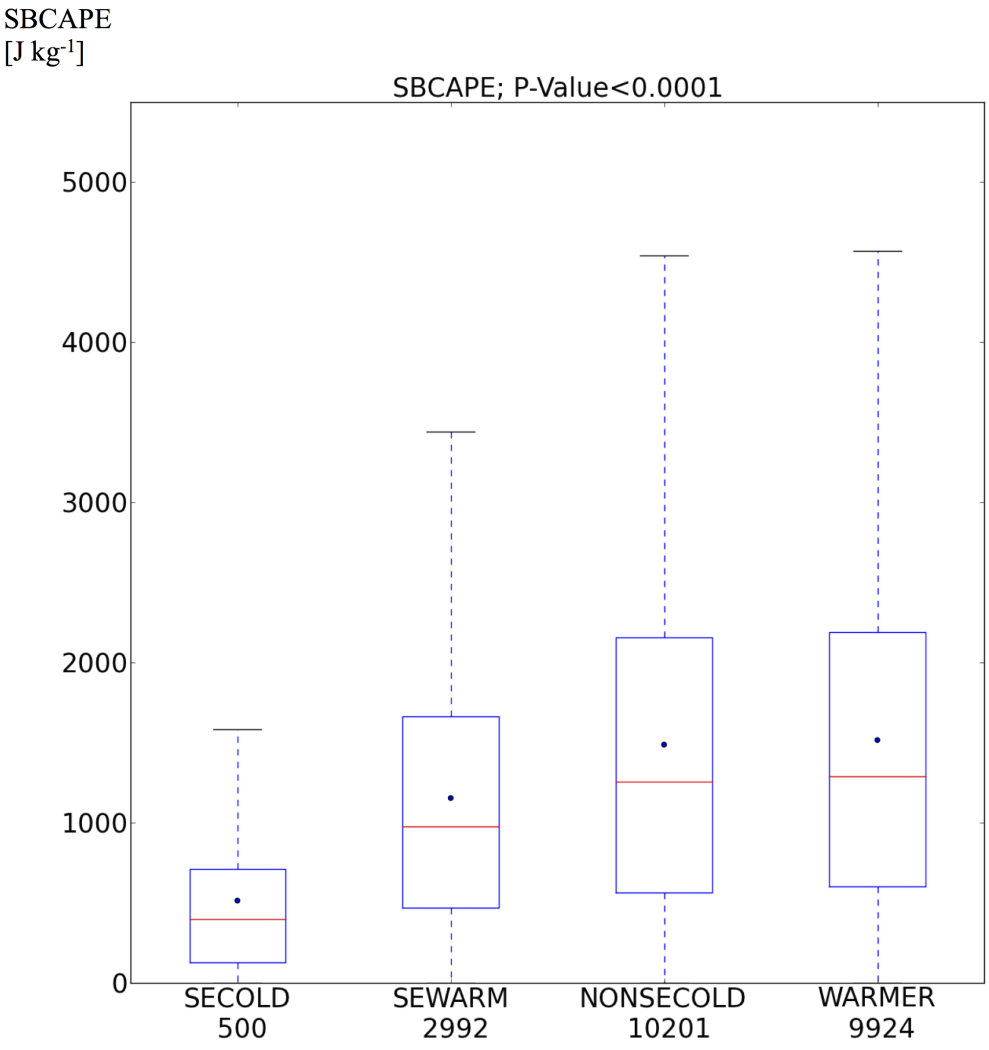

Figure 2.6: Box-and-whiskers plots corresponding to the distribution of SBCAPE for tornadoes occurring in the "SECOLD," "SEWARM," "NONSECOLD," and "WARMER" regimes, from left to right, with sample sizes listed below x-axis labels. The blue-outline box corresponds to the interquartile range, the red horizontal line corresponds to the median value, the dot marker corresponds to the mean value, and whiskers extend up to 1.5 times the interquartile range beyond the first and third quartiles. The p-value corresponding to the Kolmogorov-Smirnov statistical test of the difference in parameter values between the "SECOLD" and "NONSECOLD" regimes is listed within the title.

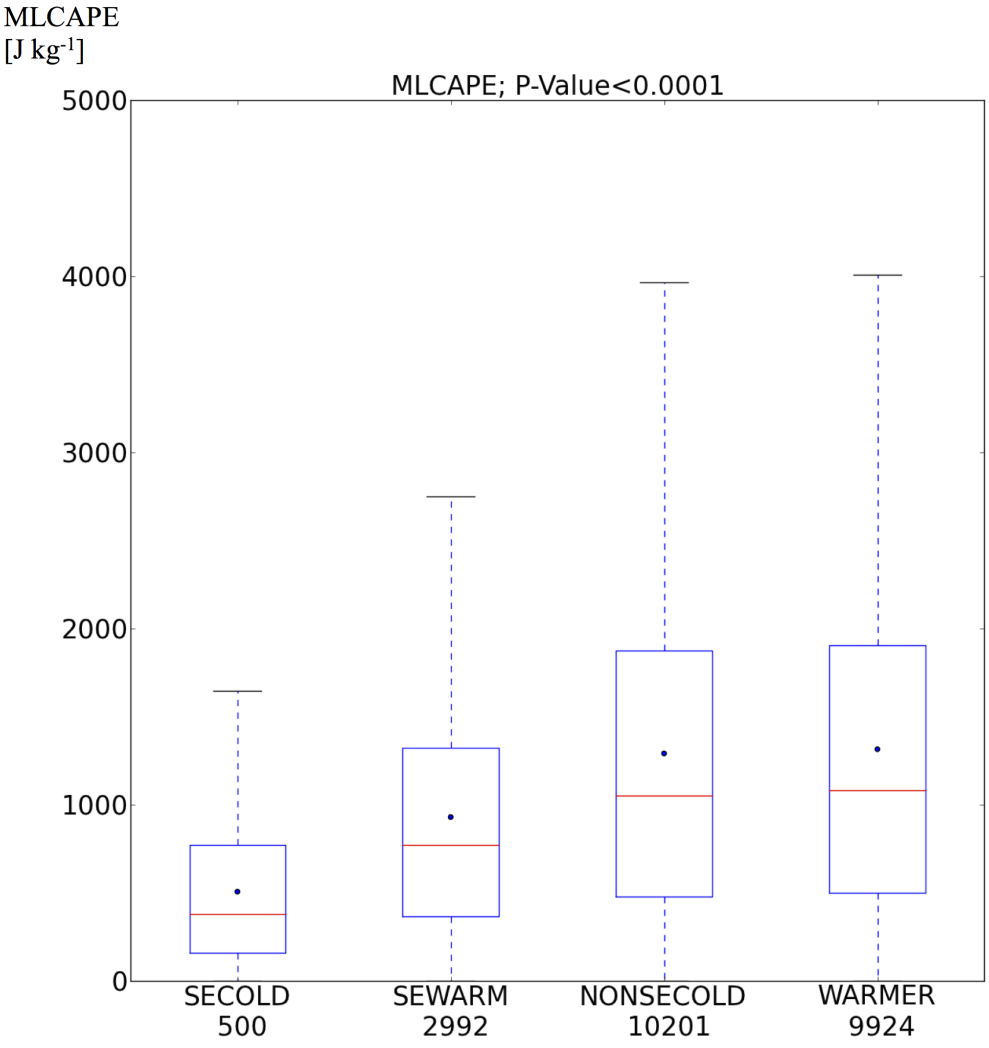

Figure 2.7: As in Fig. 2.6, except for MLCAPE.

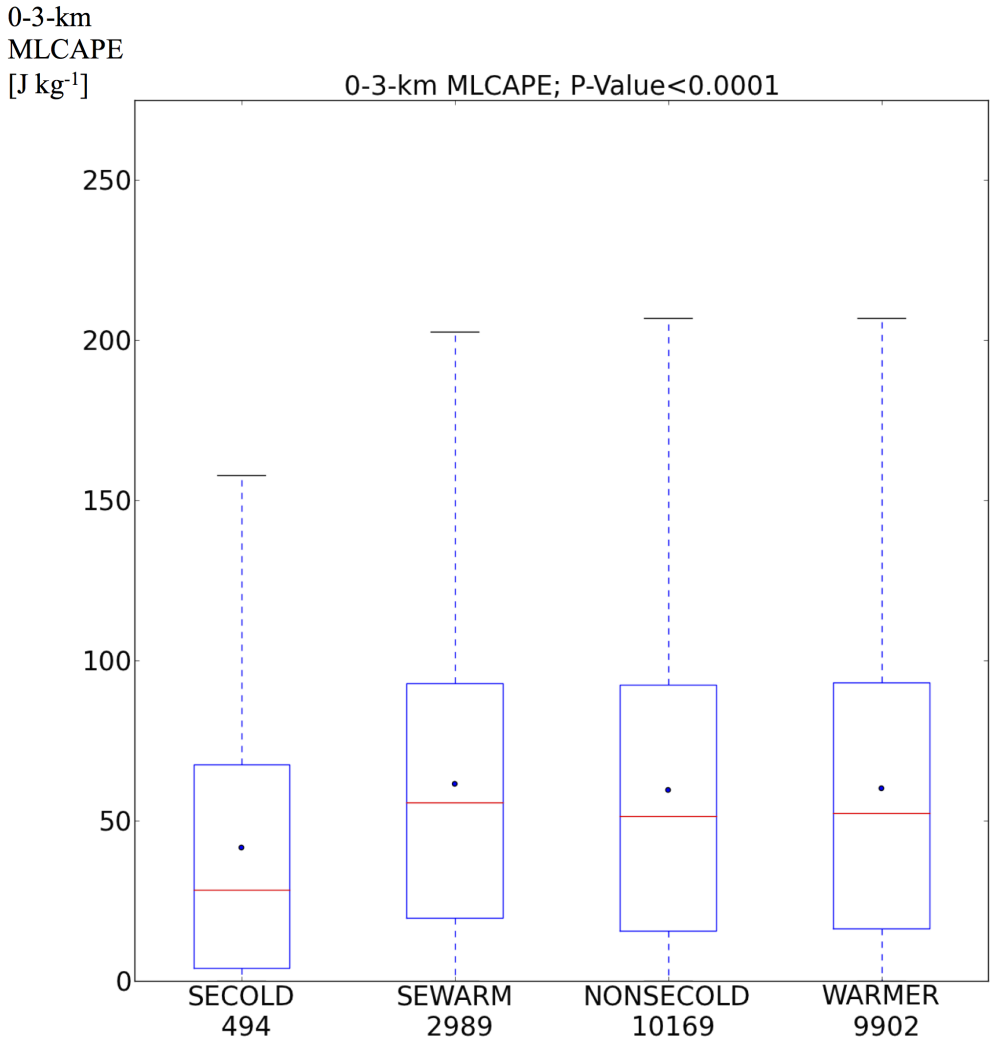

Figure 2.8: As in Fig. 2.6, except for 0-3-km MLCAPE.

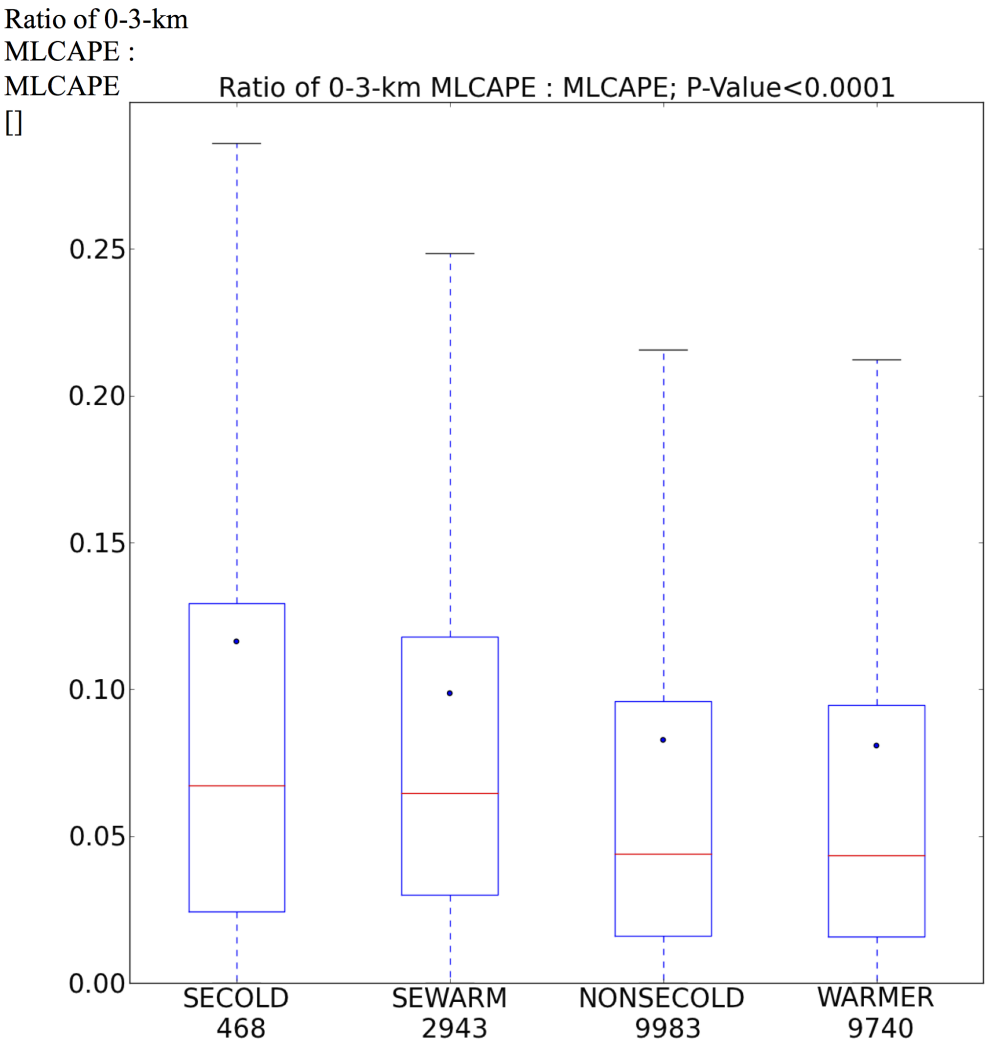

Figure 2.9: As in Fig. 2.6, except for the ratio of 0-3-km MLCAPE to total MLCAPE.

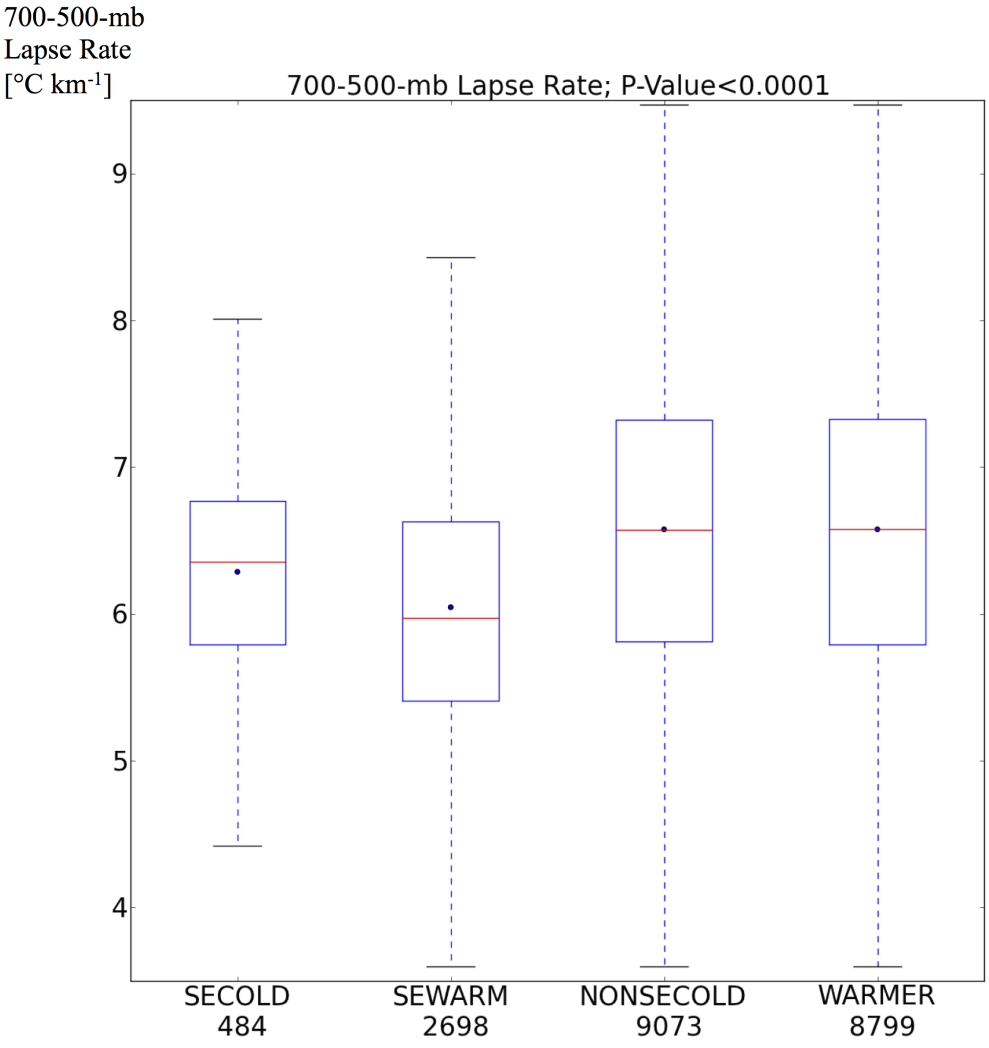

Figure 2.10: As in Fig. 2.6, except for 700-500-mb lapse rate.

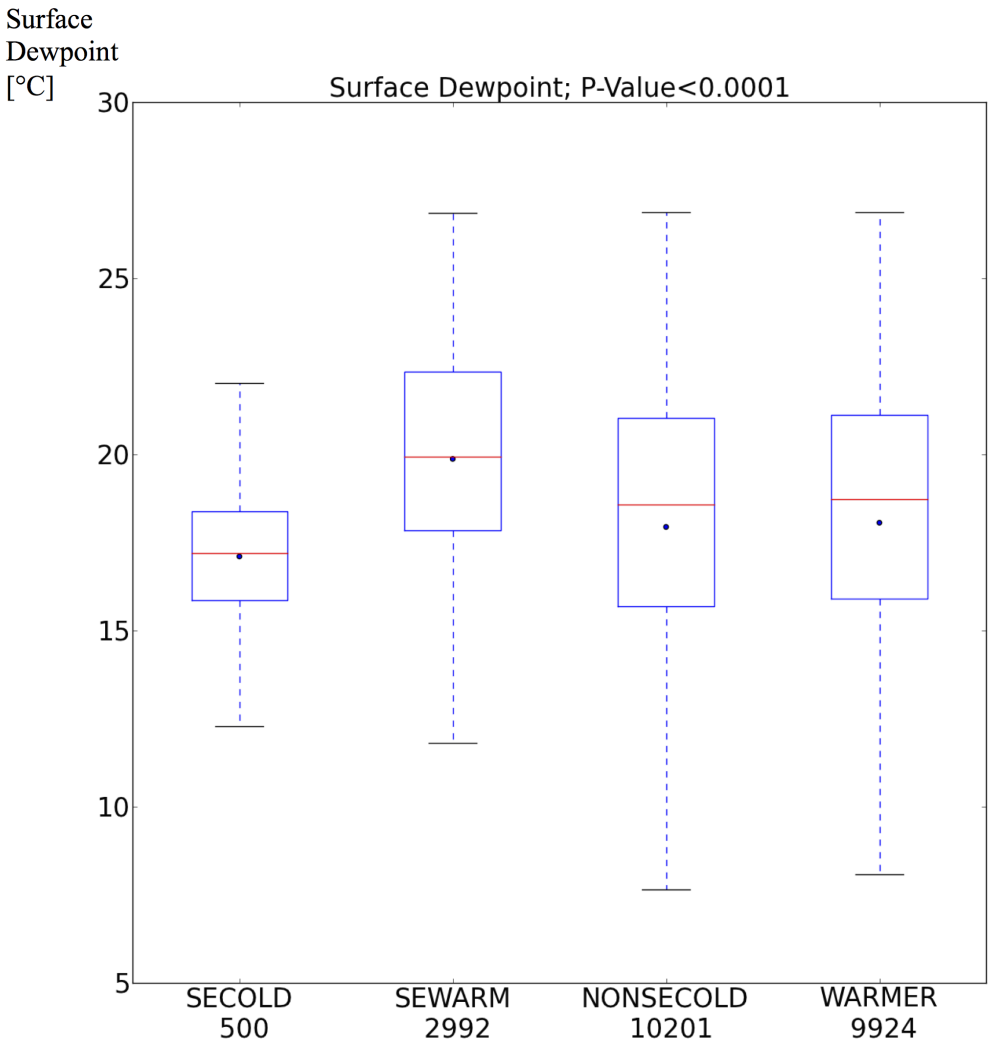

Figure 2.11: As in Fig. 2.6, except for surface dewpoint.

Regarding kinematic-related variables, substantial separation between the "SECOLD" distribution and distributions corresponding to other regimes is well portrayed in Figs. 2.12-2.15. These depict larger magnitudes of storm-relative helicity and vertical bulk shear during the "SECOLD" regime compared to the other regimes, as previously identified. With storm-relative helicity in the lowest 3 km of the atmosphere and bulk shear in the lowest 1 km directly influenced

by the vertical wind profile in the lowest portion of the atmosphere where PBL circulations affect the wind profile, this also motivates the need to explore the representation of the PBL in this distinguishable environment.

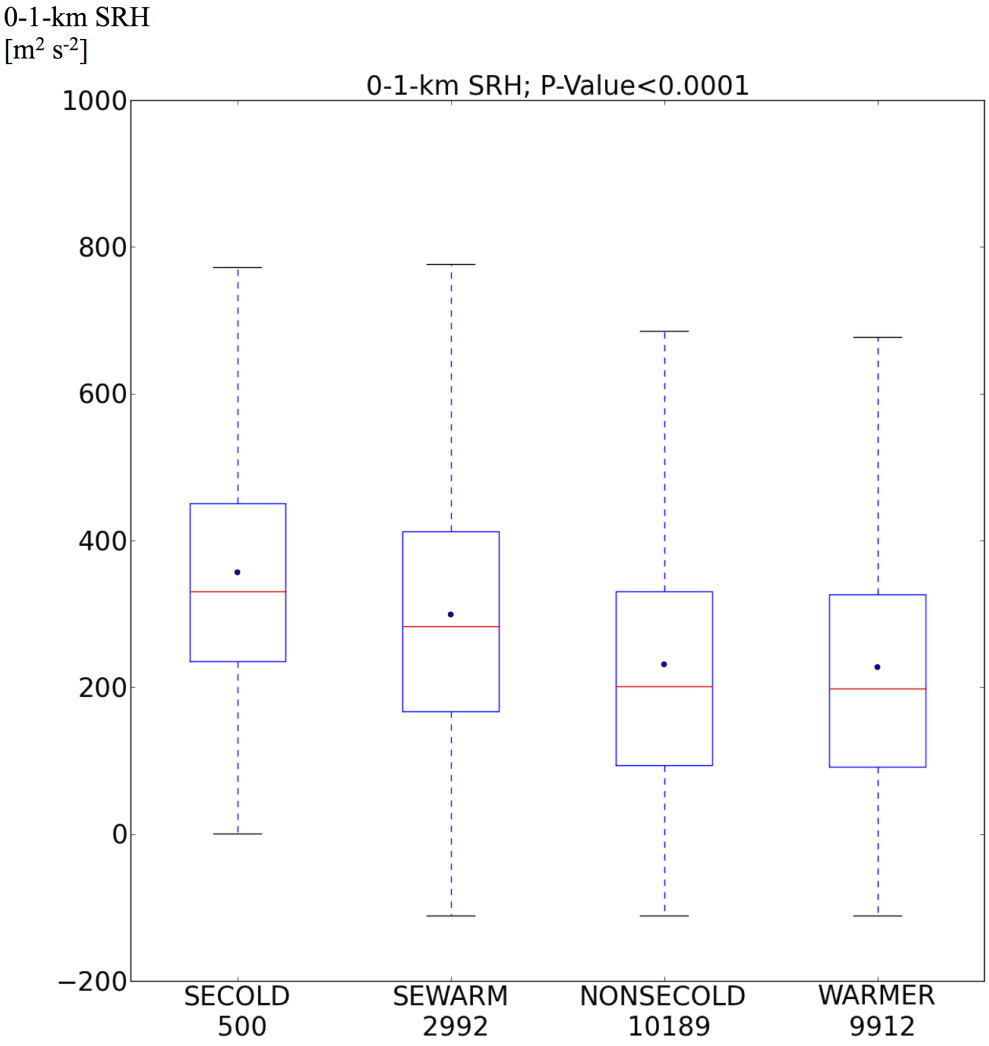

Figure 2.12: As in Fig. 2.6, except for 0-1-km SRH.

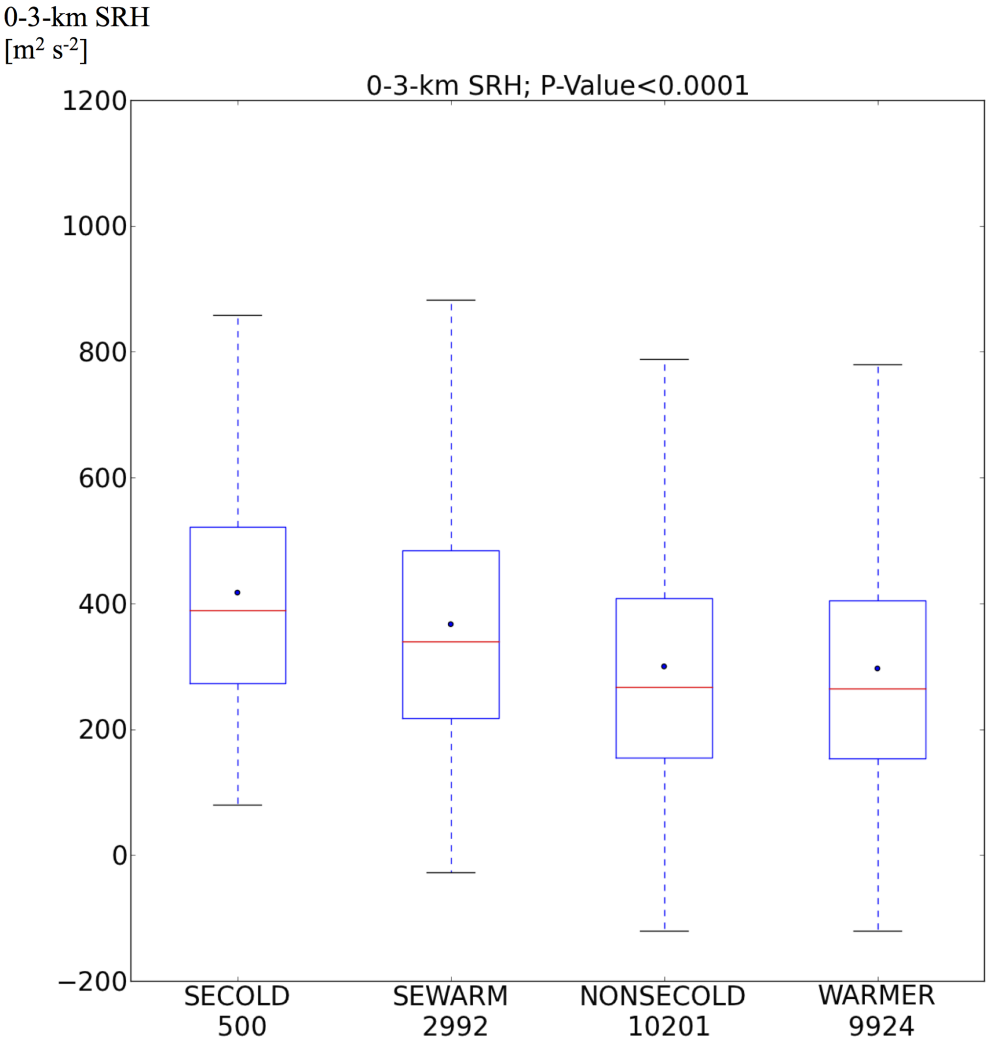

Figure 2.13: As in Fig. 2.6, except for the ratio of 0-3-km SRH.

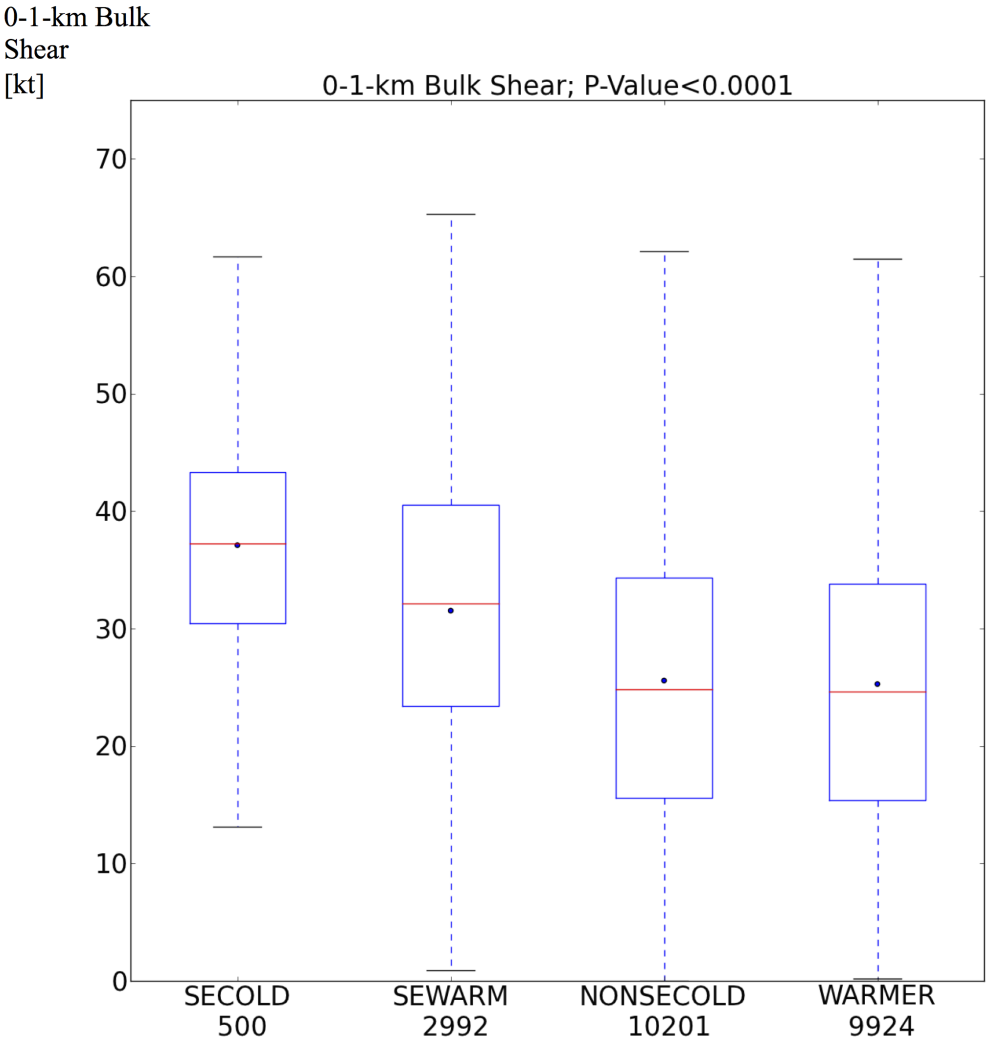

Figure 2.14: As in Fig. 2.6, except for 0-1-km bulk shear.

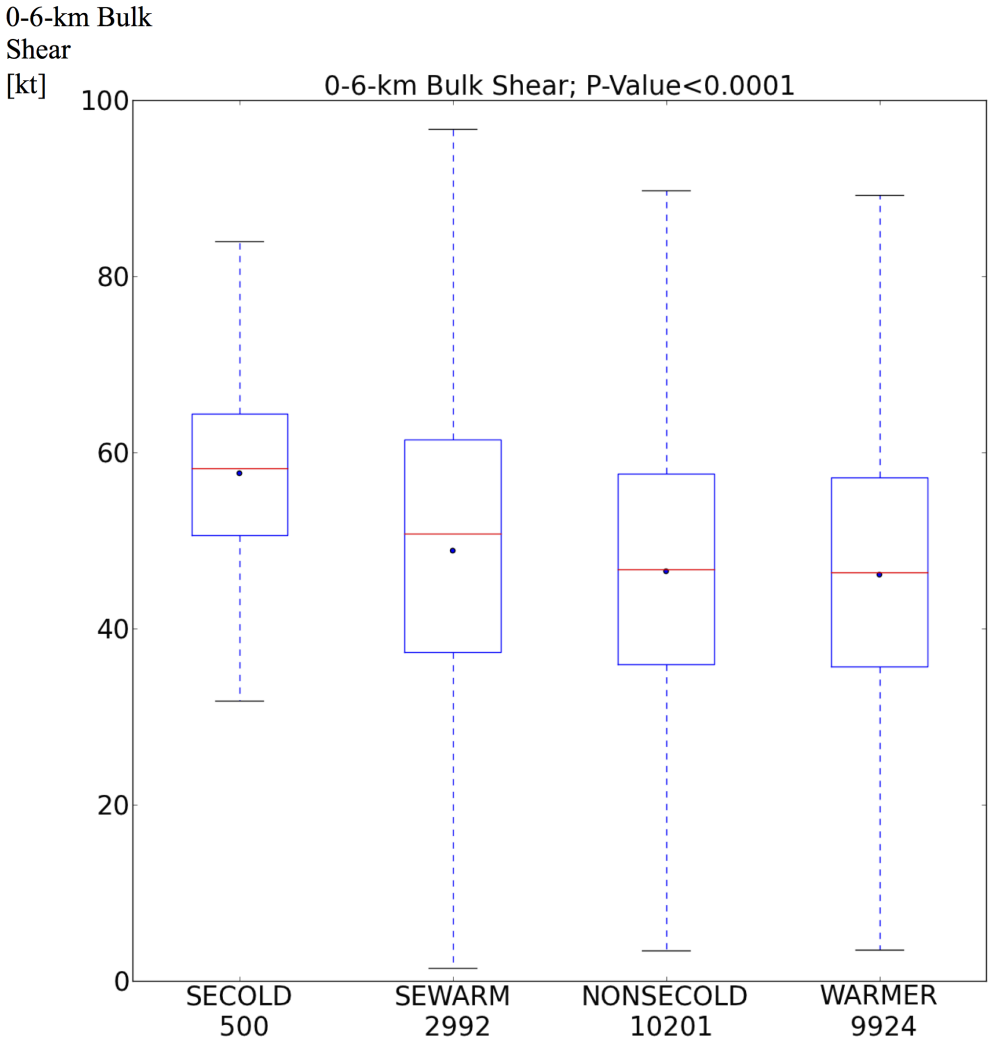

Figure 2.15: As in Fig. 2.6, except for 0-6-km bulk shear.

A subset of parameter distributions, whose corresponding box-and-whisker plots are shown in the previous section, is explored in further detail in this section. This is done by investigating histograms associated with each parameter of the subset in each regime. Multiple histograms are averaged together, each originating at equally spaced points within the first bin of the original histogram, resulting in a smoothed distribution known as an "average shifted histogram"

(Scott 1985). This analysis serves as the basis for subsequent discussion of tornado environments, with plotted histograms corresponding to indicated ranges of parameter values. Distributions of thermodynamic parameters characteristic of the "SECOLD" regime and other regimes are illustrated in Fig. 2.16, Fig. 2.17, and Fig. 2.18, and are followed by distributions of kinematic parameters (Figs. 2.19-2.21).

A difference amongst the various tornado regimes is the relatively narrow distribution of MLCAPE for the "SECOLD" regime compared to the other regimes (Fig. 2.16). Other regimes represent broader distributions of buoyancy, while the bulk of the "SECOLD" distribution is confined to marginal values of buoyancy. This directly highlights how sensitive "SECOLD" environments are to buoyancy; small differences in "SECOLD" MLCAPE are relatively large compared to typical buoyancy magnitudes for tornado events.

Mid-level lapse rates (computed in the 700-500-mb layer) are illustrated in Fig. 2.17. The "SECOLD" regime is associated with a relatively more narrow mid-level lapse rate distribution compared to the distributions for other regimes. The peak of the "SECOLD" regime mid-level lapse rates is closer to moist-adiabatic than dry adiabatic. Meanwhile, the influence of steeper mid-level lapse rates accompanying stronger elevated-terrain surface heating over the western United States is associated with the broader "NONSECOLD" and "WARMER" distributions that incorporate higher 700-500-mb lapse rate magnitudes.

Surface dewpoints for the various regimes are illustrated in Fig. 2.18. Peak dewpoints for the "SECOLD" distribution are relatively drier compared to the "SEWARM" distribution. Awareness of the distribution of surface dewpoints characteristic of the "SECOLD" regime is particularly useful for forecasters, as the relatively narrow range of dewpoint values associated with "SECOLD" tornadoes can be used as focused guidance for anticipating when sufficient moisture exists for tornadoes based on past events, conditional on the forecaster having identified a given large-scale meteorological pattern as being characteristic of one in the "SECOLD" regime.

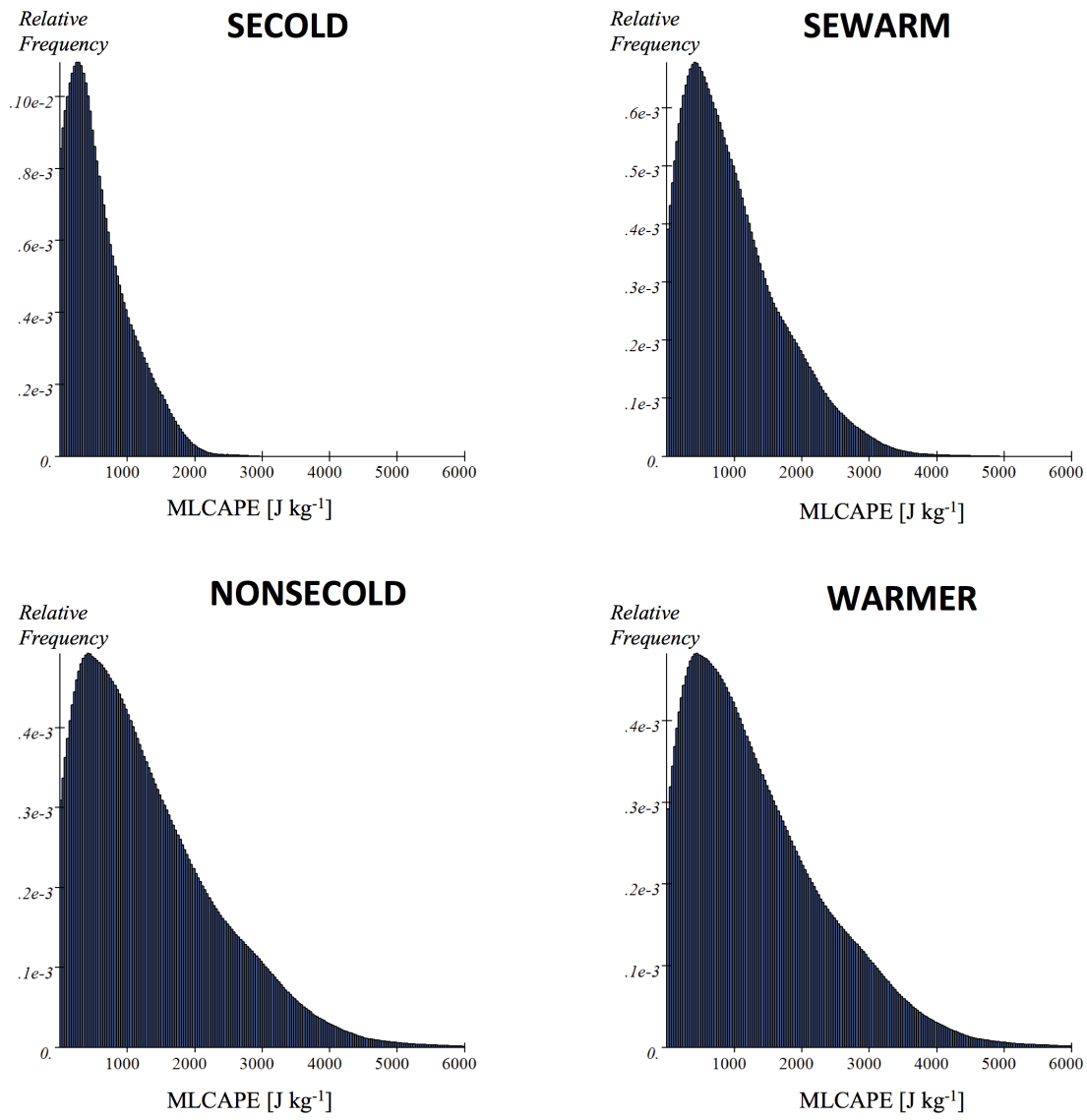

Figure 2.16: Average shifted histograms displaying MLCAPE for tornadoes occurring in the "SECOLD" regime (top left), "NONSECOLD" regime (bottom left), "SEWARM" regime (top right), and "WARMER" regime (bottom right) for the plotted ranges of parameter values. Y-axis ranges of MLCAPE vary from panel to panel to provide focus on the details of each individual distribution.

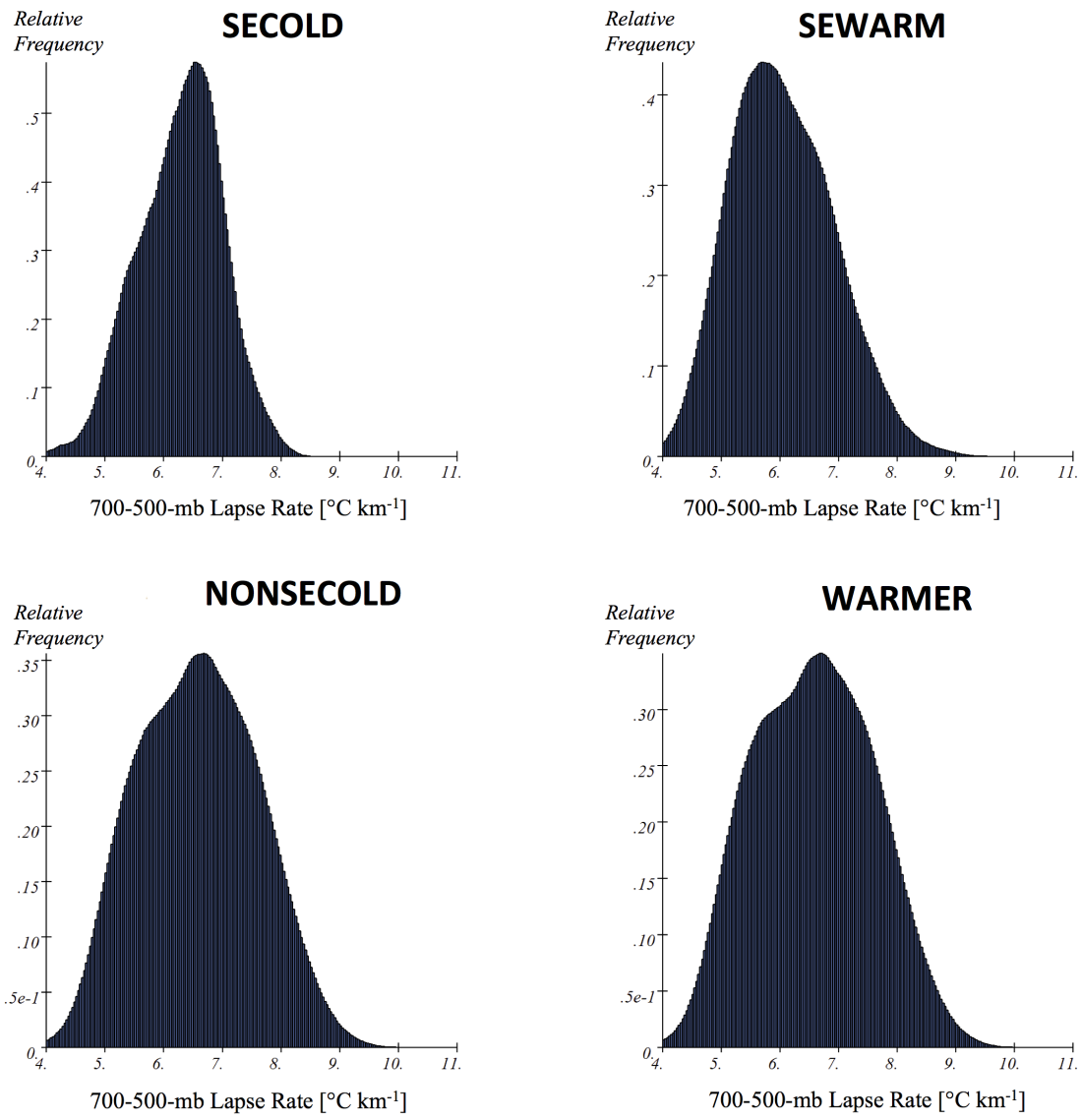

Figure 2.17: As in Fig. 2.16, except for 700-500-mb lapse rate.

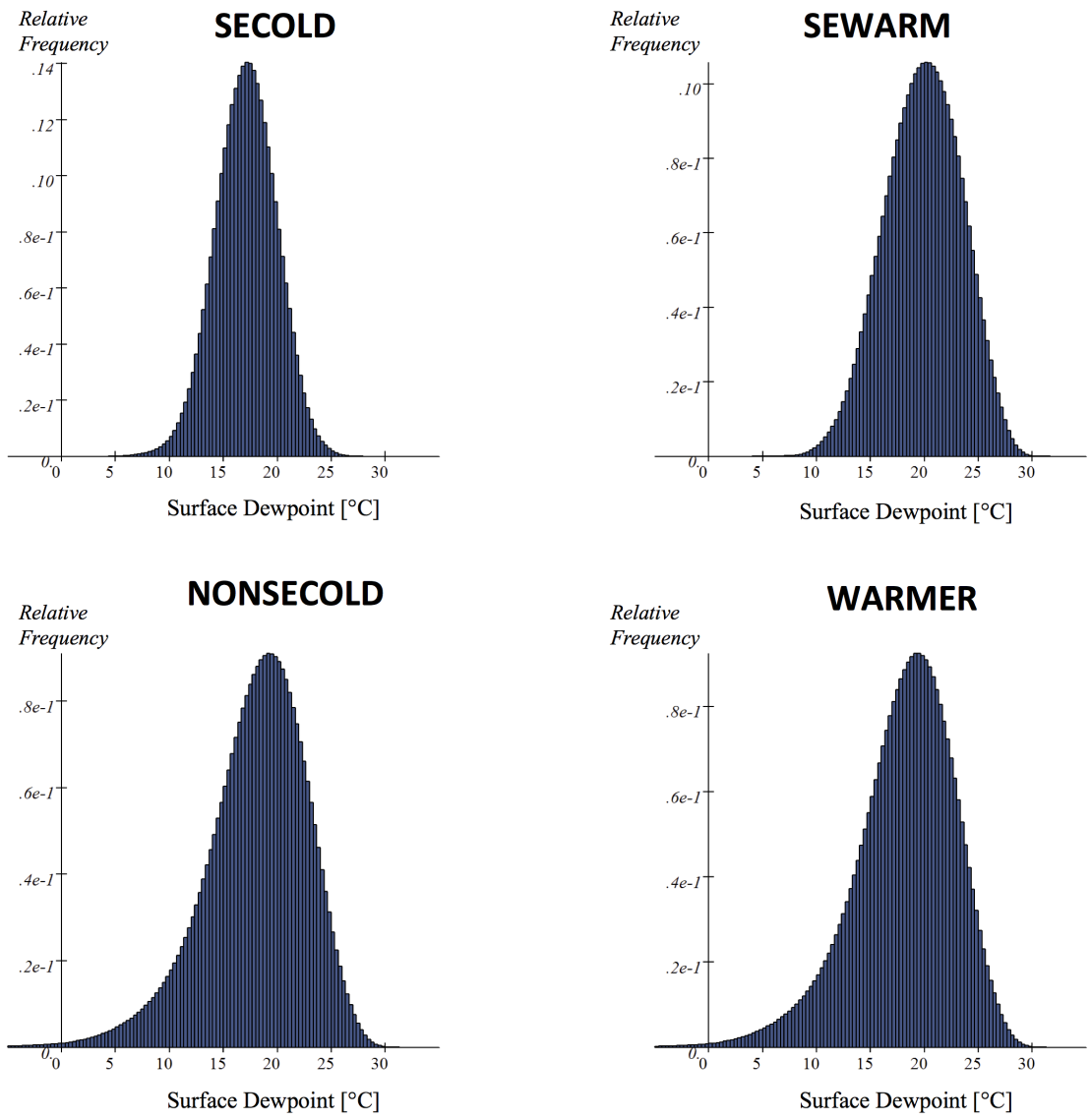

Figure 2.18: As in Fig. 2.16, except for surface dewpoint.

Distributions of kinematic parameters associated with the "SECOLD" regime are also different than those in the other regimes investigated (Figs. 2.19-2.21). The relatively stronger low-level helicity and low-level and deep-layer bulk shear are illustrated by these figures, consistent with the notions previously highlighted regarding stronger vertical shear in these environments. Comparing the

"SECOLD" regime to the "NONSECOLD" regime, a relatively larger portion of the 0-1-km storm-relative helicity (SRH) in the "SECOLD" regime extends to higher magnitudes (Fig. 2.19), while nearly symmetric distributions of the vertical bulk shear (Fig. 2.20 and Fig. 2.21) are clearly shifted to the right for the "SECOLD" regime.

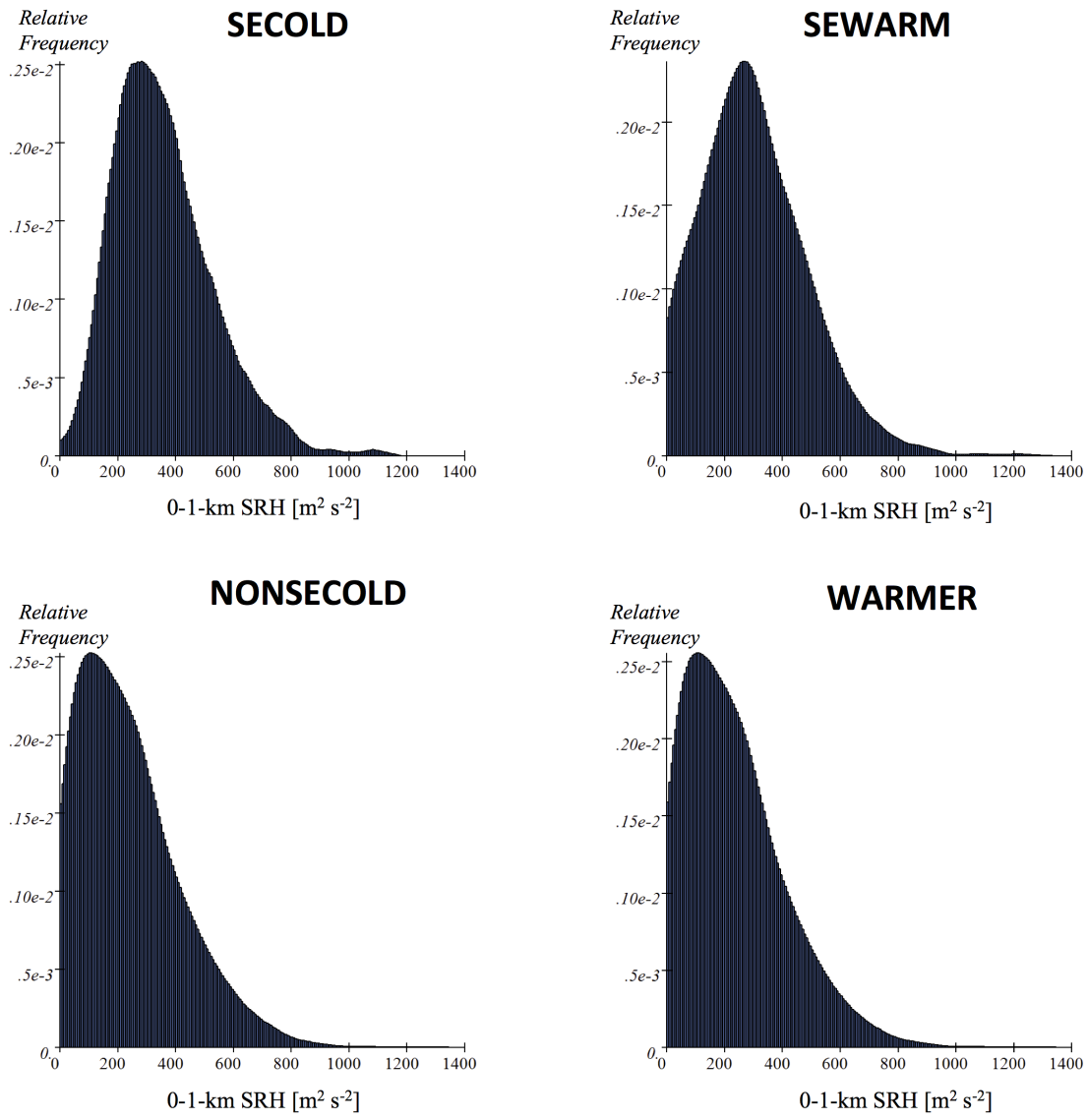

Figure 2.19: As in Fig. 2.16, except for 0-1-km SRH.

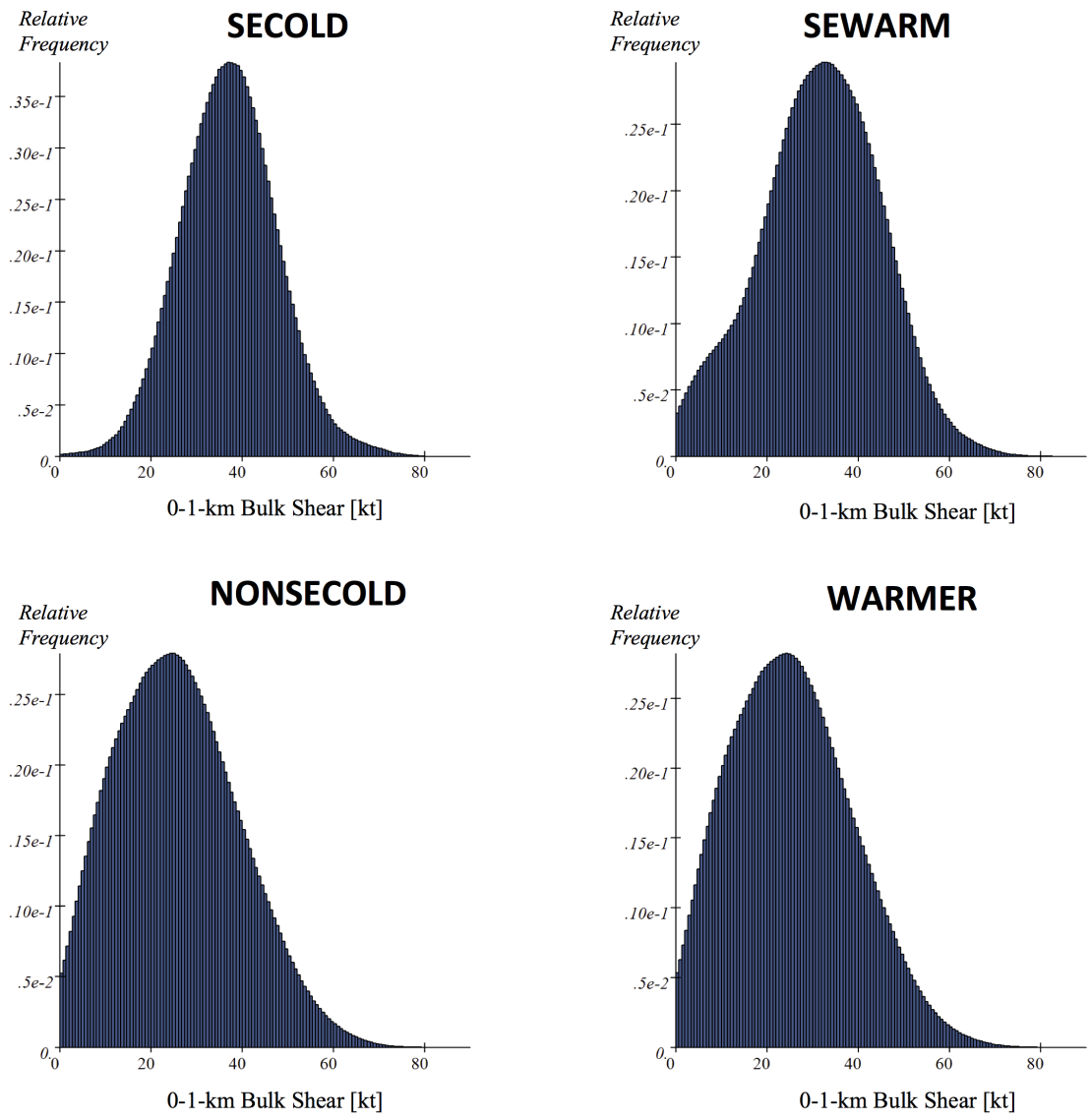

Figure 2.20: As in Fig. 2.16, except for 0-1-km bulk shear.

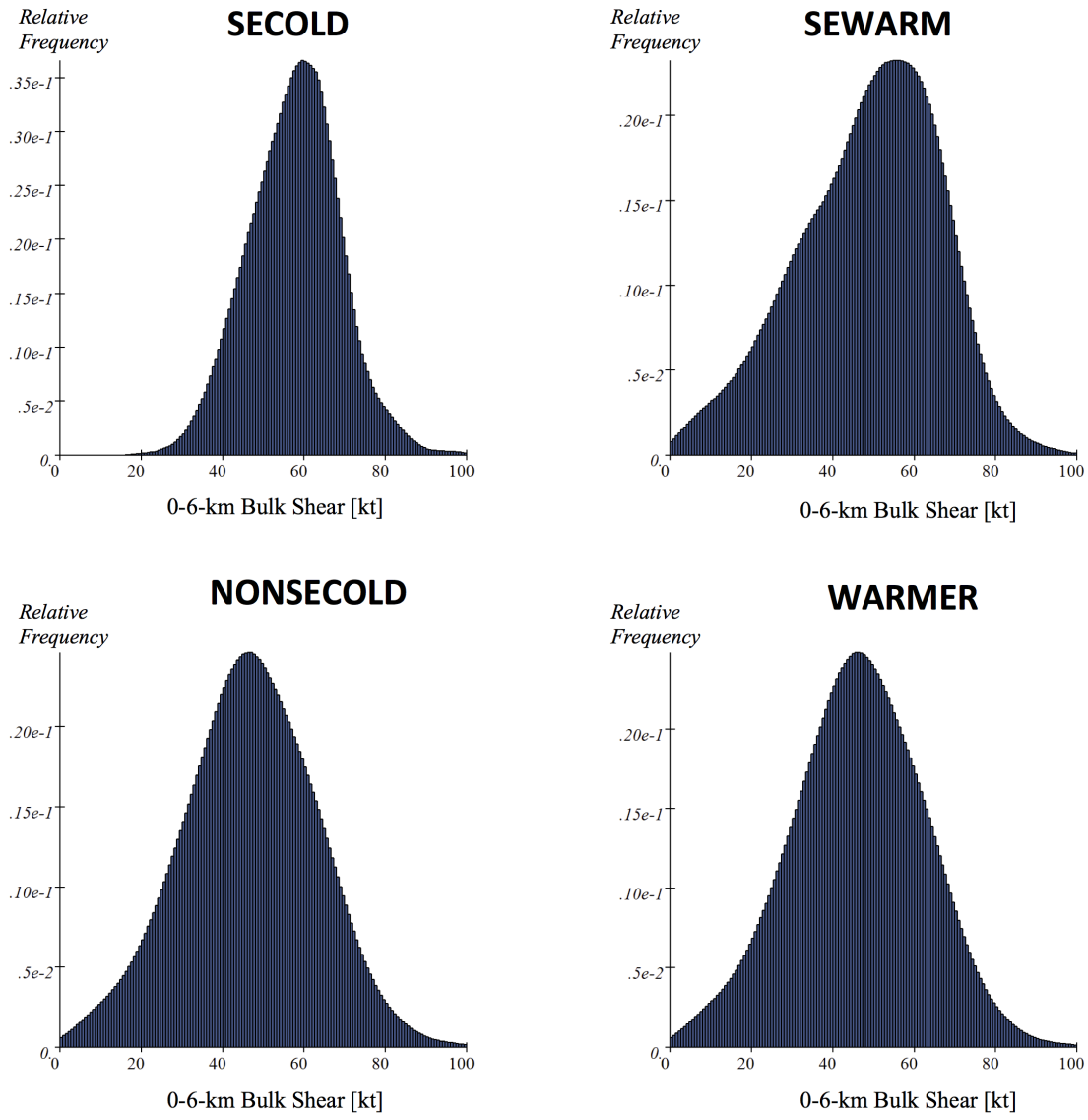

Figure 2.21: As in Fig. 2.16, except for 0-6-km bulk shear.

2.3 Convective Mode in the Southeast United States Cold Season Tornado Environment

It has been well evidenced in preceding sections that the "SECOLD" environment is indeed different than other studied regimes. Work introduced by Smith

et al. (2012), Thompson et al. (2012), and Edwards et al. (2012) permits the opportunity to investigate morphological characteristics of tornado-producing convection during this distinguished regime. Through this process, characteristic classifications of convective morphology yields identification of convective mode associated with these tornado reports. These modes provide some background for considering potential hazards produced by severe storms (Moller et al. 1994; Miller and Johns 2000; Trapp et al. 2005; Gallus et al. 2008), with tornadoes developing from QLCSs more often being relatively weaker than those developing from cells (Trapp et al. 2005). With right-moving supercells and QLCSs being the primary constituents of convective mode associated with "SECOLD" tornadoes, a subset of parameters is compared for right-moving supercell and QLCS convective modes for tornadoes occurring within the "SECOLD" regime in Figs. 2.22-2.30.

The strongest discriminators between right-moving supercell tornadoes and QLCS tornadoes in the "SECOLD" regime are thermodynamic ones, with variables such as SBCAPE (Fig. 2.22), MLCAPE (Fig. 2.23), and 700-500-mb lapse rate (Fig. 2.25) being associated with larger degrees of instability for right-moving supercell tornadoes than QLCS tornadoes. However, despite the relatively stronger buoyancy associated with right-moving tornadic supercells, only a few hundred J kg^{-1} of SBCAPE or MLCAPE variability are associated with the difference between separate convective modes, highlighting the sensitivity of the "SECOLD" regime. This further highlights the importance of correctly

evaluating buoyancy, which is, in part, derived from thermodynamic structures in the lower atmosphere influenced by turbulent mixing in the PBL.

On the other hand, kinematic variables offer less separation between tornadoes developing from right-moving supercells than QLCSs. This is apparent by considering p-values determined from the Kolmogorov-Smirnov statistical test of differences between these two modes, which are listed in Table 2.2. These collective findings highlight the need to obtain accurate depictions of ongoing and/or forecast instability to assess the possibility for a particular spectra of parameters to support QLCS or right-moving-supercell tornadoes.

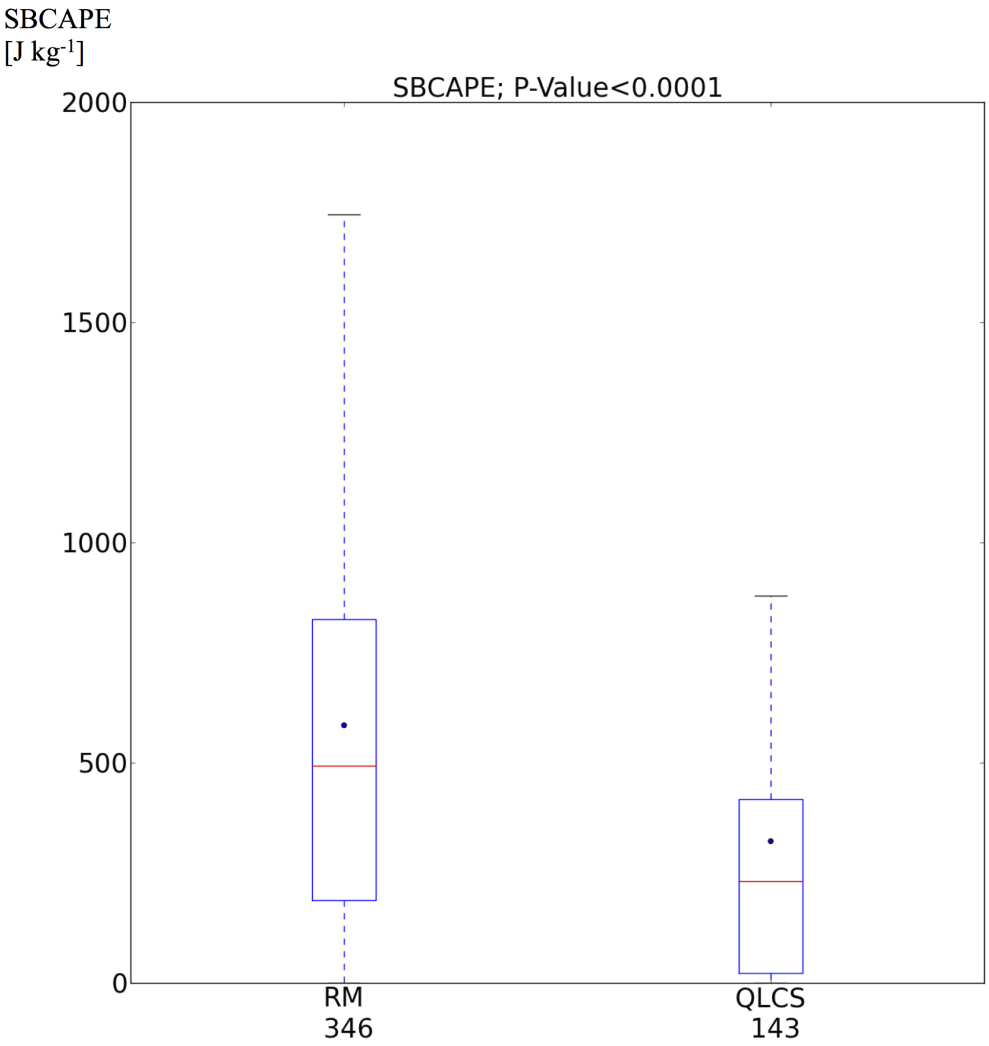

Figure 2.22: Box-and-whiskers plots corresponding to the distribution of SBCAPE for tornadoes occurring during the "SECOLD" regime for right-moving supercell (RM) tornadoes and for QLCS tornadoes. The sample sizes corresponding to each of these convective modes are listed below the x-axis. The blue-outline box corresponds to the interquartile range, the red horizontal line corresponds to the median value, the dot marker corresponds to the mean value, and whiskers extend up to 1.5 times the interquartile range beyond the first and third quartiles. The p-value corresponding to the Kolmogorov-Smirnov statistical test of the difference in parameter values between the right-moving supercell (RM) and QLCS modes is listed within the title.

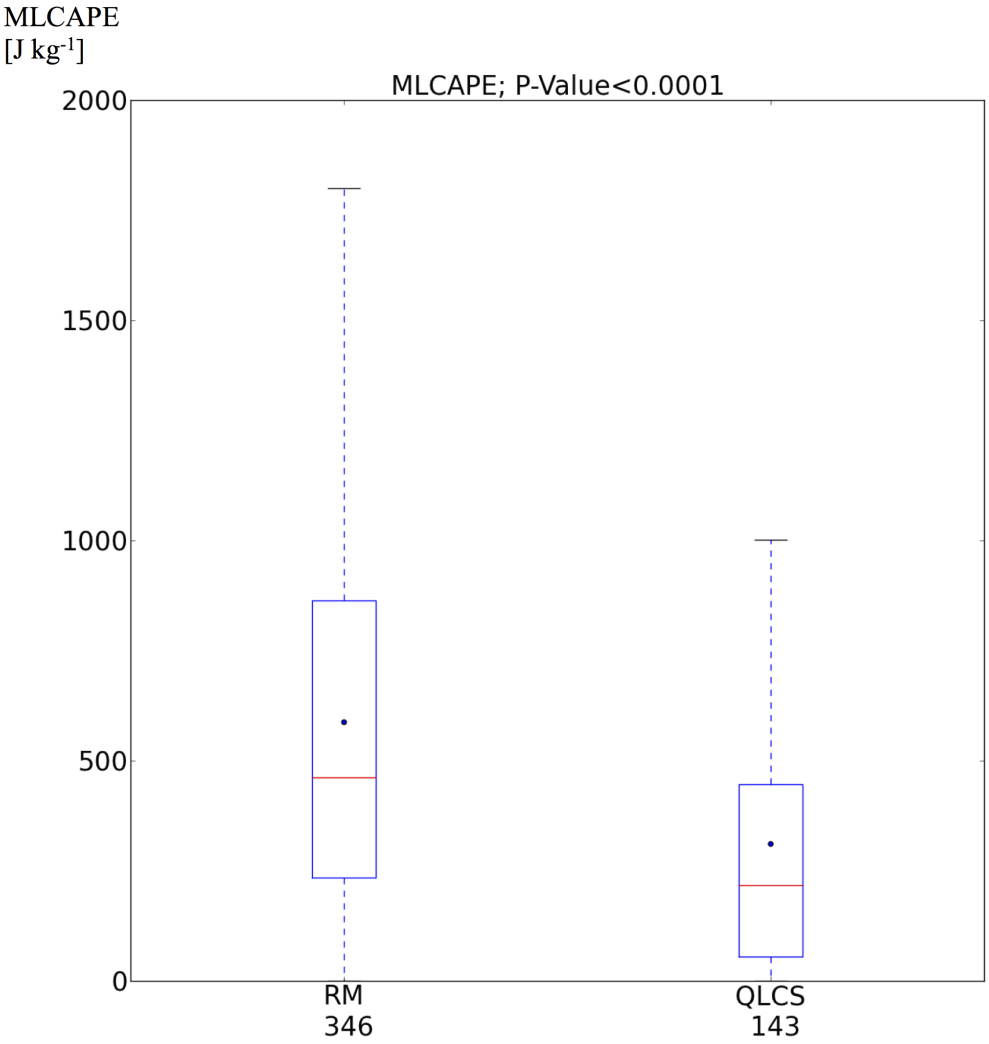

Figure 2.23: As in Fig. 2.22, except for MLCAPE.

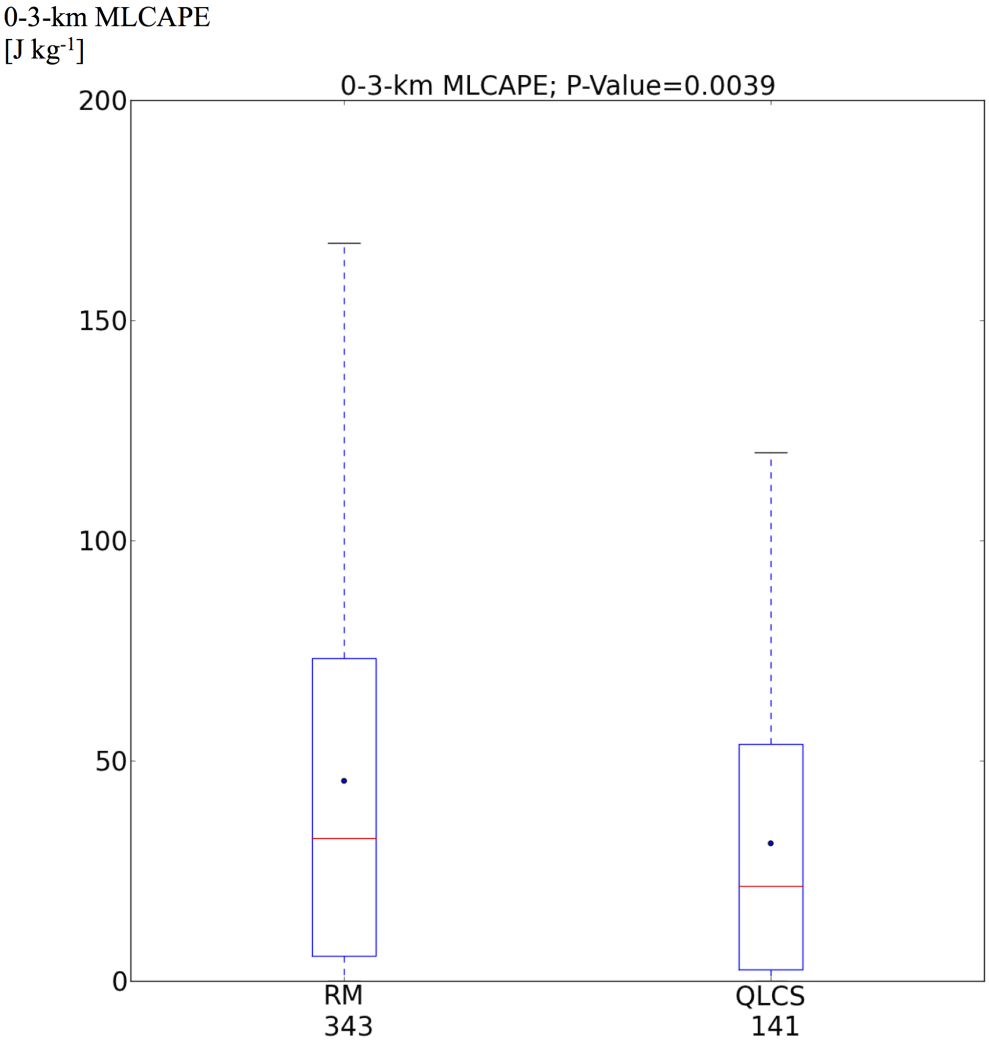

Figure 2.24: As in Fig. 2.22, except for 0-3-km MLCAPE.

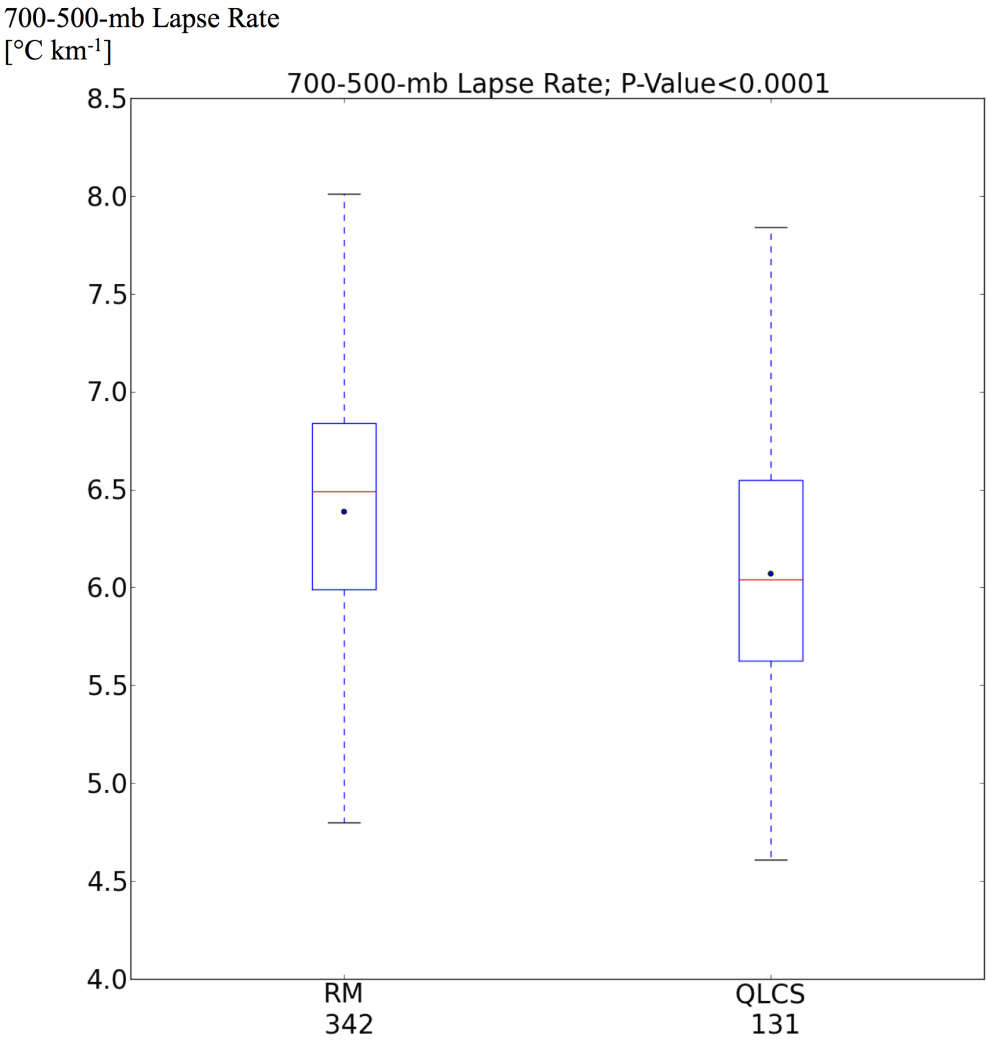

Figure 2.25: As in Fig. 2.22, except for 700-500-mb lapse rate.

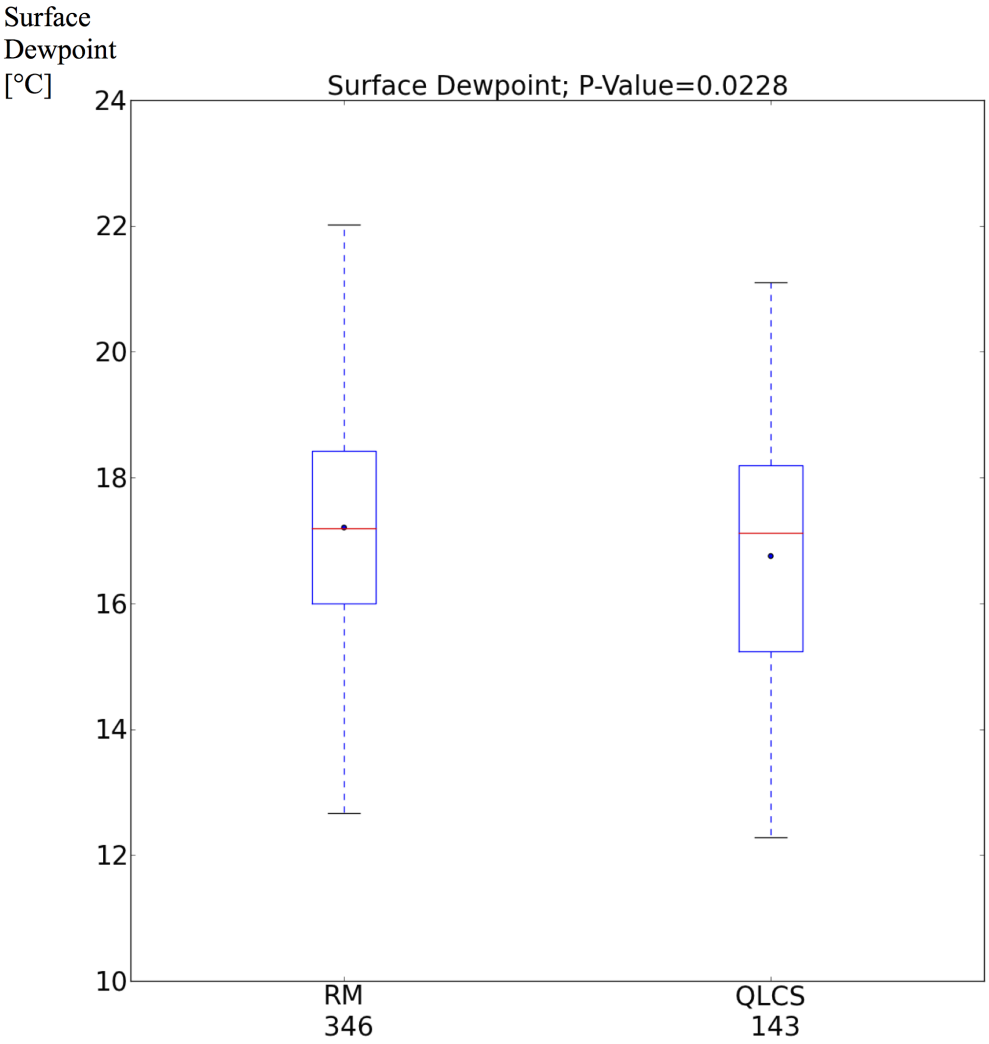

Figure 2.26: As in Fig. 2.22, except for surface dewpoint.

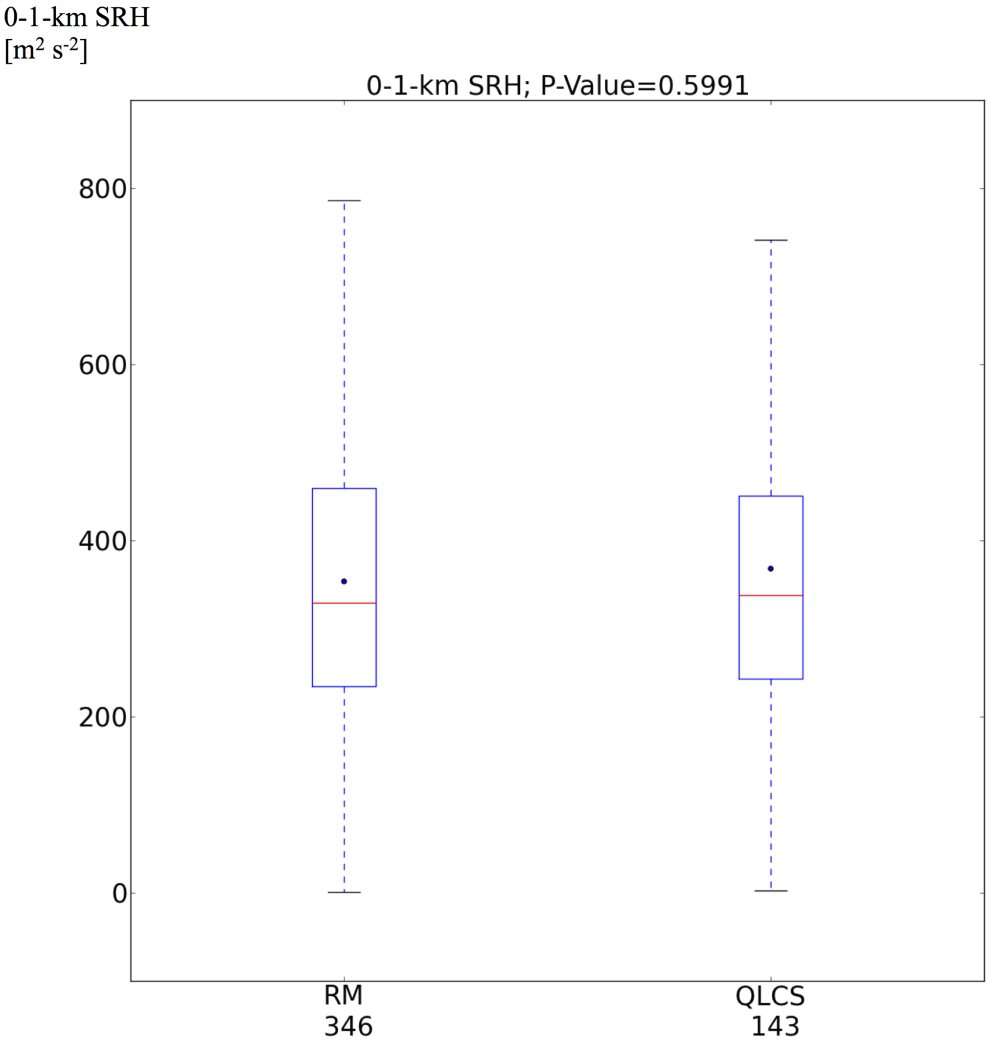

Figure 2.27: As in Fig. 2.22, except for 0-1-km SRH.

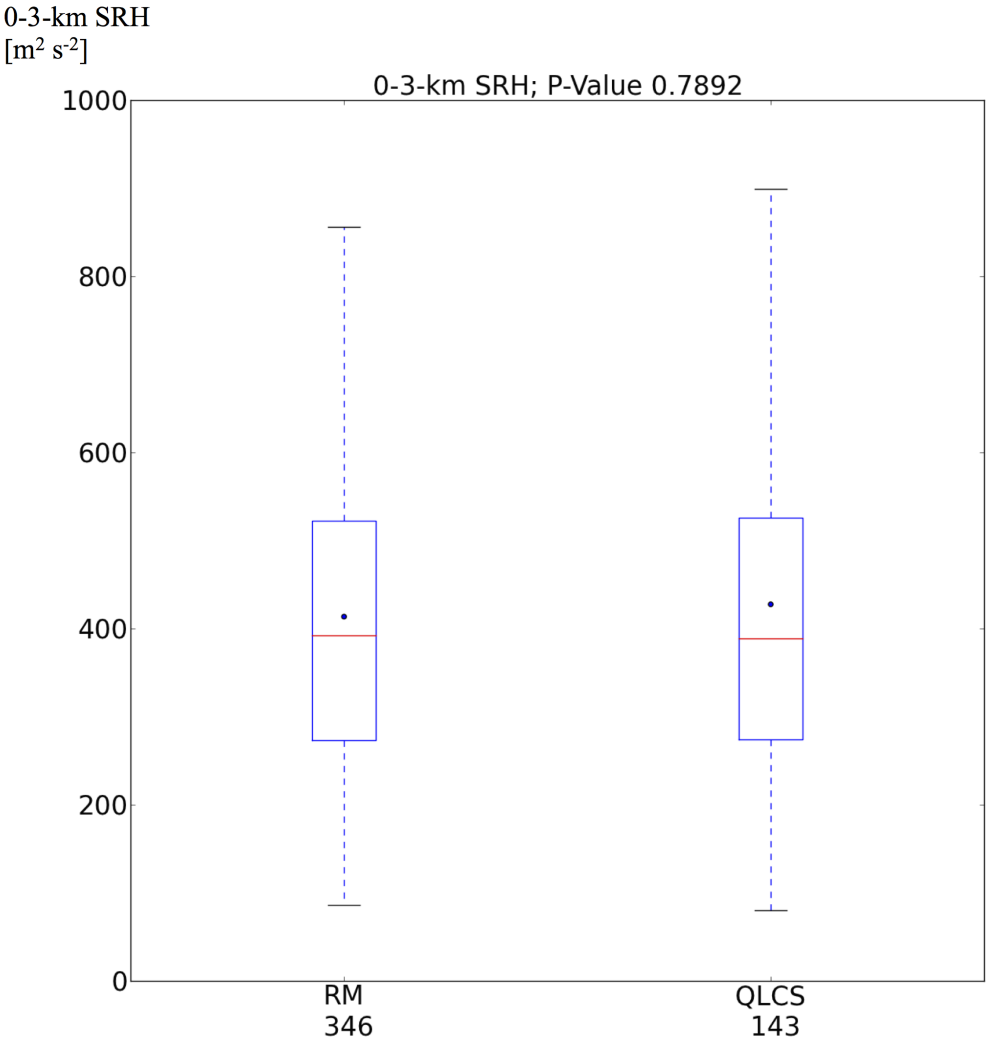

Figure 2.28: As in Fig. 2.22, except for 0-3-km SRH.

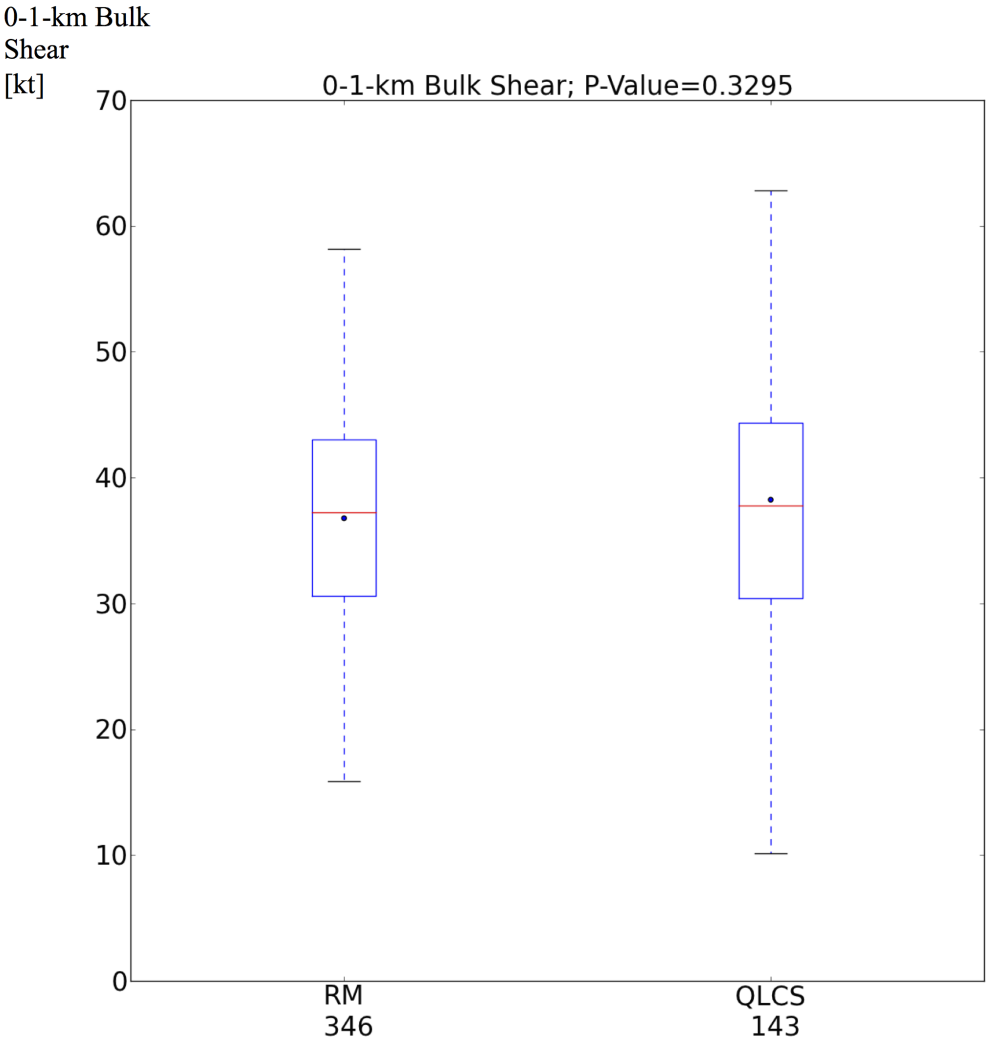

Figure 2.29: As in Fig. 2.22, except for 0-1-km bulk shear.

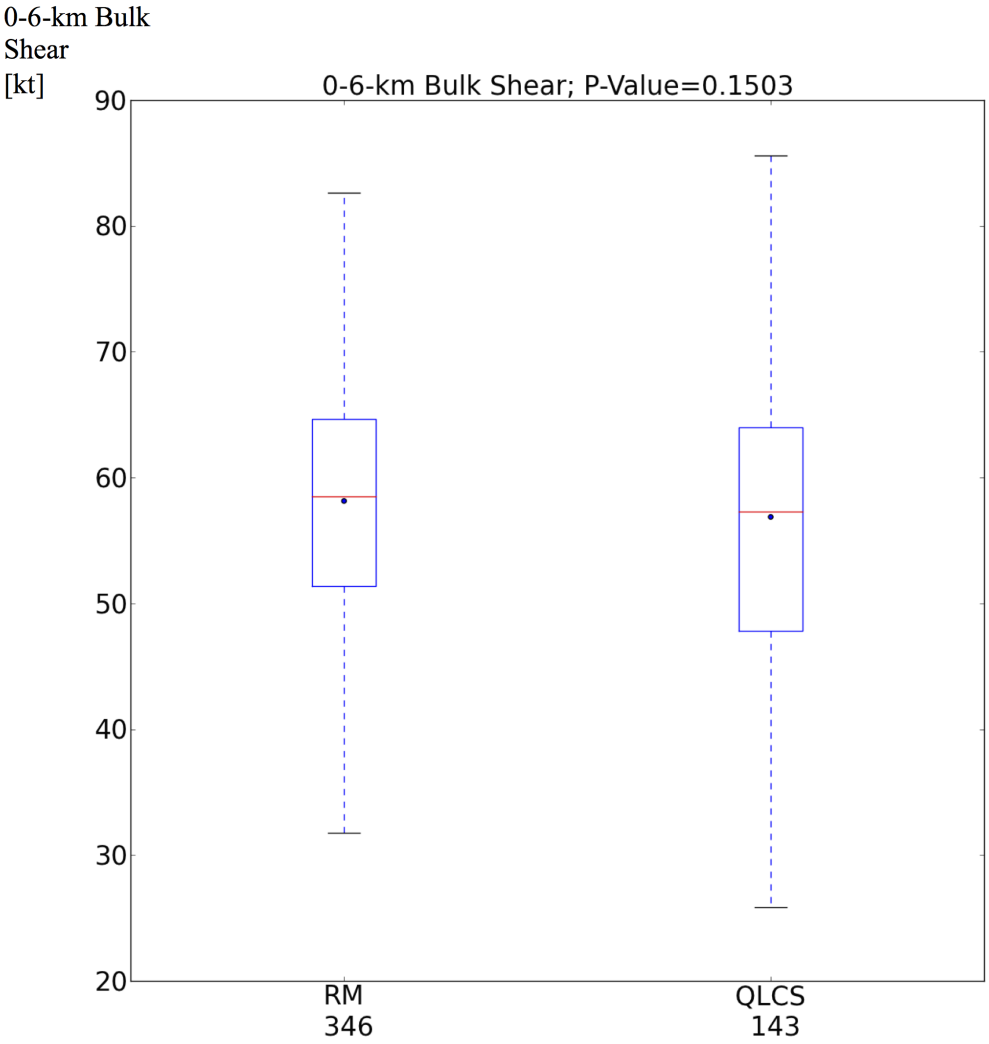

Figure 2.30: As in Fig. 2.22, except for 0-6-km bulk shear.

Table 2.2: P-values corresponding to the Kolmogorov-Smirnov statistical test of the difference in parameter values between the right-moving supercell and QLCS convective modes for the "SECOLD" regime.

Variable	*P-Value*
surface-based convective available potential energy	<0.0001
mixed-layer convective available potential energy	<0.0001
0-3-km mixed-layer convective available potential energy	0.0039
700-500-mb lapse rate	<0.0001
surface dewpoint temperature	0.0228
0-1-km storm-relative helicity	0.5991
0-3-km storm-relative helicity	0.7892
0-1-km bulk shear	0.3295
0-6-km bulk shear	0.1503

2.4 Daytime versus Nighttime Variability in the Southeast United States Cold Season Tornado Environment

Throughout this chapter, the distinguishable characteristics of kinematic and thermodynamic parameter magnitudes characterizing the "SECOLD" regime have been identified and tested. This chapter concludes with an investigation of the daytime versus nighttime variability of some of these parameters. The objective of this investigation is to determine if the behavior of the temporal variability of these parameters during "SECOLD" differs from other regimes.

Daytime versus nighttime variability of thermodynamic parameters such as SBCAPE (Fig. 2.31), MLCAPE (Fig. 2.32), and surface dewpoint (Fig. 2.33)

during warmer-season influenced regimes ("SEWARM", "NONSECOLD", and "WARMER") roughly resembles the variability expected with a more quiescently evolving PBL (e.g., Stull 1988; Stensrud 2007). Specifically, surface heating associated with insolation is associated with increases in SBCAPE (Fig. 2.31) and MLCAPE (Fig. 2.32), while stronger vertical mixing instigated by the surface heating and related deepening of the PBL during the day are associated with daytime decreases in surface dewpoints (Fig. 2.33) as drier air aloft is mixed to the surface. Alternatively, for the "SECOLD" regime, these fluctuations are dampened, during a time when large-scale moisture transport, cloud coverage, vertical-shear-enhanced turbulence, and precipitation processes associated with large-scale weather systems can all negate the more quiescent evolution of the PBL. This is manifested in the distinguishable behavior of these thermodynamic parameters in the "SECOLD" regime compared to the other regimes.

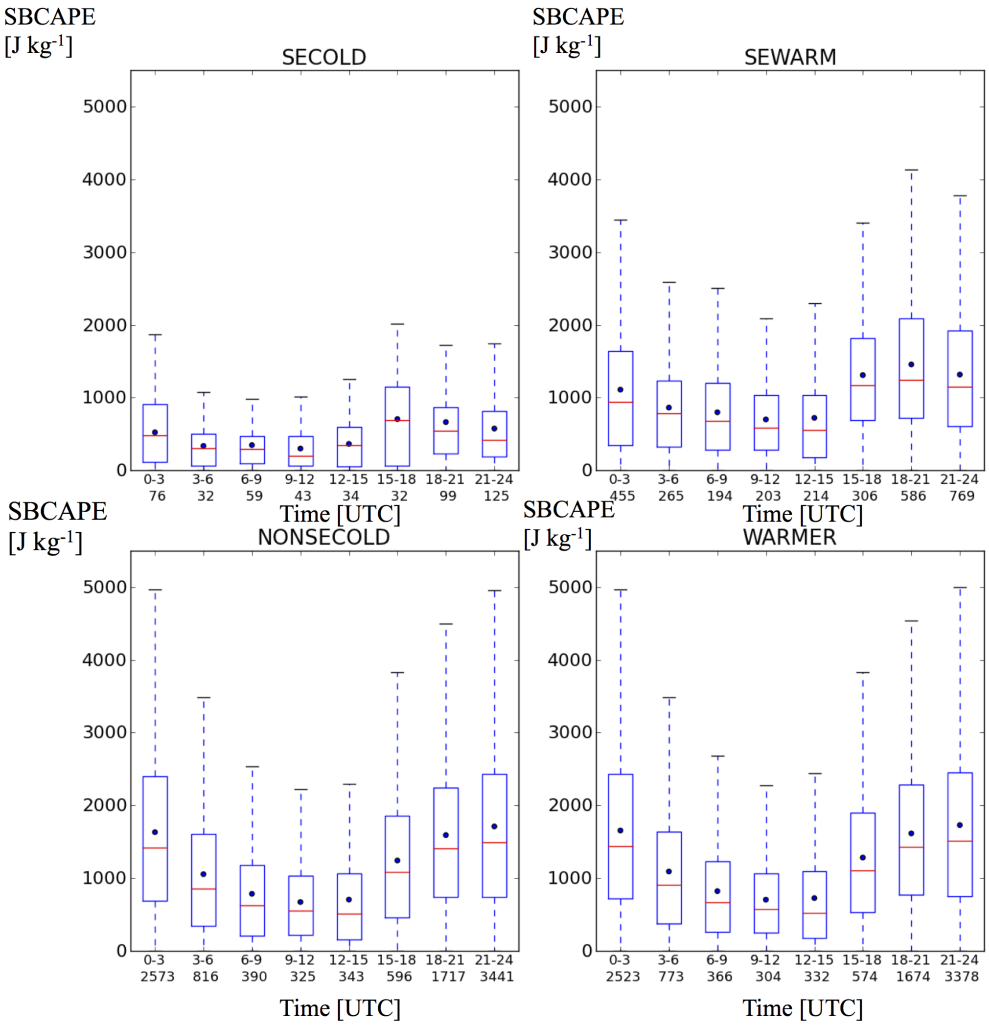

Figure 2.31: Time series of box-and-whiskers plots corresponding to the distribution of SBCAPE for tornadoes occurring in the "SECOLD" (top left), "NONSECOLD" (bottom left), "SEWARM" (top right), and "WARMER" (bottom right) regimes grouped within time periods identified along the x-axis. Time periods are listed from start time to end time in UTC (e.g., "0-3" corresponds to the three-hour period beginning at 0000 UTC), with sample sizes listed below the labeled time periods. The blue-outline box corresponds to the interquartile range, the red horizontal line corresponds to the median value, the dot marker corresponds to the mean value, and whiskers extend up to 1.5 times the interquartile range beyond the first and third quartiles.

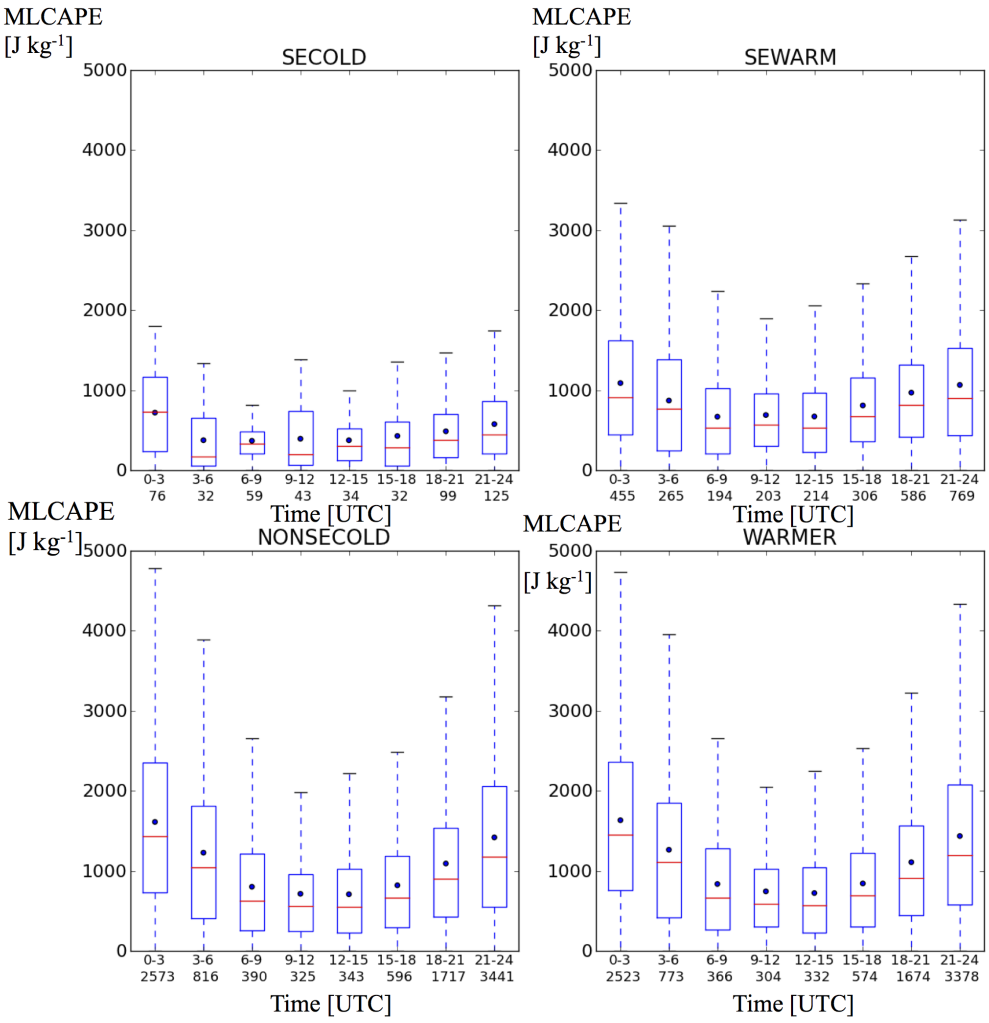

Figure 2.32: As in Fig. 2.31, except for MLCAPE.

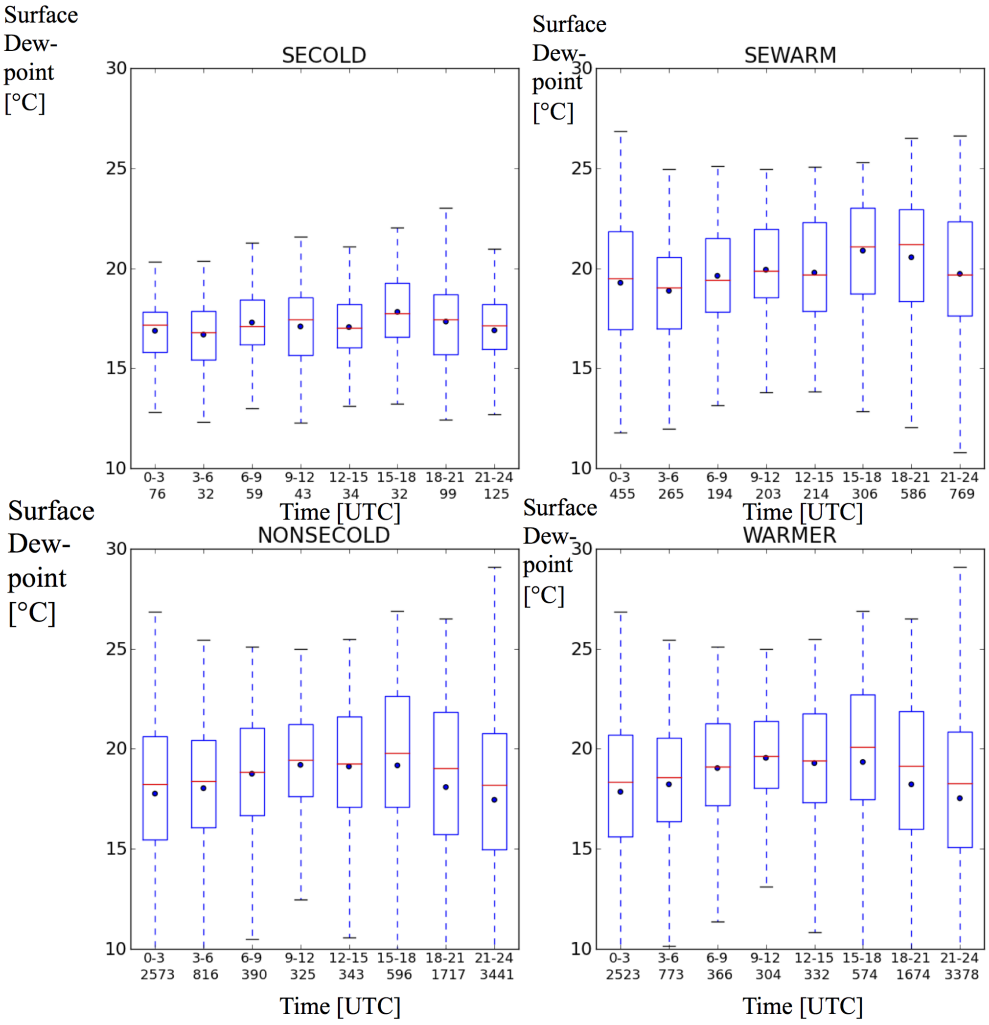

Figure 2.33: As in Fig. 2.31, except for surface dewpoint.

The behaviors of kinematic parameters representing the "SECOLD" regime that are influenced by lower-atmospheric mixing processes also exhibit differences compared to other regimes, based upon 0-1-km SRH (Fig. 2.34) and 0-1-km bulk shear (Fig. 2.35). The "SEWARM", "NONSECOLD", and "WARMER" regimes are associated with daytime losses in low-level SRH and vertical bulk shear followed by nighttime increases in the magnitudes of these parameters

(e.g., Stull 1988; Stensrud 2007). This is consistent with smoothing of the vertical wind profile in association with enhanced vertical mixing during the day followed by increases in vertical shear attendant to decoupling of the PBL at night. These processes and their reflection on 0-1-km SRH and bulk shear are more characteristic of a quiescently evolving PBL. On the other hand, and similar to thermodynamic parameters, the "SECOLD" regime is associated with a much dampened variability pattern associated with daytime heating and nighttime cooling cycles characteristic of the other regimes.

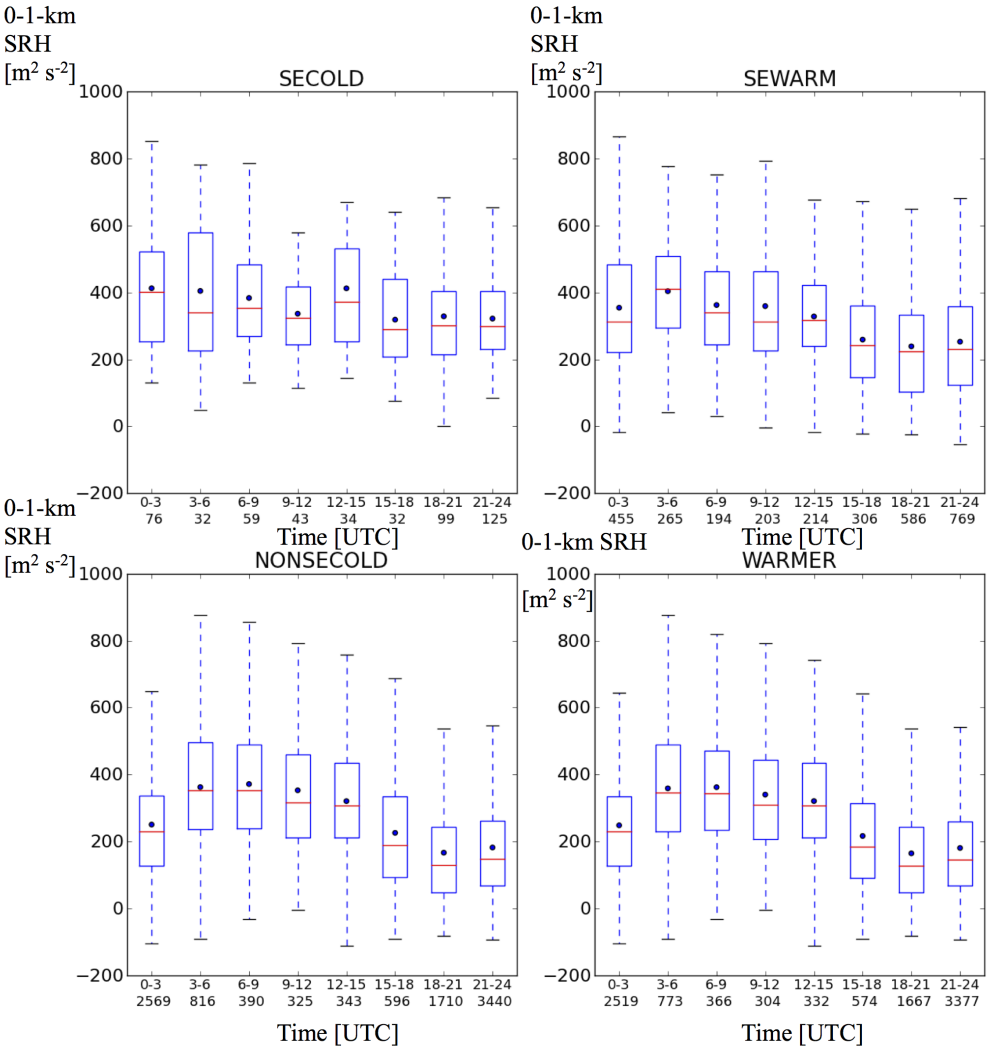

Figure 2.34: As in Fig. 2.31, except for 0-1-km SRH.

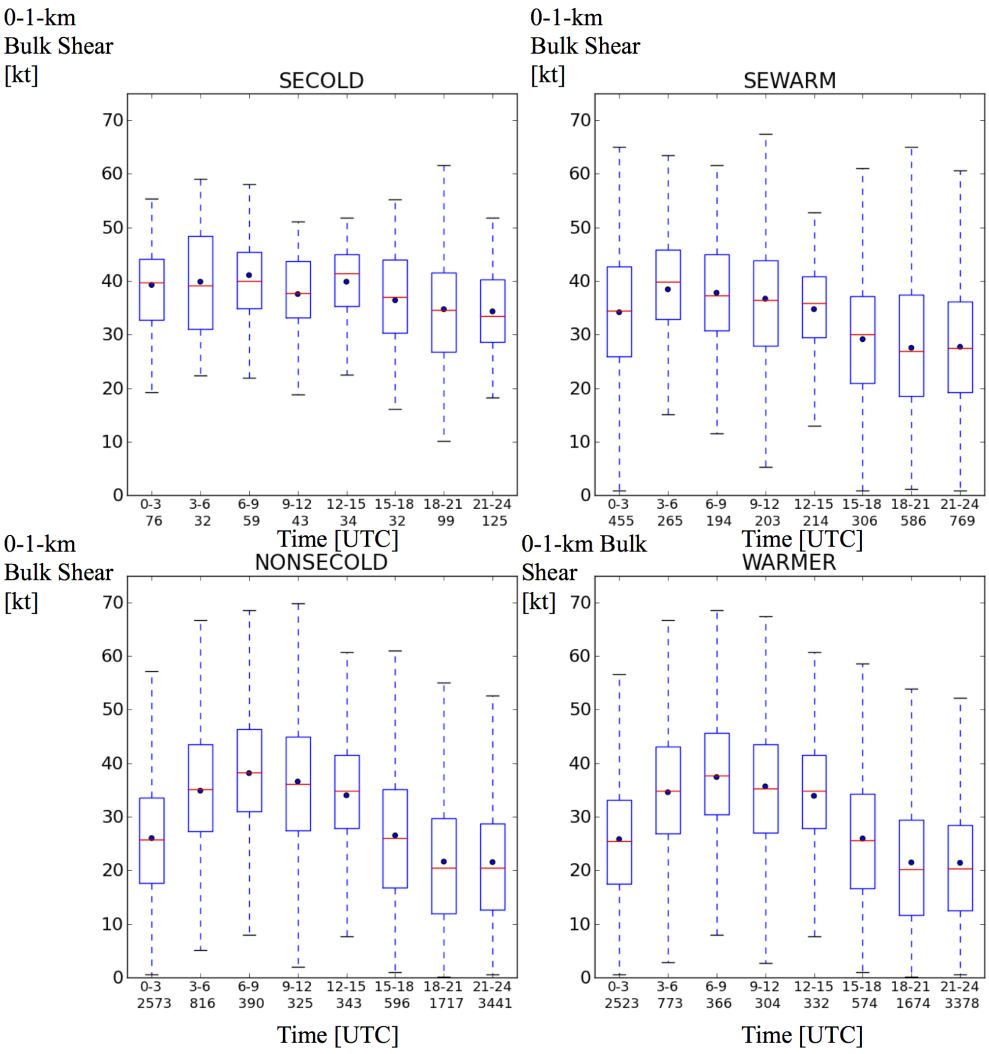

Figure 2.35: As in Fig. 2.31, except for 0-1-km bulk shear.

It has been shown that daytime versus nighttime variability of thermodynamic and kinematic parameters representing the "SECOLD" regime is suppressed compared to the other regimes that resemble more quiescent PBL evolution. This is consistent with parameters of the "SECOLD" regime being different than those of other regimes, specifically with the "SECOLD" regime being associated with a buoyancy distribution that is compressed while confined to more

marginal values and with stronger vertical shear compared to other regimes. Because many of these parameters are strongly influenced by thermodynamic and kinematic properties of the lowest portion of the atmosphere, which are affected by turbulent processes occurring in the PBL, and because these parameters are shown to have distinguishable characteristics in the "SECOLD" regime, the PBL of the "SECOLD" regime is the focus of subsequent discussion. C15 provide initial attempts to better understand PBL-influenced meteorological parameters in the "SECOLD" regime for numerical simulations, and subsequent work builds upon C15. Ultimately, more accurate representations of the PBL in this regime could support improved forecasts of parameters used for forecasting tornadoes.

Chapter 3

Planetary Boundary Layer Parameterization Schemes

3.1 Purpose of Planetary Boundary Layer Parameterization Schemes

The importance of accurately representing processes occurring within the PBL has been inferred, as they directly influence the accuracy of numerical simulations of high-impact weather phenomena. This is of particular importance for severe-weather patterns where one or more of the necessary conditions for severe storms is marginal and the assessment of the hazardous-weather threat is sensitive to small fluctuations of the marginal quantities favoring severe thunderstorms. Small forecast inaccuracies in such scenarios may be of particular importance, and a source of these inaccuracies comes from a model's representation of the low-level wind profile and the low-level thermodynamic profile (e.g., Jankov et al. 2005; Stensrud 2007; Hacker 2010; Hu et al. 2010; Nielsen-Gammon et al. 2010). Ultimately, this motivates the need to minimize errors in forecast vertical profiles to better depict characteristics of the convective environment, which plays a major role in more accurately assessing the severe-weather threat (e.g., Kain et al. 2003, 2005, 2013).

As was previously discussed, turbulent eddies facilitate the exchanges of momentum, heat, and moisture in the PBL within which properties of surface conditions are communicated on time scales under an hour (e.g., Stull 1988; Stensrud 2007). Because these eddies are not able to be explicitly resolved by mesoscale models, their effects are parameterized using PBL parameterization schemes. The theoretical development of these schemes is addressed by multiple sources (e.g., Stull 1988; Holton 2004; Stensrud 2007). The Advanced Research version of the Weather Research and Forecasting (WRF) Model (ARW; Skamarock et al. 2008) offers options for selecting from several different PBL parameterization schemes to be used in numerical simulations of weather events. However, some schemes are more appropriate to be used for certain atmospheric regimes than others (e.g., "SECOLD" versus other regimes).

C15 provide a detailed summary of the various PBL schemes that the WRF offers for use by numerical modelers, as well as advantages and disadvantages to using each scheme. They also summarize basic foundational work in the development of PBL parameterization schemes by synthesizing explanations provided by Stensrud (2007) and Stull (1988). Some of the core details of this process described in greater detail by C15 are provided in the subsequent subsection, which is followed by a section focused on characteristics of the performance of these schemes.

3.2 Theoretical Underpinnings of Planetary Boundary Layer Parameterization Schemes

C15 describe the process by which variables within the equations of motion are partitioned into two components: time-averaged, mean components that represent the background state of the atmosphere and perturbation components that depict differences from the average state corresponding to turbulent eddies within the PBL. The equations containing perturbation quantities always carry fewer known terms than unknown terms. To effectively solve, or close, these equations requires the use of empirical relationships linking unknown terms of moment $n + 1$ with known terms of lower moment, where n is an integer. This is referenced as nth-order turbulence closure. An example of a first moment is the mean of a state variable such as zonal and meridional wind component and temperature, an example of a second moment is a covariance variable involving the mean of the products of two state-variable perturbations, while an example of a third moment is a triple-correlation term involving the mean of the products of three state-variable perturbations. C15 provide a detailed overview of the order of closure associated with the several PBL scheme options available in the WRF.

Aside from differences in the order of turbulence closure, PBL parameterization schemes differ from each other regarding the depth through which

known variables are permitted to affect a given model point, which is an important source of variability amongst PBL schemes that C15 address. Schemes can be classified as local or nonlocal. For local closure schemes, only vertical levels that are in immediate proximity to a given point within the model directly influence variables representing this point, whereas other vertical levels within the PBL can also influence variables for nonlocal closure schemes. Nonlocal closure schemes are able to represent the effects of deeper PBL circulations supporting countergradient fluxes within the lower atmosphere that oppose downward-directed heat fluxes associated with maxima in stability. As such, nonlocal schemes can improve model accuracy for regimes in which larger eddies exist in the lower atmosphere.

Stensrud (2007) highlights a major disadvantage of employing strictly local closure, which effectively reflects stunted deepening of the PBL in the presence of localized stable layers. In the real atmosphere, these stable layers may have minimal effect on vertical mixing within the PBL, which is facilitated by the largest eddies encouraging deeper mixing of mass, heat, and momentum. While nonlocal schemes are able to account for effects from these eddies, higher orders of closure used in local schemes have been found to offer some improvement in numerical simulations (e.g., Mellor and Yamada 1982; Nakanishi and Niino 2009; Coniglio et al. 2013). However, using such higher orders of turbulence closure comes at relatively greater computational expense. Some schemes have been developed that incorporate concepts of both local and nonlocal closure,

which will be the focus of later discussion, with a focus on the Asymmetric Convective Model (ACM) whose design is illustrated in Fig. 3.1 as originally presented by Pleim (2007a,b).

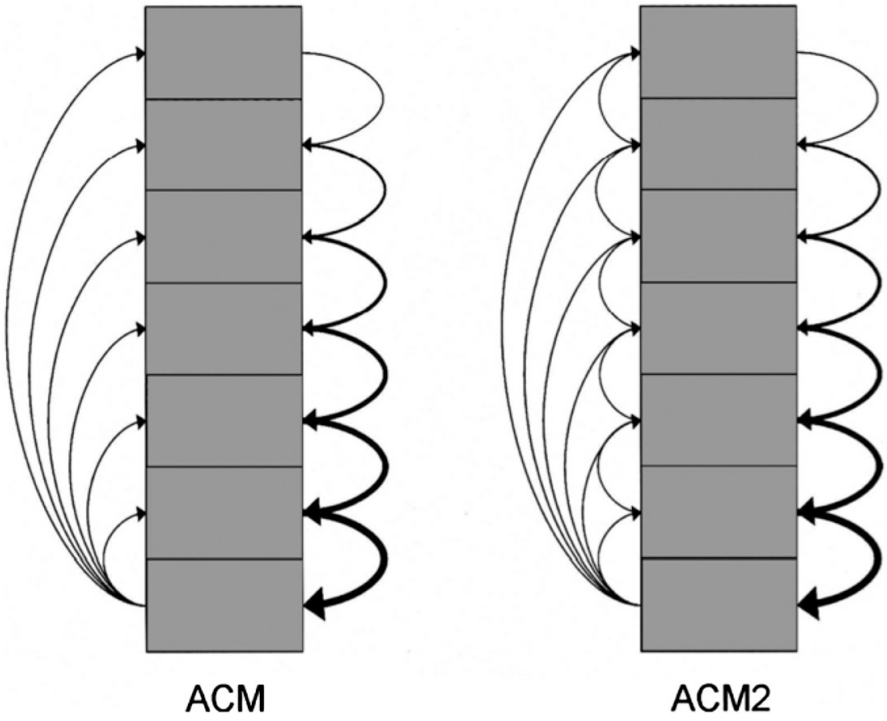

Figure 3.1: Reproduction of Fig. 1 of Pleim (2007a) that illustrates the structural development of the ACM, with arrows indicating which model layers are engaged in mixing processes within the simulation of the PBL.

3.3 Performance by Planetary Boundary Layer Parameterization Schemes

C15 provide an in-depth collection of typical biases associated with PBL schemes used in the WRF that have been explored throughout the broader literature. For example, across the south-central United States in the summer, tested schemes using a non-local component provide smallest errors in lower-atmospheric moisture and temperature profiles in association with daytime mixing, offering drier

and warmer PBLs. These findings are supported by Gibbs et al. (2011) in studying characteristics of the dry convective boundary layer. Nonlocal schemes are found to simulate deeper and more accurate PBLs in the Hong Kong area compared to those simulated by strictly local schemes (Xie et al. 2012). As another example of PBL scheme evaluation for specific regimes, more accurate PBL depictions are produced when both local and nonlocal processes are included in situations involving shallow cumulus and stratocumulus clouds (Huang et al. 2013).

Subsequent discussion and analysis focus on a sampling of five PBL schemes, specifically two local, two nonlocal, and one hybrid local-nonlocal and four variants of the hybrid. The two local schemes considered are the Mellor-Yamada-Janjić (MYJ; Janjić 1990, 1994) and quasi-normal scale elimination (QNSE; Sukoriansky et al. 2005) schemes, the two nonlocal schemes considered are the Medium-Range Forecast model (MRF; Hong and Pan 1996) and Yonsei University (YSU; Hong et al. 2006) schemes, and the hybrid local-nonlocal scheme for which variants are created herein is the version 2 of the Asymmetric Convective Model (ACM2; Pleim 2007a). This set of five PBL schemes and variants is intended to reflect the physical dispersiveness of model simulations arising from the two principally different techniques of representing vertical mixing using PBL parameterization schemes: local versus nonlocal mixing.

A tabular summary of these PBL schemes and others, along with associated advantages and disadvantages based on a variety of sources, is provided by C15.

Combining these results, C15 and references therein suggest deeper and more accurate mixing associated with convective PBLs for the nonlocal schemes, with overly deep PBLs found in some circumstances. The local schemes are characterized by more shallow mixing and are more appropriately used for stable thermodynamic profiles. However, their tendency is for insufficiently deep vertical mixing with respect to convectively enhanced boundary layers. On the other hand, the ACM2 scheme represents both nonlocal and local processes via upward mixing and local mixing for downward-directed fluxes, offering greater accuracy of PBL heights (Pleim 2007b). However, similar to some of the nonlocal schemes, the ACM2 (nonlocal/local) scheme exaggerates the depth of vertical mixing for simulations of spring, convective environments (Coniglio et al. 2013).

Meteorological regimes for which previous studies have addressed evaluation of PBL schemes have not included a sole focus on the southeast United States cold season severe weather patterns. Vertical motion at larger spatial scales, shear-driven eddies, as well as daytime surface heating all influence thermodynamic and kinematic structures in the low levels of the atmosphere, which are found to be associated with distinguishable characteristics of parameters in the "SECOLD" regime. C15 highlight examples of observed and model-forecast soundings that do not display attributes of well or poorly mixed PBLs, yet such PBLs need to be accurately portrayed by model simulations using PBL parameterization schemes to resolve the highly sensitive instability parameter space

characteristic of this regime. While they begin to address this problem through an analysis of two southeast U.S. cold season severe weather events, much additional work is needed to better refine our understanding of PBL parameterization schemes in this regime. However, they do reiterate similarities between the southeast U.S. cold season severe weather regime and European severe storm environments studied by Brooks (2009) that assist in contextualization of the formerly mentioned environments.

Specifically, C15 partly base investigation of PBL schemes in the United States cold season severe weather regime from analysis of PBL schemes in the European warm season following work from Haylock et al. (2008) and García-Díez et al. (2013). It is found that the MYJ (local) scheme yields more substantial daytime cold biases when compared to the YSU (nonlocal) and ACM2 (nonlocal/local) schemes, with the YSU (nonlocal) depicting deeper PBLs during the day and with warm-season bias reduction in temperatures using the YSU (nonlocal) scheme (García-Díez et al. 2013). As such, C15 conclude that, based upon model evaluation in the European warm season, the nonlocal YSU (nonlocal) scheme could assist in more accurately simulating southeast United States cold season severe weather environments. In fact, García-Díez et al. (2013) suggest the importance of focusing on specific spatiotemporal regimes for the improvement of PBL schemes in certain environments, which further motivates this area of research in the following chapter.

Chapter 4

Application of Planetary Boundary Layer Parameterization Schemes to Southeast United States Cold Season Tornado Environments

4.1 Experiment Motivation

The performance of PBL schemes will highly influence the ability of a numerical model to accurately simulate the challenging southeast United States cold season severe weather environment (C15). C15 investigate two "SECOLD"-regime severe-weather events, which highlight differences in the thermodynamic and kinematic structures between this regime and those of a more quiescently evolving PBL. They illustrate the Southeast cold-season tornado environment using an observed sounding, to show its characteristic low static stability in the low levels with strong vertical wind shear. However, no portion of the observed sounding highlights well mixed layers characterized by uniform potential temperature and/or wind velocity.

Through an evaluation of the ACM2 (nonlocal/local), YSU (nonlocal), MRF (nonlocal), MYJ (local), and QNSE (local) PBL schemes for both events, they find that nonlocal mixing is necessary to properly simulate the relatively steeper

low-level lapse rates within the warm sectors of extratropical cyclones favoring the severe weather, as local schemes yield lapse rates that are too weak. This is consistent with simulated PBLs in the European warm season, where nonlocal schemes are more likely to include effects of entrainment within the PBL. However, C15 find nonlocal schemes to depict weaker SRH than local schemes in association with a somewhat smoother vertical wind profile, but still sufficiently strong to suggest that the deeper mixing inherent to the nonlocal schemes does not produce too smooth of a wind profile to preclude tornadoes. Overestimates of MLCAPE are common amongst all schemes, enhanced by nonlocal schemes. The conclusions of C15 provide motivation for the present study, in terms of extending the analysis to a more robust sample. As such, this work extends the investigation of PBL schemes in the "SECOLD" regime by incorporating many additional cases. This is for the purpose of better generalizing results and better substantiating an understanding of the tendencies of the PBL schemes through an investigation of multiple convective parameters. Ultimately, this will allow for an assessment of the performance of the PBL schemes, which can provide a basis for determining which schemes best depict the "SECOLD" regime and can also provide an opportunity to improve upon the parameterization schemes for this regime.

Furthermore, the notion that the "SECOLD" regime represents a more intermediate-mixing (neither highly statically stable nor statically unstable but

still yielding convective available potential energy) regime lends interest in investigating the performance of the ACM2 scheme that combines both nonlocal and local mixing processes. The nonlocal mixing component and related depictions of a deeper PBL may effectively represent the effects of vertical-shear-enhanced mixing in these environments, whereas the local mixing component may effectively represent the inherent higher-static-stability environment compared to one that is well mixed. The combination of these components and related offsetting biases are hypothesized to improve performance of PBL parameterization schemes in the "SECOLD" regime.

4.2 Experiment Design

The overall simulation design and model-evaluation technique follow those presented by C15, with equivalent comparisons in the extension to a more robust sample for the present work. Model simulations are run using version 3.3.1 of the ARW (Skamarock et al. 2008), with a horizontal grid length of 4 km and 50 levels in the vertical. The domain covers the southeastern United States and vicinity including portions of the Gulf of Mexico, which is illustrated in Fig. 4.1.

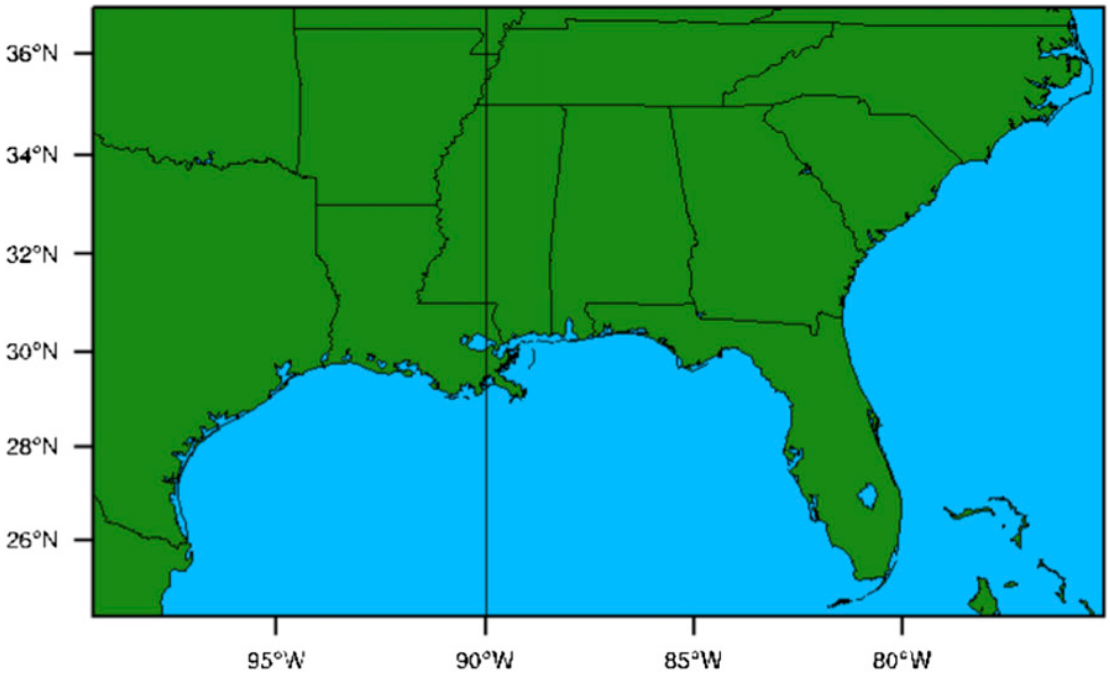

Figure 4.1: The domain used for WRF simulations. The horizontal grid length is 4 km for the simulations.

C15 specify other characteristics of these WRF simulations, including consistent pairing of the PBL schemes to land surface schemes, initial and boundary conditions using the National Centers for Environmental Prediction Final (FNL) Operational Global Analysis (NCAR 2015), single-moment 6-class microphysics scheme (Hong and Lim 2006), the Rapid Radiative Transfer Model relevant for general circulation models (RRTMG; Iacono et al. 2008) long- and shortwave radiation schemes, the Noah land surface model (Ek et al. 2003), a model time step of 12 s, and a radiation time step of 30 min. The RRTMG scheme for longwave radiation includes a procedure for dampening cold biases previously noted in the upper levels of WRF simulations (Cavallo et al. 2011).

Nineteen events are simulated, each involving separate 24-hour periods from 1200 UTC on one day to 1200 UTC on the next day during which severe weather, including tornadoes, occurred over the Southeast. In addition to the two cases from C15, this results in a total of twenty-one separate severe-weather events, providing robust sample sizes in resulting model analyses and across many "SEC-OLD" regime episodes. These events were chosen based on a subjective assessment of their production of high-density severe weather reports requiring the issuance of watches and warnings from the National Weather Service. The storm reports from each of these events are illustrated in Figs. 4.2-4.22, along with the 4 locations considered for forecast sounding evaluation in each event. The decision to select 4 locations is somewhat arbitrary, but is intended to provide a sample of some spatial diversity of the environment for each event, and is consistent with the analysis procedure carried out by C15. The 4 particular locations are based on proximity to severe thunderstorm reports, particularly tornadoes.

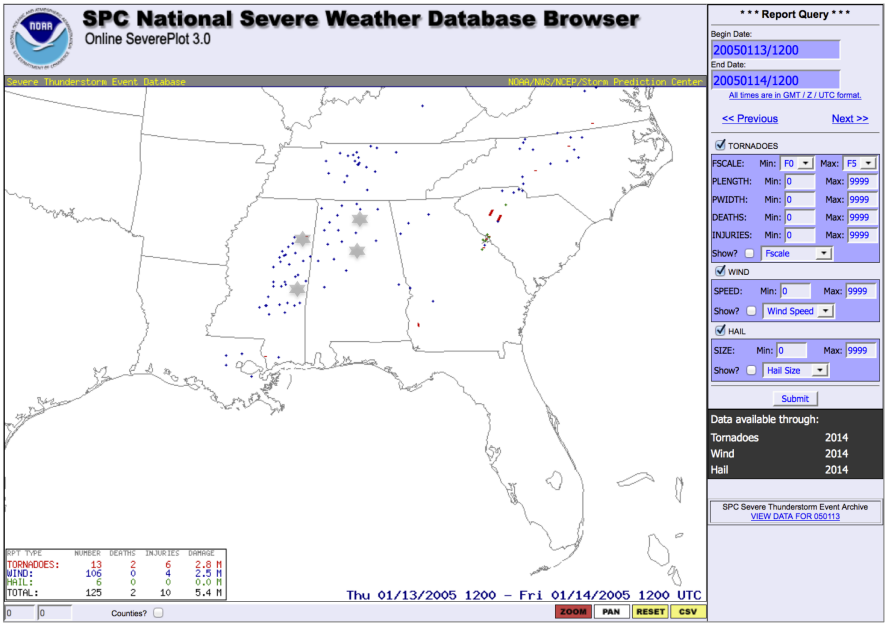

Figure 4.2: Severe thunderstorm reports (tornadoes in red, wind in blue, and hail in green) for 1200 UTC 13 Jan 2005 to 1200 UTC 14 Jan 2005 using Storm Prediction Center (2015b) overlaid with gray-shaded-star markers denoting the four locations used for forecast sounding evaluation for this event.

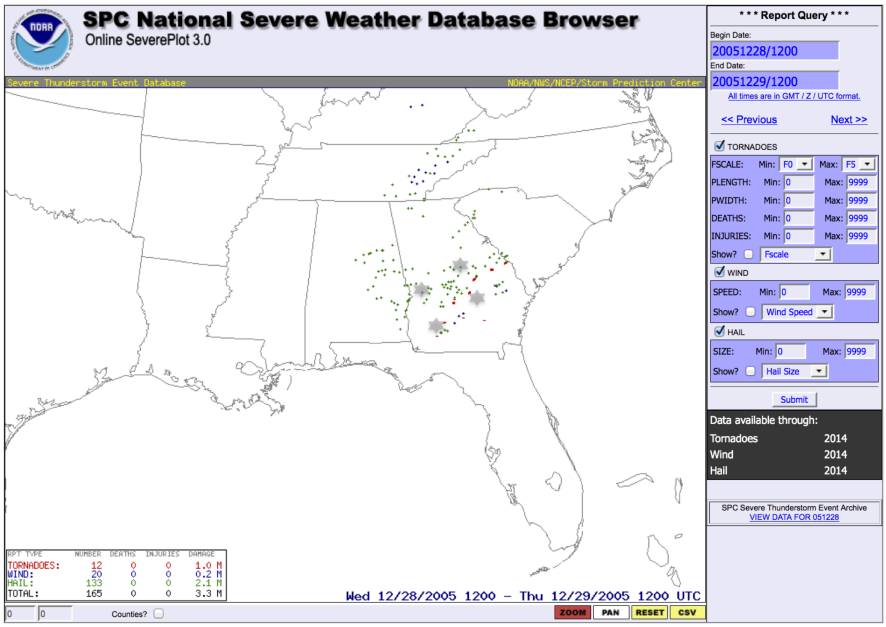

Figure 4.3: As in Fig. 4.2, except for 1200 UTC 28 Dec 2005 to 1200 UTC 29 Dec 2005.

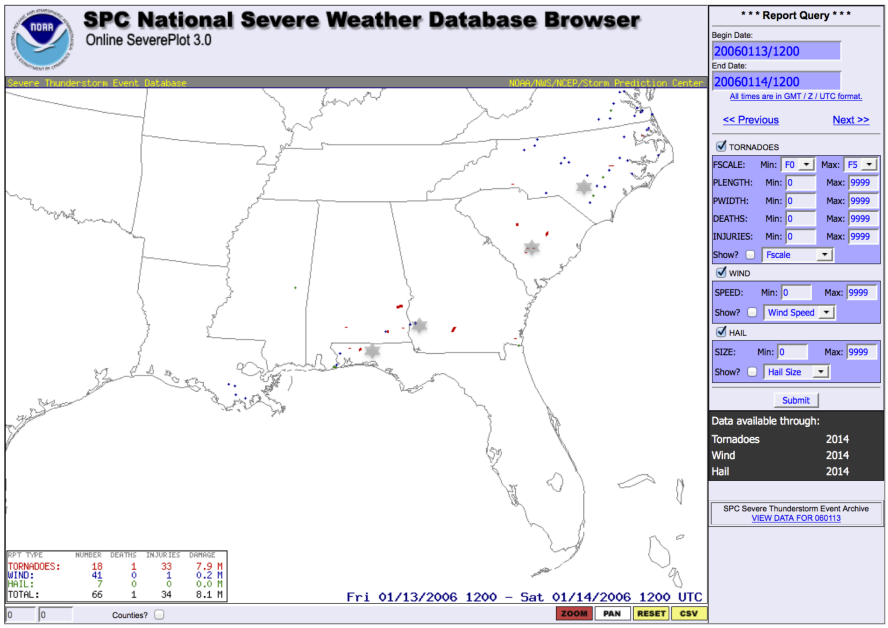

Figure 4.4: As in Fig. 4.2, except for 1200 UTC 13 Jan 2006 to 1200 UTC 14 Jan 2006.

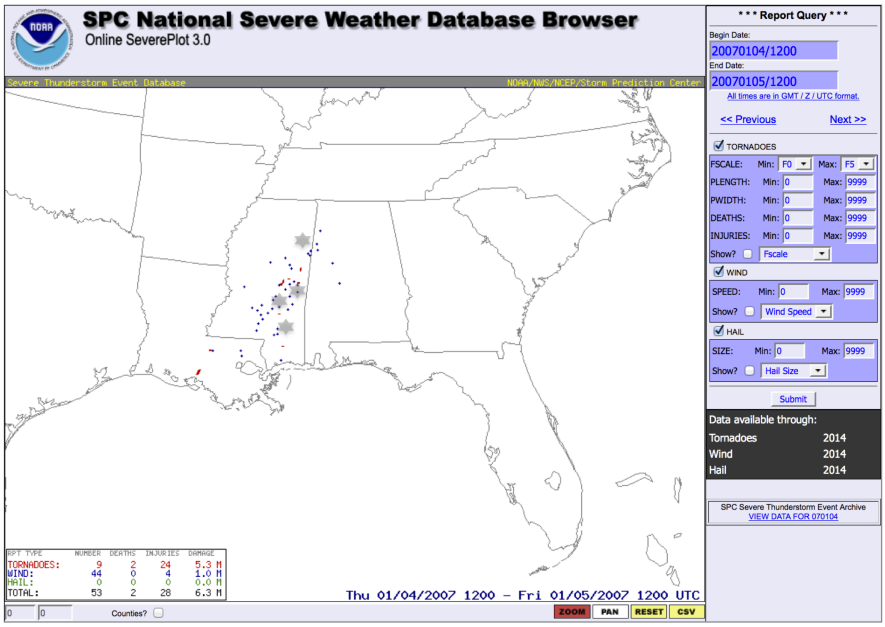

Figure 4.5: As in Fig. 4.2, except for 1200 UTC 4 Jan 2007 to 1200 UTC 5 Jan 2007.

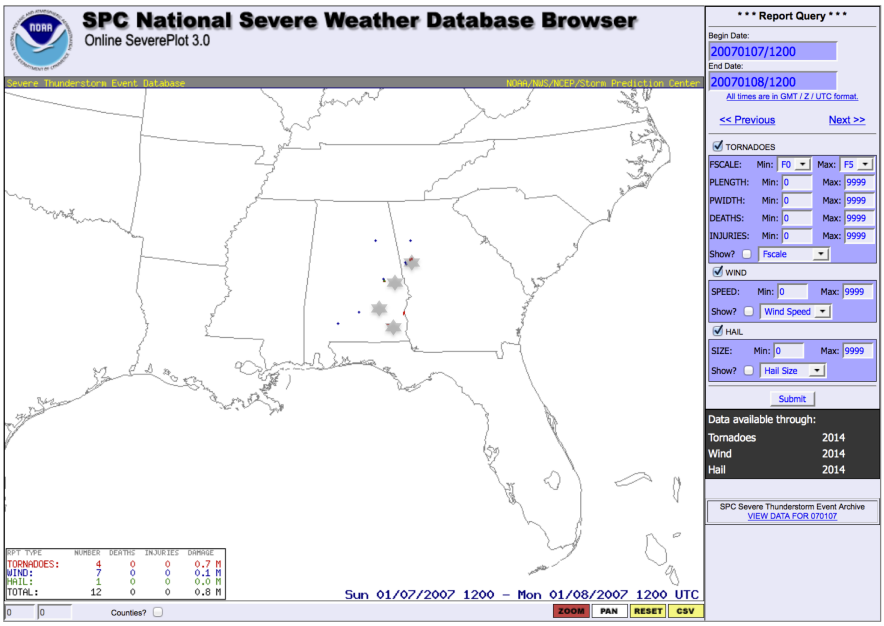

Figure 4.6: As in Fig. 4.2, except for 1200 UTC 7 Jan 2007 to 1200 UTC 8 Jan 2007.

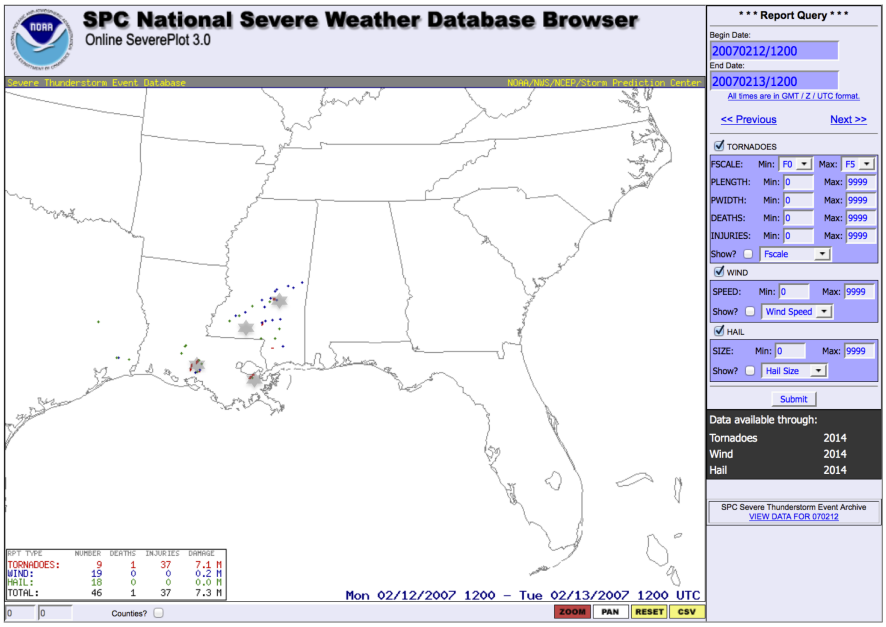

Figure 4.7: As in Fig. 4.2, except for 1200 UTC 12 Feb 2007 to 1200 UTC 13 Feb 2007.

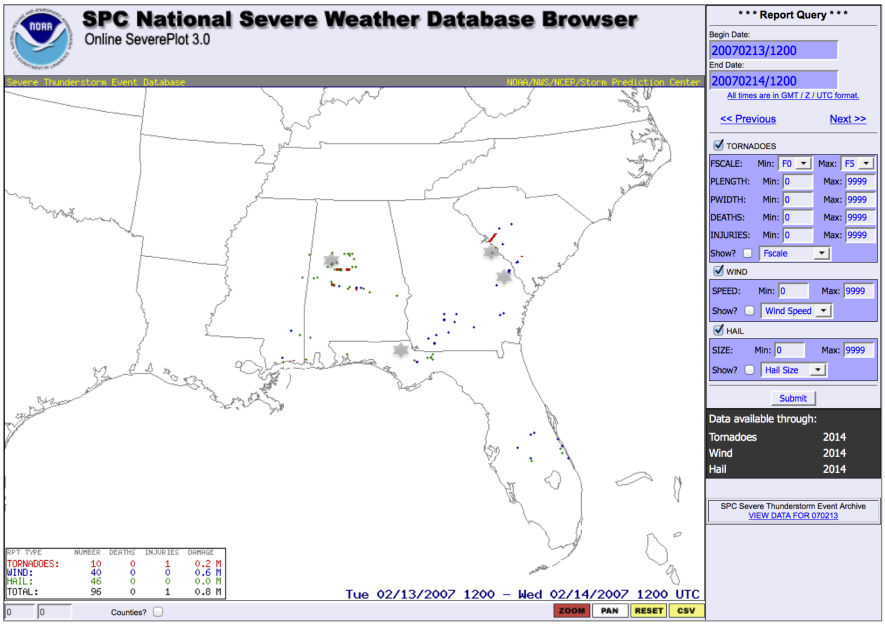

Figure 4.8: As in Fig. 4.2, except for 1200 UTC 13 Feb 2007 to 1200 UTC 14 Feb 2007.

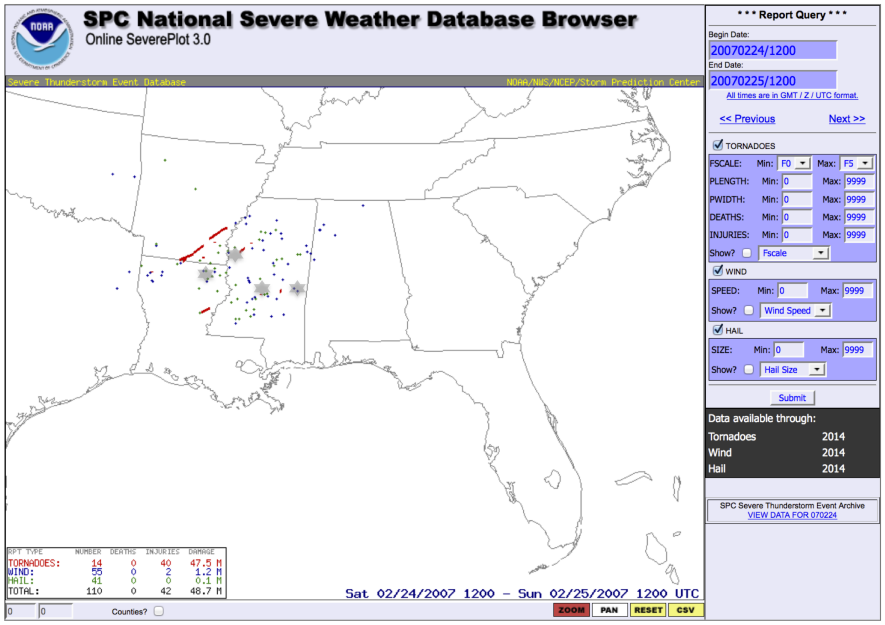

Figure 4.9: As in Fig. 4.2, except for 1200 UTC 24 Feb 2007 to 1200 UTC 25 Feb 2007.

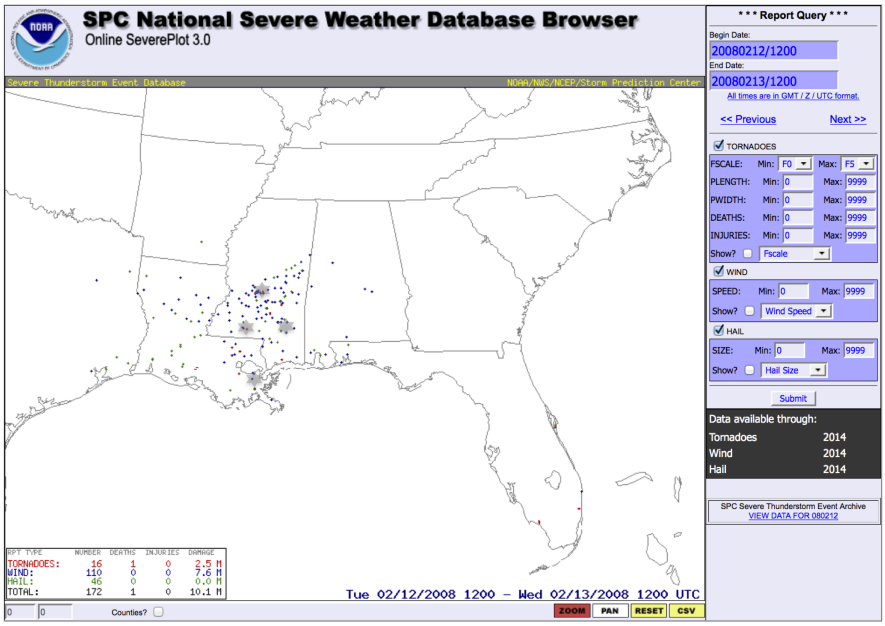

Figure 4.10: As in Fig. 4.2, except for 1200 UTC 12 Feb 2008 to 1200 UTC 13 Feb 2008.

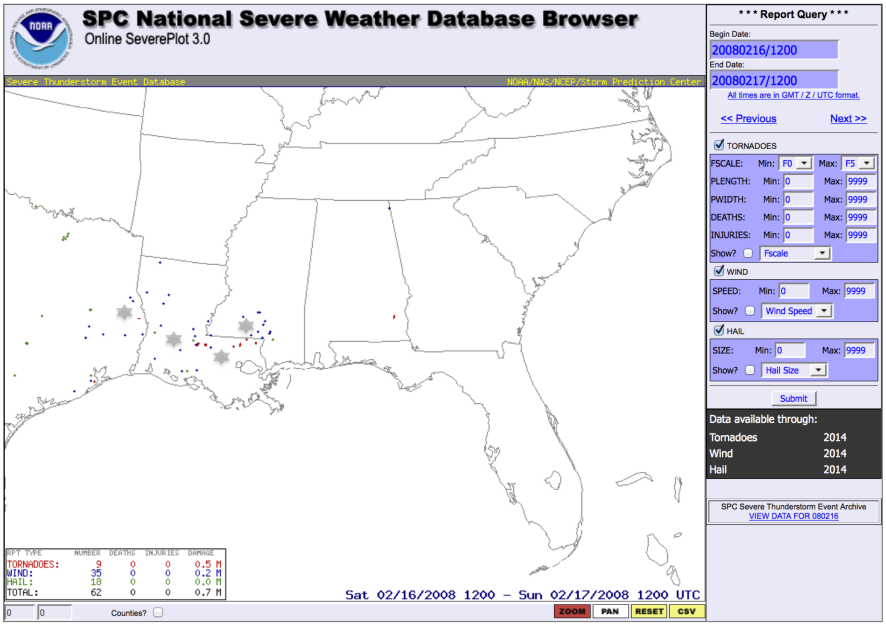

Figure 4.11: As in Fig. 4.2, except for 1200 UTC 16 Feb 2008 to 1200 UTC 17 Feb 2008.

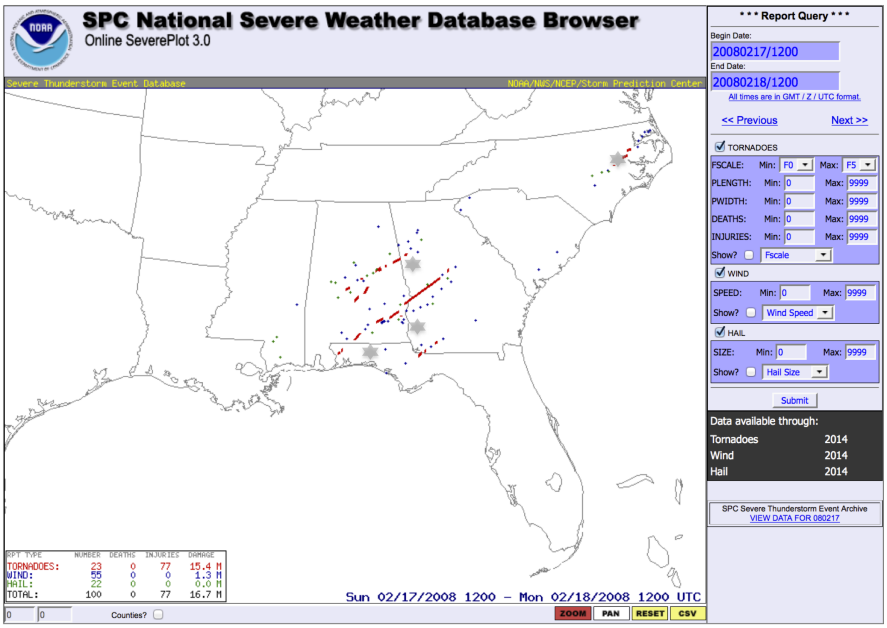

Figure 4.12: As in Fig. 4.2, except for 1200 UTC 17 Feb 2008 to 1200 UTC 18 Feb 2008.

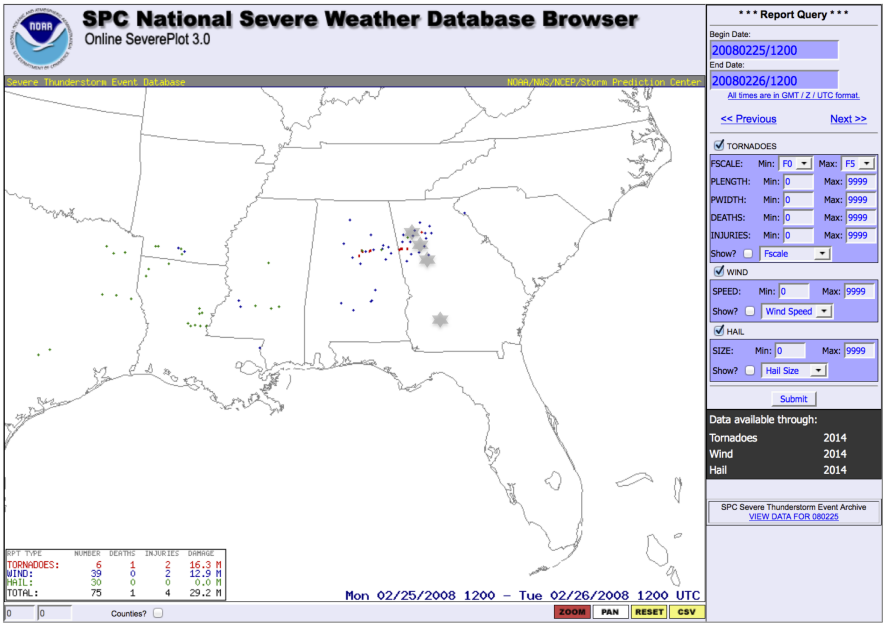

Figure 4.13: As in Fig. 4.2, except for 1200 UTC 25 Feb 2008 to 1200 UTC 26 Feb 2008.

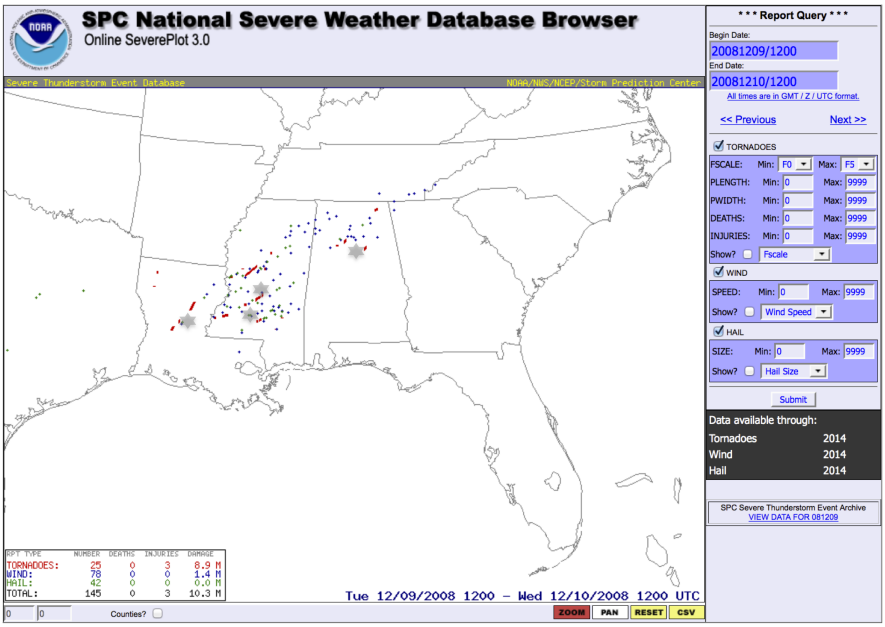

Figure 4.14: As in Fig. 4.2, except for 1200 UTC 9 Dec 2008 to 1200 UTC 10 Dec 2008.

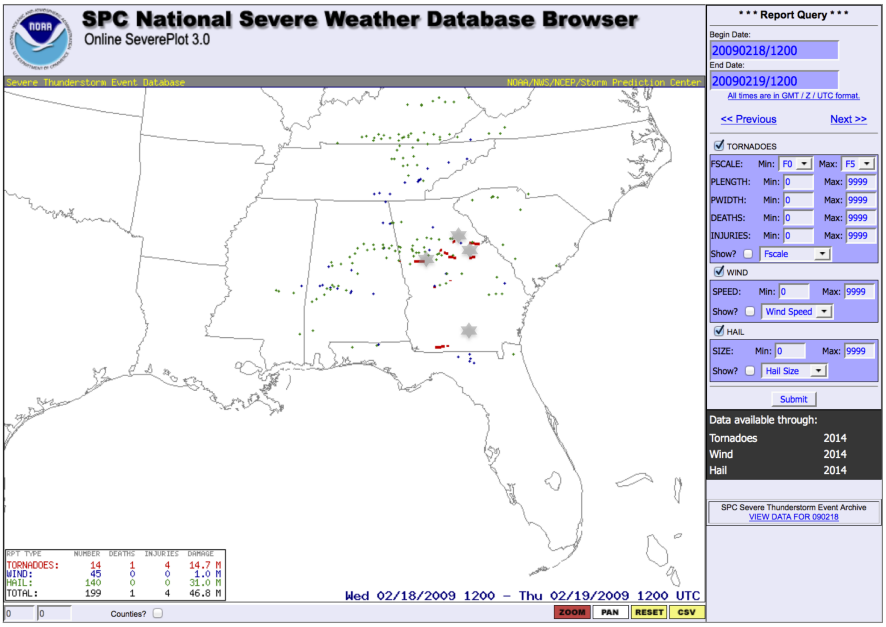

Figure 4.15: As in Fig. 4.2, except for 1200 UTC 18 Feb 2009 to 1200 UTC 19 Feb 2009.

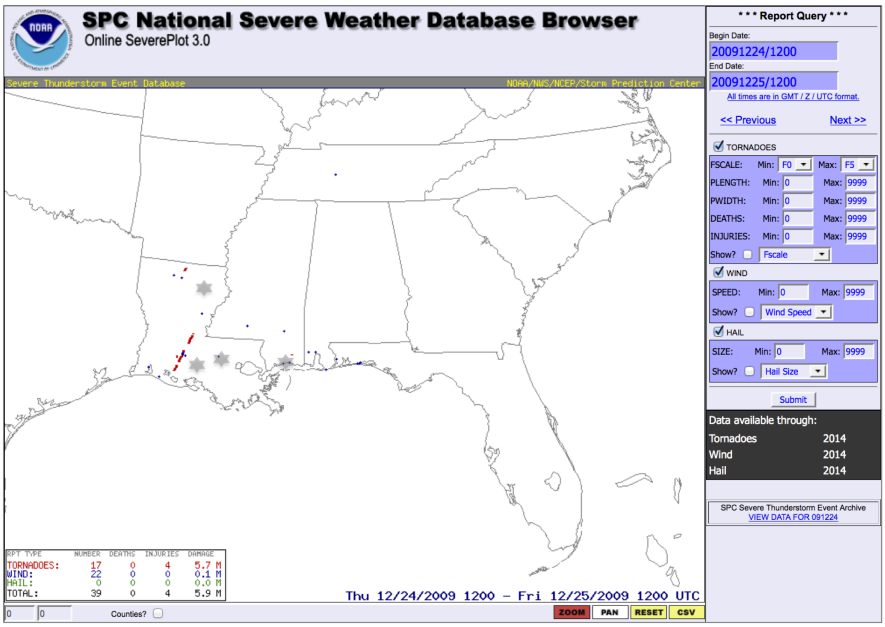

Figure 4.16: As in Fig. 4.2, except for 1200 UTC 24 Dec 2009 to 1200 UTC 25 Dec 2009.

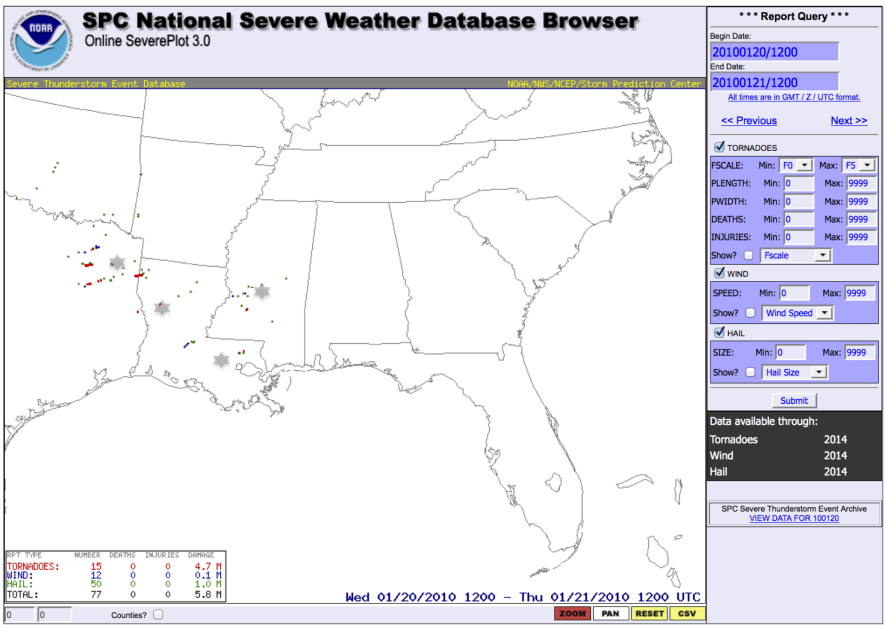

Figure 4.17: As in Fig. 4.2, except for 1200 UTC 20 Jan 2010 to 1200 UTC 21 Jan 2010.

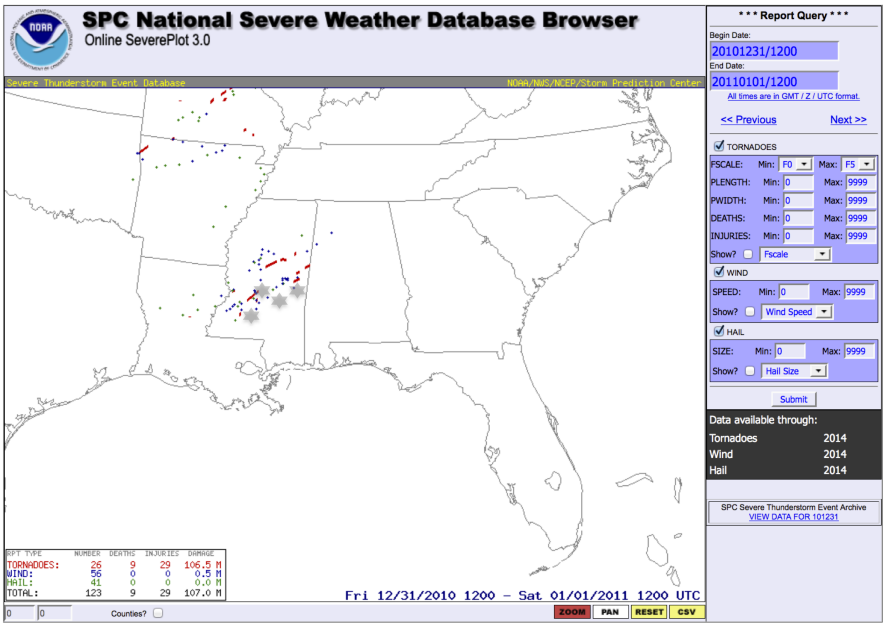

Figure 4.18: As in Fig. 4.2, except for 1200 UTC 31 Dec 2010 to 1200 UTC 1 Jan 2011.

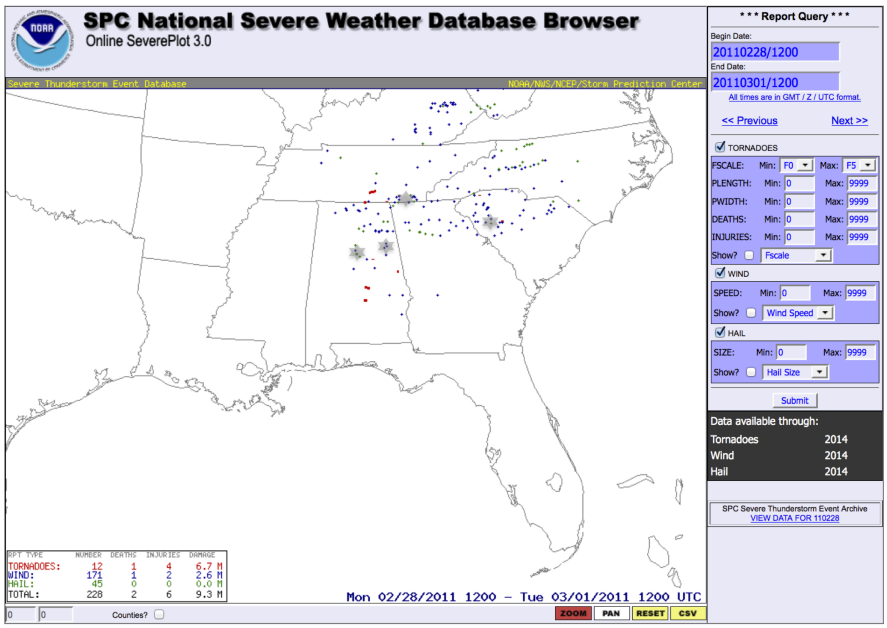

Figure 4.19: As in Fig. 4.2, except for 1200 UTC 28 Feb 2011 to 1200 UTC 1 Mar 2011.

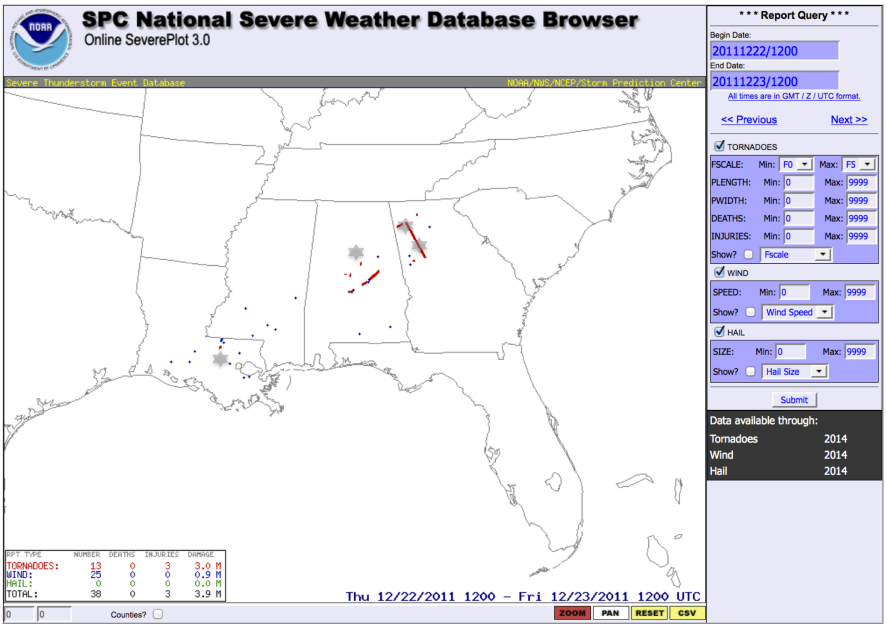

Figure 4.20: As in Fig. 4.2, except for 1200 UTC 22 Dec 2011 to 1200 UTC 23 Dec 2011.

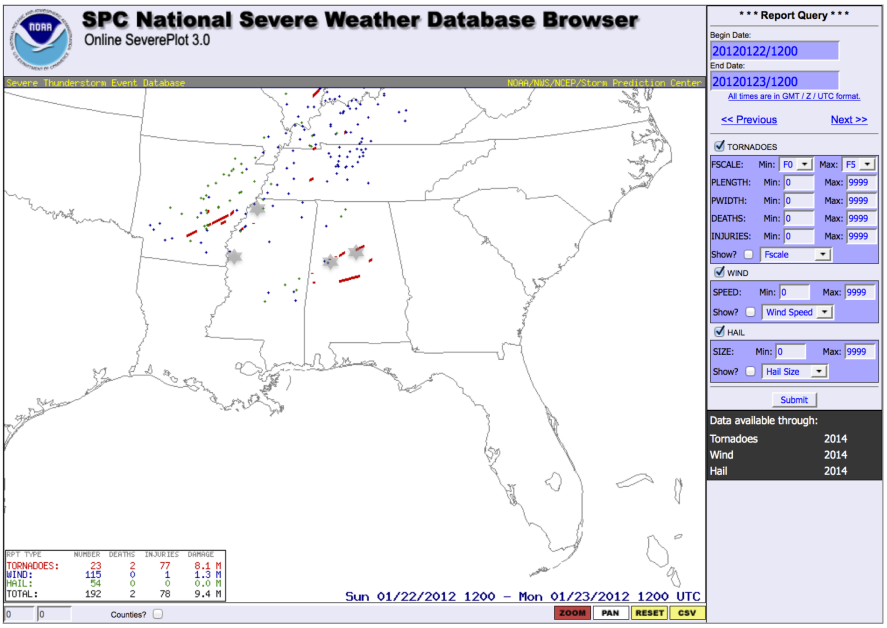

Figure 4.21: As in Fig. 4.2, except for 1200 UTC 22 Jan 2012 to 1200 UTC 23 Jan 2012.

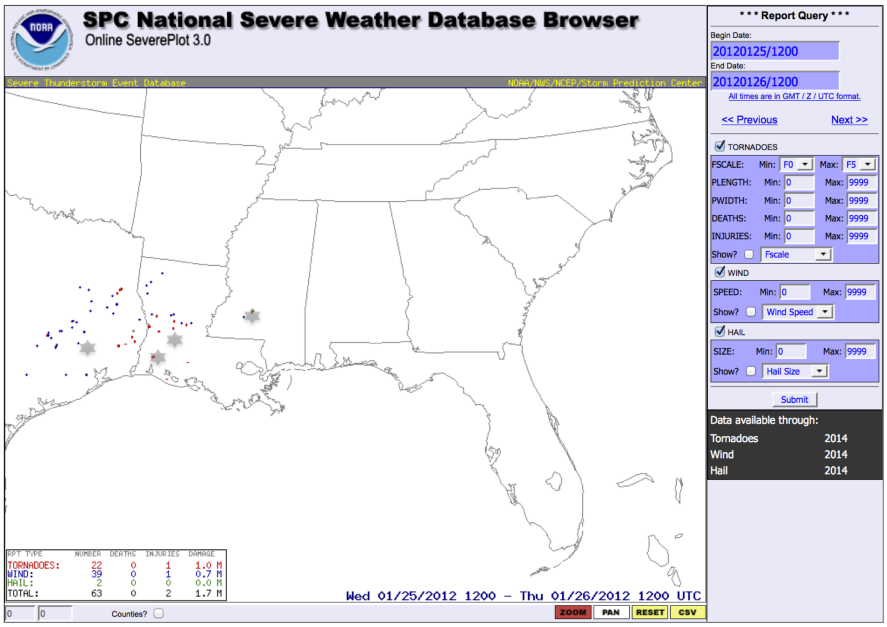

Figure 4.22: As in Fig. 4.2, except for 1200 UTC 25 Jan 2012 to 1200 UTC 26 Jan 2012.

4.3 Testing the Sensitivity of the ACM2 Scheme

An evaluation of the same PBL schemes tested by C15 (ACM2 (nonlocal/local), YSU (nonlocal), MRF (nonlocal), MYJ (local), and QNSE (local)) is provided. Because of inherent biases in strictly nonlocal and local schemes, it is hypothesized that the ACM2 scheme, which combines both nonlocal and local viewpoints, may prove to be more accurate in reproducing the environment of the "SECOLD" regime.

Furthermore, the PBL depth simulated by the ACM2 (nonlocal/local) scheme depends on the critical Richardson number, which can be modified. This provides an opportunity to potentially further improve its depictions of thermodynamic and kinematic structures of the PBL. The Richardson number corresponds

to the ratio of static stability to vertical wind shear. In general, a larger Richardson number corresponds to greater suppression of turbulence. Variations of the ACM2 (nonlocal/local) scheme are incorporated by making adjustments to its corresponding physics code. This is aimed at depicting its sensitivity to the selection of the critical Richardson number in assessing the top of the PBL. For unstable conditions, Pleim (2007a) indicates the PBL top as being set at the level where the simulated Richardson number (computed using differences in variables from the surface to locations above the ground), reaches a critical Richardson number threshold, while the PBL top is also treated as a function of the critical Richardson number threshold for stable cases. Accordingly, higher critical Richardson numbers would typically correspond to deeper PBLs being simulated using the ACM2 (nonlocal/local) configuration. This will be tested in the subsequent PBL scheme evaluation. Ultimately, the Richardson number provides definition for the portion of the atmosphere that is characterized by the PBL in these model simulations. This is the primary reason why this parameter is selected for additional analysis, especially given the distinguishability of the instability and kinematic properties of the "SECOLD" regime that also influence the Richardson number.

Ultimately, the overall purpose of perturbing the ACM2 (nonlocal/local) scheme is to investigate whether improvements can be made to a scheme that already incorporates both local and nonlocal mixing formulations, potentially offering the greatest benefit to simulations of the "SECOLD" regime. Its design

incorporates vertical wind shear via the critical Richardson number, which is an important aspect of this regime owing to its strength and ability to enhance turbulent mixing. The control ACM2 (nonlocal/local) scheme uses 0.25 as the critical Richardson number, and four variants to the ACM2 (nonlocal/local) scheme associated with changes to the critical Richardson number are introduced: critical Richardson number variant of 0.05 corresponding to "ACM05," 0.15 to "ACM15," 0.35 to "ACM35," and 0.45 to "ACM45," with each variant representing the nonlocal/local hybrid configuration. While these critical Richardson number values are somewhat arbitrary, they represent dispersion on either side of the critical Richardson number control value to determine sensitivity associated with this variability.

4.4 Evaluation Process

A consistent, reproducible evaluation of the simulations corresponding to different PBL parameterization schemes is particularly challenging owing to the scarcity of regular observations of meteorological variables through the troposphere in locations characterizing the near-storm environment of the tornadoes. However, this evaluation is particularly important in the search for the best way of parameterizing PBL processes for a regime that is not well studied. As such, C15 take the approach of combining surface observations with model analysis output to create an evaluation dataset. In particular, they describe the way in

which model output from the RUC is merged with objective analyses of surface observations to create a consistent dataset describing the real environment, similar to the process invoked for the generation of mesoanalysis data (Bothwell et al. 2002), such that the surface-observation-influenced data lie at the base of the vertical profiles. Specifically, vertical profiles of relative humidity, temperature, and wind are extracted from 20-km grid-length RUC output available from the NOAA National Model Archive and Distribution System (NOAA/NCDC 2014a,b) every 25 mb above the surface each hour, and this is repeated for each hour of each 24-hour-long simulation. Then, corresponding surface variables each hour originating from SFCOA output (Bothwell et al. 2002) serve as the base of each profile, and the organization of such profiles is supported by using the NCAR Command Language (NCL; NCAR 2014). This permits consistent computations of thermodynamic and kinematic parameters relevant for model evaluation, following the methodology carried out by C15 and Coniglio et al. (2013). The corresponding dataset will subsequently be referred to as the "RUC/SFCOA" dataset.

Similar to C15, four locations in proximity to the severe thunderstorm reports in Figs. 4.2-4.22 are chosen to provide the background verifying thermodynamic and kinematic profiles from the RUC/SFCOA dataset on an hourly basis throughout the simulations. A focus on near-tornado environments is made. In order to specifically focus on environments that are representative of the warm-sector air that is relevant for supporting tornadoes, sounding-based

parameter thresholds are set for comparisons between forecast soundings and RUC/SFCOA soundings. Thresholds of 25 J kg^{-1} and 25 m^2 s^{-2} of most-unstable CAPE and 0-3-km SRH are used, respectively (i.e., representing overlap of at least very limited buoyancy and SRH supporting severe weather in the "SECOLD" regime), for a sounding to be considered for comparison, and all initial-hour soundings are omitted from the analysis to permit models to spin up from initial conditions. These thresholds slightly differ from the more general, positively buoyant and convectively uncontaminated characteristics that C15 use as thresholds. At a given hour, both forecast and RUC/SFCOA soundings must meet these requirements to be considered for comparison. If a sounding from either a WRF forecast or the RUC/SFCOA is omitted from the analysis, the corresponding sounding from the other source is also omitted to facilitate consistent comparisons between available forecasts and available RUC/SFCOA profiles. The irregularity amongst forecast sounding availability owing to variations in the choice of PBL scheme explains the slight differences in sample size for comparisons amongst the different PBL schemes as subsequently shown. All valid forecast soundings and corresponding RUC/SFCOA soundings and related parameters are pooled together for each PBL scheme for the statistical analysis provided in the next subsection.

The RUC/SFCOA dataset is limited by errors inherent to the RUC model, surface objective analyses, and potential inconsistencies between the RUC and SFCOA fields. This estimate of the atmosphere is constructed similarly to the

SPC mesoanalysis system. Additionally, the surface objective analysis fields are found to be accurate in severe weather regimes affecting the central United States (Coniglio 2012), though the accuracy of these fields has not been tested for the "SECOLD" regime yielding uncertainty regarding this accuracy in the "SECOLD" regime.

Some of the error evident in the RUC/SFCOA dataset is illustrated in Fig. 4.23 that compares vertical thermodynamic and kinematic profiles between the RUC/SFCOA dataset and the fully observed sounding corresponding to Jackson, Mississippi for a single time associated with the "SECOLD" regime. Comparisons to profiles associated with different PBL schemes are also provided in this figure. This figure highlights some of the differences between the RUC/SFCOA dataset and the fully observed sounding, implying some error (albeit relatively modest in magnitude) inherent to the RUC/SFCOA dataset that is treated as representative of the real atmosphere. A more rigorous comparison between the RUC/SFCOA dataset and fully observed soundings would need to be performed for this particular regime to further identify error characteristics of the RUC/SFCOA dataset, though this figure illustrates an initial attempt at performing this comparison.

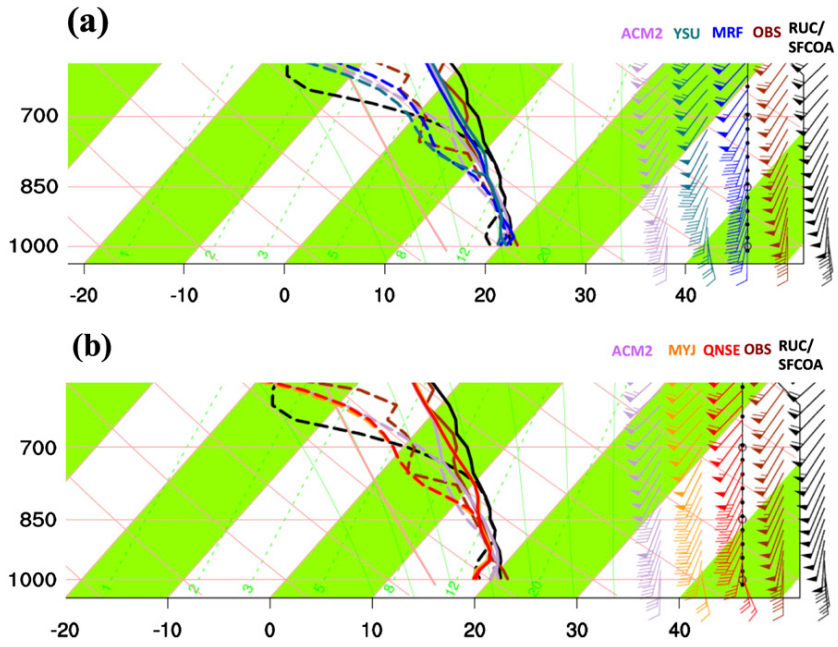

Figure 4.23: Reproduction of Fig. 16 of C15 representing overlays of soundings from WRF simulations at 0400 UTC 1 Jan 2011 corresponding to Jackson, Mississippi using (a) the nonlocal YSU and MRF PBL schemes and the hybrid nonlocal/local ACM2 PBL scheme around and below the 600-mb level, and using (b) the local MYJ and QNSE PBL schemes and the hybrid nonlocal/local ACM2 PBL scheme around and below the 600-mb level. In both of these panels containing WRF soundings, the observed sounding (OBS) and the RUC/SFCOA sounding corresponding to Jackson, Mississippi at the same time are also overlaid. Profiles in each panel correspond to the color-coded format identified above the plotted wind profile in each panel. The temperature profiles are plotted using the thick solid traces, the dewpoint profiles are plotted using thick dashed traces, and the wind profiles are plotted to the right of these traces.

However, despite this error inherent to the RUC/SFCOA dataset, the aforementioned scarcity of observational data fully resolving the troposphere, and irregular spatial sampling of surface observations, prevent a more accurate dataset from being available. Furthermore, the RUC/SFCOA rendition of the real atmosphere is constructed similarly to the SPC mesoanalysis system that is considered to be an important clue of real-time data. Corresponding data from the SPC mesoanalysis system are considered to provide a reliable depiction of the

atmosphere by the convective community. Finally, the robust sample of forecast soundings evaluated for each PBL scheme across a vast array of simulated Southeast cold season severe weather events lends confidence in the ensuing evaluation statistics.

4.5 Statistical Analysis Introduction

The problem of forecast model evaluation for different PBL parameterization schemes is addressed by considering multiple metrics for verification to provide a broad array of model versus observed comparisons for multiple thermodynamic and kinematic parameters for convective forecasting. There are many different aspects of this process that no single indicator can fully address, and different portions of a parameter space may be associated with different levels of performance. These parameters represent a focused set of variables that incorporate important aspects of the forecast problem, and are associated with differences between the schemes that can aid in choosing the most appropriate scheme for the "SECOLD" regime.

The approach of model evaluation begins with an analysis of model performance for particular RUC/SFCOA parameter-magnitude groupings that are treated as "observations" or "actual" values, which will be used interchangeably hereafter. This addresses the following question: "How well do PBL schemes reproduce actual thermodynamic and kinematic regimes?" For each parameter

subsequently investigated, observed parameter regimes are binned based upon narrow, fixed ranges, within which corresponding model forecast parameter values are pooled for each of the nine PBL parameterization schemes (ACM2 (nonlocal/local), YSU (nonlocal), MRF (nonlocal), MYJ (local), QNSE (local), ACM05 (nonlocal/local), ACM15 (nonlocal/local), ACM35 (nonlocal/local), and ACM45 (nonlocal/local)).

Box-and-whiskers plots corresponding to each of these schemes are provided to illustrate the tendency for these schemes to result in over-, under-, or accurate forecasts of the various observed parameter. For the purpose of generating concise statements from these plots and related distributions, follow-up statistical analyses are required, which are addressed in subsequent plots for each parameter.

Linear regressions are then generated for model forecast parameters on actual parameter values, effectively fitting a line to the various PBL schemes whose distributions are plotted in the box-and-whiskers diagrams. This particular selection of linear-type regressions is motivated by Murphy et al. (1989) who use linear regression to evaluate forecasts of temperatures, which succinctly provides additional insight regarding differences between forecast and actual parameter values as subsequently described. In addition to plotted lines, which mirror the interquartile ranges of the box-and-whiskers diagrams, slopes and

y-intercepts are provided with the linear regression equation alongside each corresponding regression coefficient (r^2). Aside from the listed r^2 regression coefficient values in the diagrams, no other measures of validity of linear regression analysis are demonstrated including tests of normality related to the distributions. Under- and over-forecasts are readily apparent from such diagrams in different parameter regimes, through their comparison with the plot of $y = x$ representing the perfect forecast. Slopes that increasingly deviate from the slope of this perfect-forecast line, unity, represent increasing conditional bias, where the degree of under- and over-forecasts depend upon the magnitude of the actual values. To succinctly extract relevant characteristics of each of these lines, slope and y-intercept values corresponding to each of the PBL schemes are plotted on scatterplots for each parameter, such that values of slope approaching unity correspond to decreasing conditional bias.

Average actual parameter values over the entire distribution are compared with average simulation values for each of the PBL schemes over the entire distribution. This permits the analysis of overall mean differences between simulation results using the different PBL schemes and observations.

Following the aforementioned analysis of forecast versus actual distributions and related conditional biases, along with mean differences, metrics of forecast evaluation introduced by C15 to assess model performance amongst the nine PBL parameterization schemes are applied. In particular, they apply two metrics for the evaluation of the schemes. One is Theil's inequality coefficient, U (Theil

1961, 1966; Clements and Frenkel 1980; Pindyck and Rubinfeld 1981; Trnka et al. 2006). The definition of U is as follows:

$$U = \frac{\sqrt{\frac{1}{T}\sum_{t=1}^{T}(Y_t^s - Y_t^a)^2}}{\sqrt{\frac{1}{T}\sum_{t=1}^{T}(Y_t^s)^2} + \sqrt{\frac{1}{T}\sum_{t=1}^{T}(Y_t^a)^2}}, \tag{4.1}$$

where Y_t^s represents forecasts, and Y_t^a represents observations. U represents normalization of the root-mean-square error, allowing for parameters whose magnitudes vary relatively widely amongst one another to be compared in a standardized manner (C15). The range of U values is from zero to one. Low values of U indicate a relatively better forecast, with a perfect forecast corresponding to a U value of zero. Progressively higher values of U indicate less accurate forecasts, and the worst possible forecast corresponds to a U value of one. C15 also refer to the bias component of error, U_m. The definition of U_m is as follows:

$$U_m = \frac{(\overline{Y}^s - \overline{Y}^a)^2}{\frac{1}{T}\sum_{t=1}^{T}(Y_t^s - Y_t^a)^2}, \tag{4.2}$$

where Y_t^s represents forecasts, and Y_t^a represents observations. U_m measures the degree of systematic error inherent to simulation results by comparing the overall simulation mean to the overall actual mean. The range of U_m values is from zero to one. A value of U_m of zero represents no systematic bias, while relatively larger values of U_m correspond to greater forecast bias. Pindyck and Rubinfeld (1981) suggest U_m values over 0.1 or 0.2 being associated with appreciable systematic bias, necessitating adjustments to the model for its improvement. By

comparing U and U_m across different PBL schemes, one can determine the relative degree of forecast error for each PBL scheme and evaluate how much of that is systematic. A forecast model with large U and large U_m would imply large error associated with a large systematic component, and poor model performance. On the other hand, a forecast model with small U and small U_m would imply minimal error and good model performance. One consideration for this analysis using Theil's inequality coefficient is that in the theoretical limit of a perfect simulation where U is zero, the decomposition of U into components such as U_m is undefined. However, this consideration is not of concern for this work, since none of the simulations result in perfect forecasts as will be subsequently shown.

4.6 Statistical Analysis of 0-3-km Lapse Rate

Simulated lapse rates in the lowest 3 km above ground typically are too steep in the poor actual lapse-rate regimes and too weak in the stronger actual lapse-rate regimes (Fig. 4.24) amongst all PBL parameterization schemes. This represents an overall underforecast of actual variability associated with RUC/SFCOA soundings for all simulations, and conditional bias amongst all schemes. It is evident that, in the stronger lapse-rate regimes, the MYJ (local) and QNSE (local) schemes provide relatively greater underforecasts of lapse rates. This is consistent with local schemes producing insufficiently deep vertical mixing with respect to the PBL in regimes where deeper PBLs exist. Graphically, it appears that the ACM2 (nonlocal/local) scheme and its variants most commonly reproduce actual lapse rates.

Using linear regression of simulated 0-3-km lapse rates on actual values reveals slopes of lines below unity, which is consistent with the underforecast of variability of lapse rates depicted by Fig. 4.24, and this is demonstrated in Fig. 4.25 and Fig. 4.26. The ACM2 (nonlocal/local) scheme and its variants provide slopes closest to 1, indicating the least conditional bias. Strictly local and nonlocal schemes provide relatively greater conditional biases with lower slopes for 0-3-km lapse rate regressions.

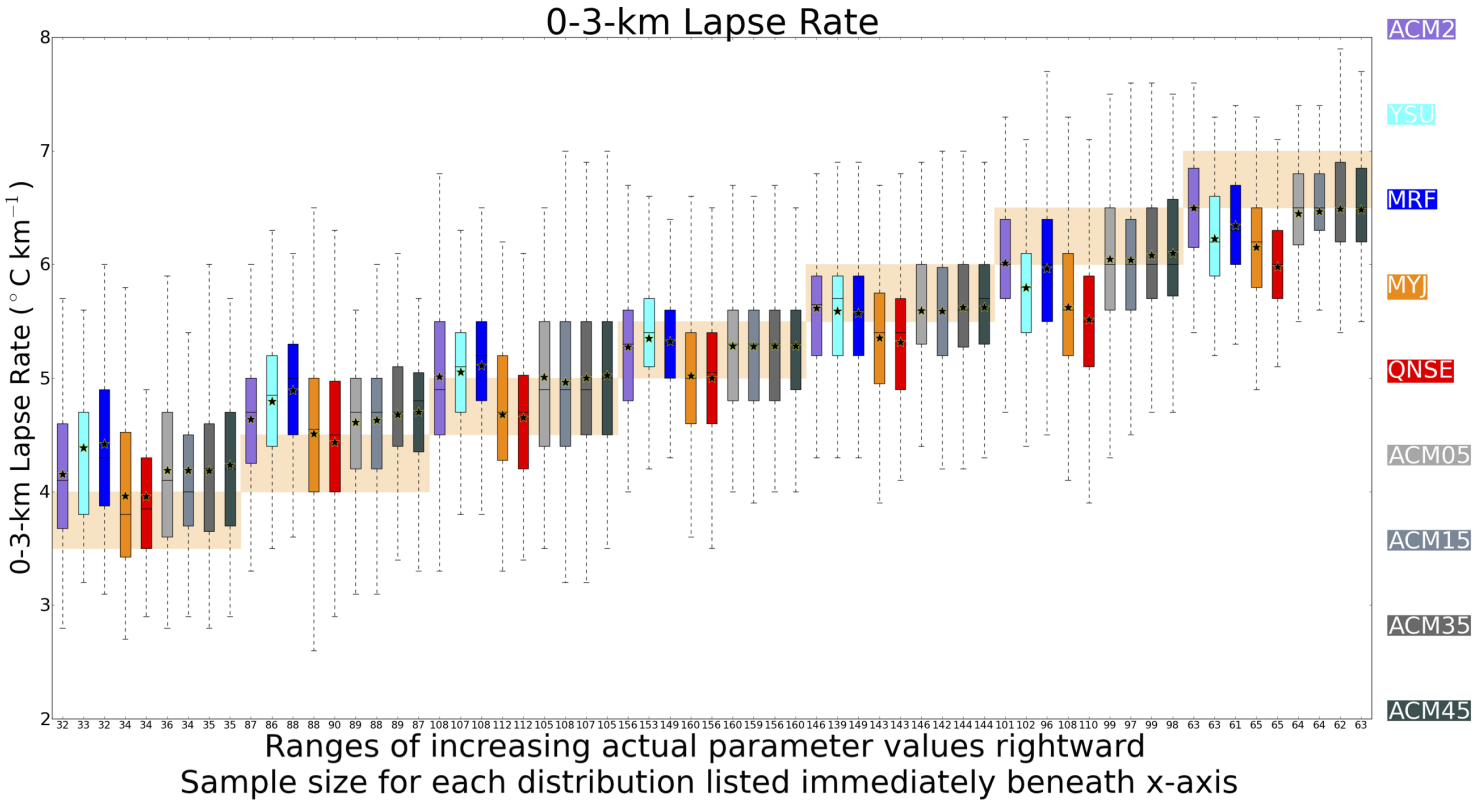

Figure 4.24: Box-and-whiskers plots corresponding to the distributions of simulated 0-3-km lapse rate within fixed ranges of RUC/SFCOA ("observed" or "actual") 0-3-km lapse rates for all PBL parameterization schemes. These fixed ranges are denoted by the tan rectangles that span various ranges of actual 0-3-km lapse rate, whose magnitudes correspond to the y-axis. The different schemes are identified based on the color of the interquartile range, as depicted on the legend listed at the rightmost part of the figure. Whiskers extend up to 1.5 times the interquartile range beyond the first and third quartiles, and small stars depict the mean values of the simulated distributions. Sample sizes for each distribution are listed below the x-axis.

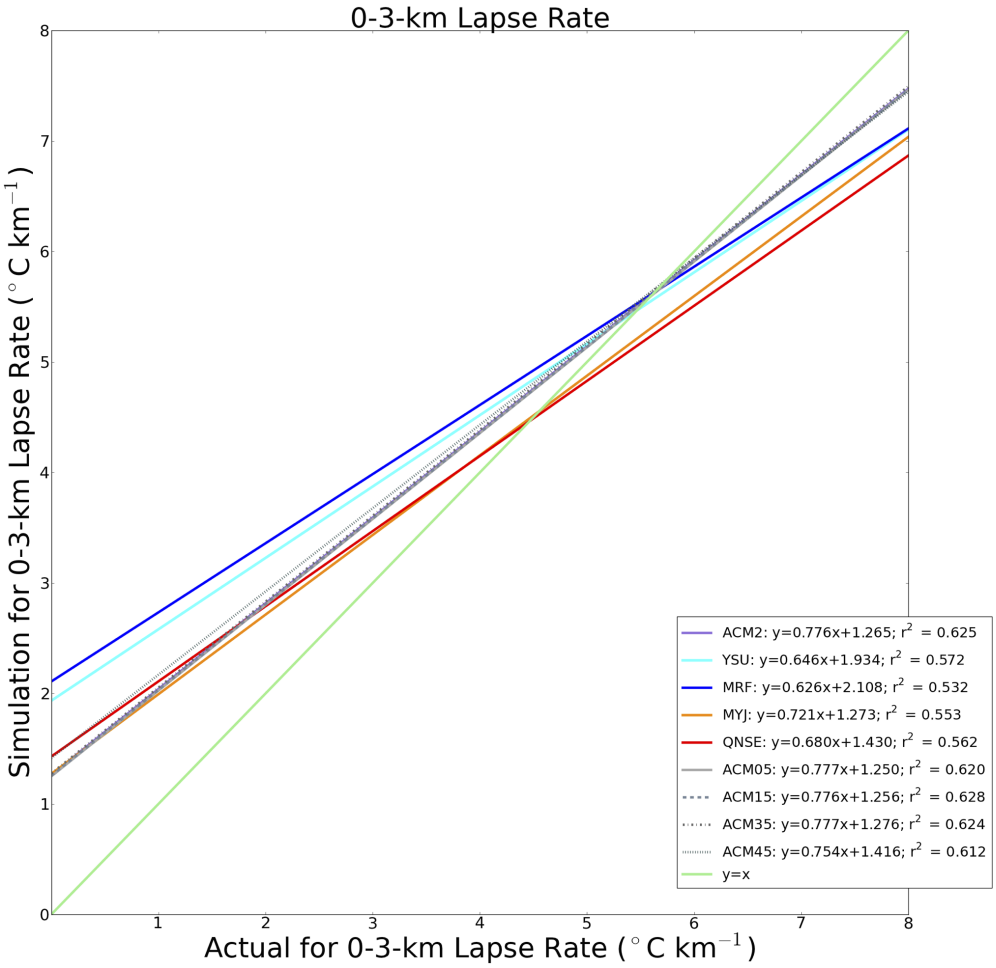

Figure 4.25: Plots of lines resulting from regression of simulated 0-3-km lapse rate on actual 0-3-km lapse rate for the PBL parameterization schemes. Lines are color-coded and correspond to the legend in the bottom-right part of the diagram. The equation corresponding to each line is listed within this legend, along with the r^2 regression coefficient. Overlaid on this plot includes the line characterized by the equation $y = x$, which corresponds to a perfect forecast.

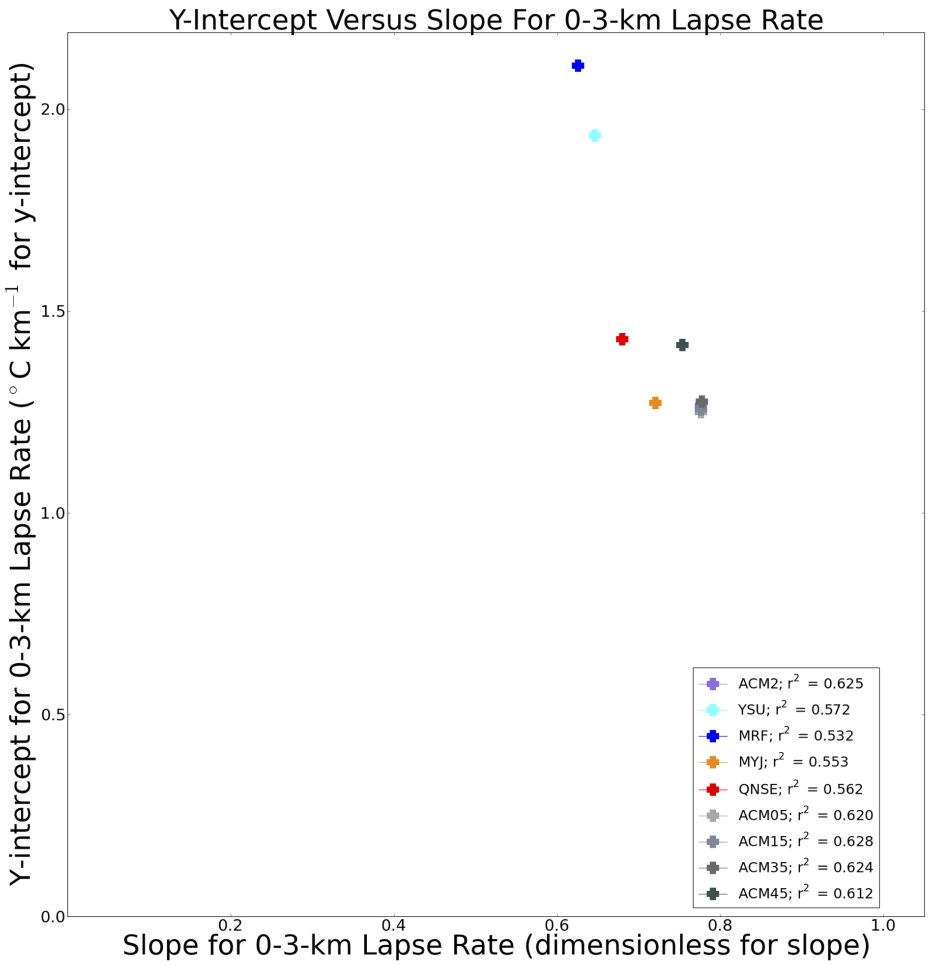

Figure 4.26: Scatterplot of y-intercept versus slope corresponding to each PBL scheme regression line for 0-3-km lapse rate. Markers depict slope-y-intercept pairs that are color-coded based on the legend in the bottom-right part of the diagram, which also lists the r^2 regression coefficient associated with each PBL scheme linear regression.

Average simulated 0-3-km lapse rate comes closest to the RUC/SFCOA average values for non-local schemes, along with the ACM2 (nonlocal/local) scheme and its variants, whereas the MYJ (local) and QNSE (local) schemes are associated with substantial mean underforecasts based on comparisons to RUC/SFCOA means (Fig. 4.27). The mean underforecast of 0-3-km lapse rate corresponding to local schemes is associated with their relatively greater 0-3-km lapse rate underforecast in steeper lapse-rate regimes (Fig. 4.24). Ultimately, it takes nonlocal-influenced PBL parameterization schemes to reduce these large negative differences offered by local schemes, consistent with findings from C15.

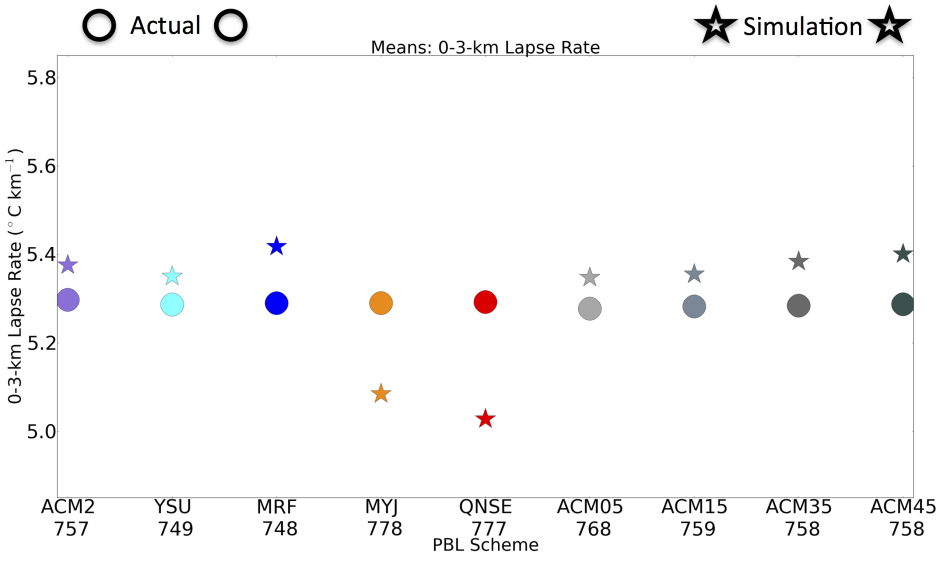

Figure 4.27: For each PBL scheme, comparison of average 0-3-km lapse rate averaged from RUC/SFCOA soundings (shaded circle) and simulations (shaded star). Depictions of mean values are color-coded based on the PBL scheme used, with selected colors corresponding to those displayed in Figs. 4.24-4.26. Sample size for each PBL scheme is provided below the x-axis.

Theil's inequality coefficient (U) for 0-3-km lapse rate is relatively similar amongst all PBL schemes, although slightly lower for ACM2 (nonlocal/local) and its variants, along with the YSU (nonlocal) scheme, which also minimize the bias component (U_m) (Fig. 4.28). Consistent with earlier plots, local schemes (MYJ and QNSE) provide the largest bias component, U_m, values.

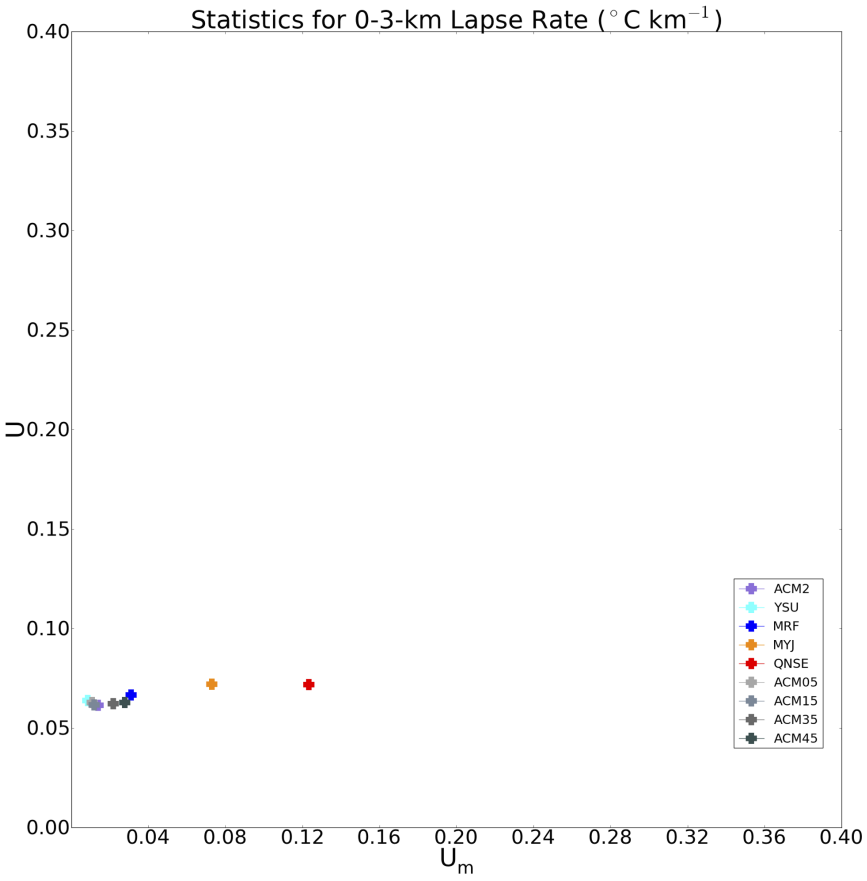

Figure 4.28: Scatterplot of Theil's inequality coefficient (U) versus bias component of error (U_m) for 0-3-km lapse rate. Each marker corresponds to each PBL parameterization scheme, with markers color-coded based on PBL scheme type and identified in the legend in the bottom-right part of the figure. Vertical and horizontal axes are scaled equivalently for this and all subsequent scatterplots of U versus U_m to permit relative comparisons of error and its bias component (i.e., U and U_m values closer to 0 indicating less error and less bias component, respectively).

4.7 Statistical Analysis of Mixing Ratio

Amongst the various regimes of observed lowest-100-mb mean mixing ratios, Fig. 4.29 indicates most schemes performing relatively similarly to observed values. In observed drier environments, the MRF (nonlocal) scheme is too moist. Meanwhile, for moister observed regimes, local schemes (MYJ and QNSE) produce too dry conditions in the lowest 100 mb, as does the YSU (nonlocal) scheme. It is noteworthy that at these moister environments, the YSU (nonlocal) scheme also offers similar drier output to the MYJ (local) and QNSE (local). Fig. 4.30 and Fig. 4.31 indicate little difference in slope across the different PBL schemes, with the ACM2 (nonlocal/local) and its variants offering linear-regression slopes closest to unity indicating the smallest conditional bias.

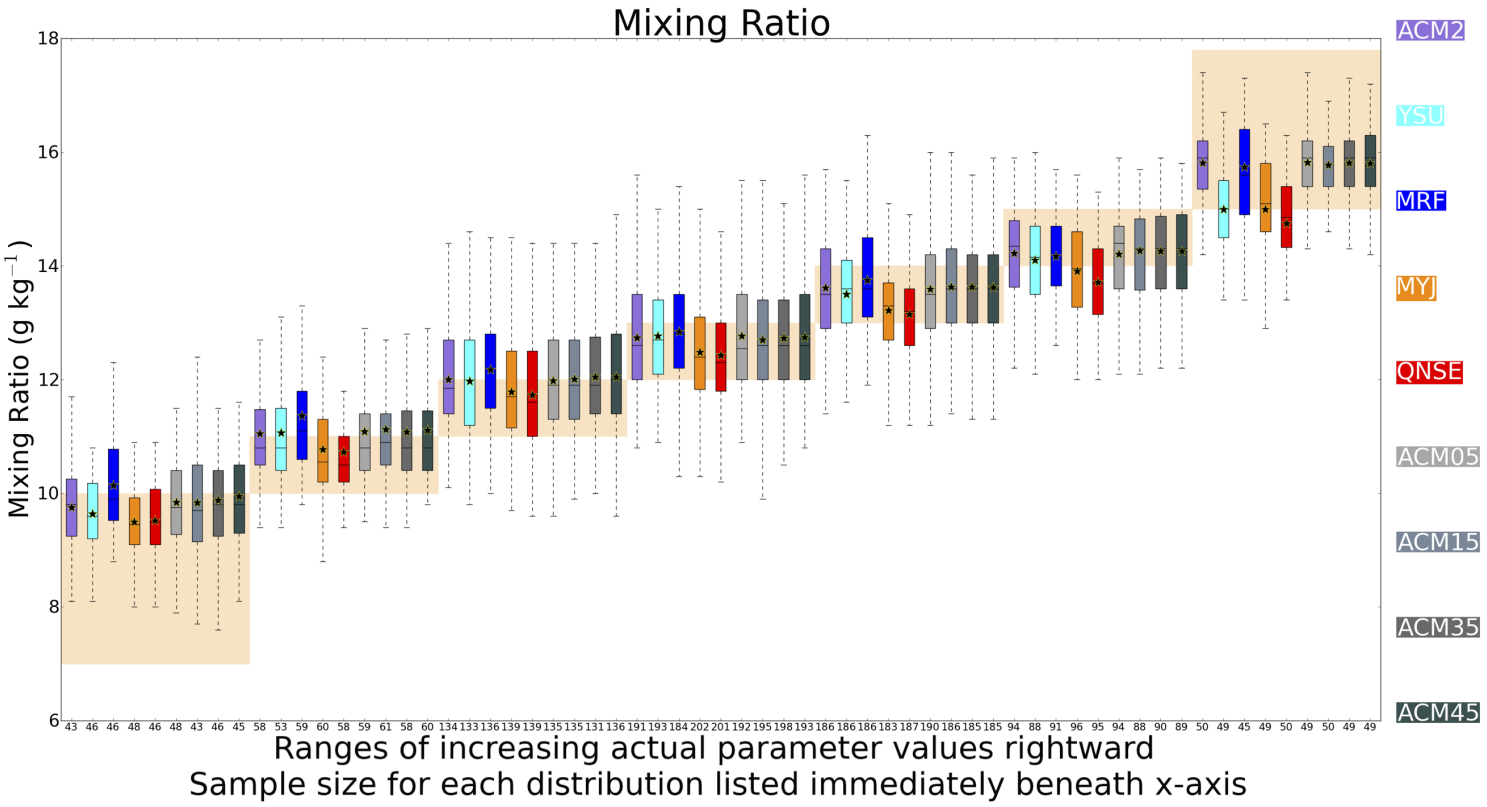

Figure 4.29: As in Fig. 4.24, except for mean mixing ratio in the lowest 100 mb.

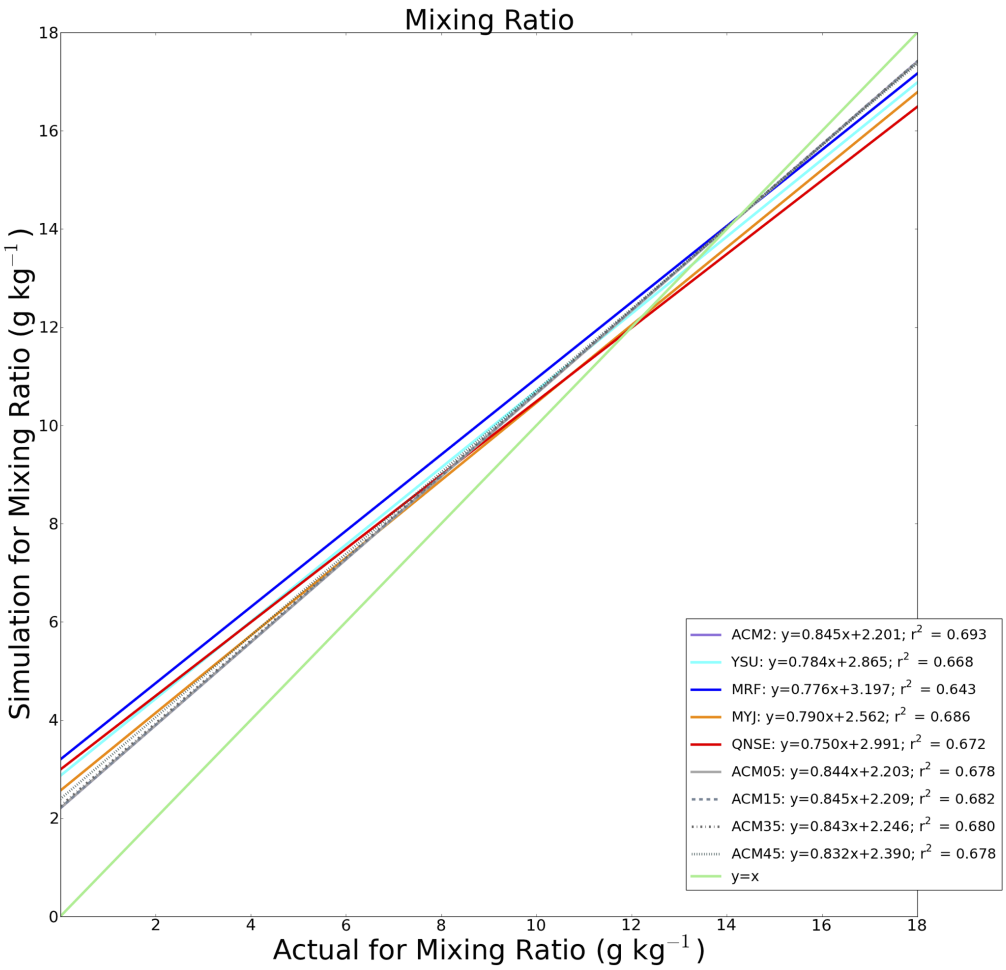

Figure 4.30: As in Fig. 4.25, except for mean mixing ratio in the lowest 100 mb.

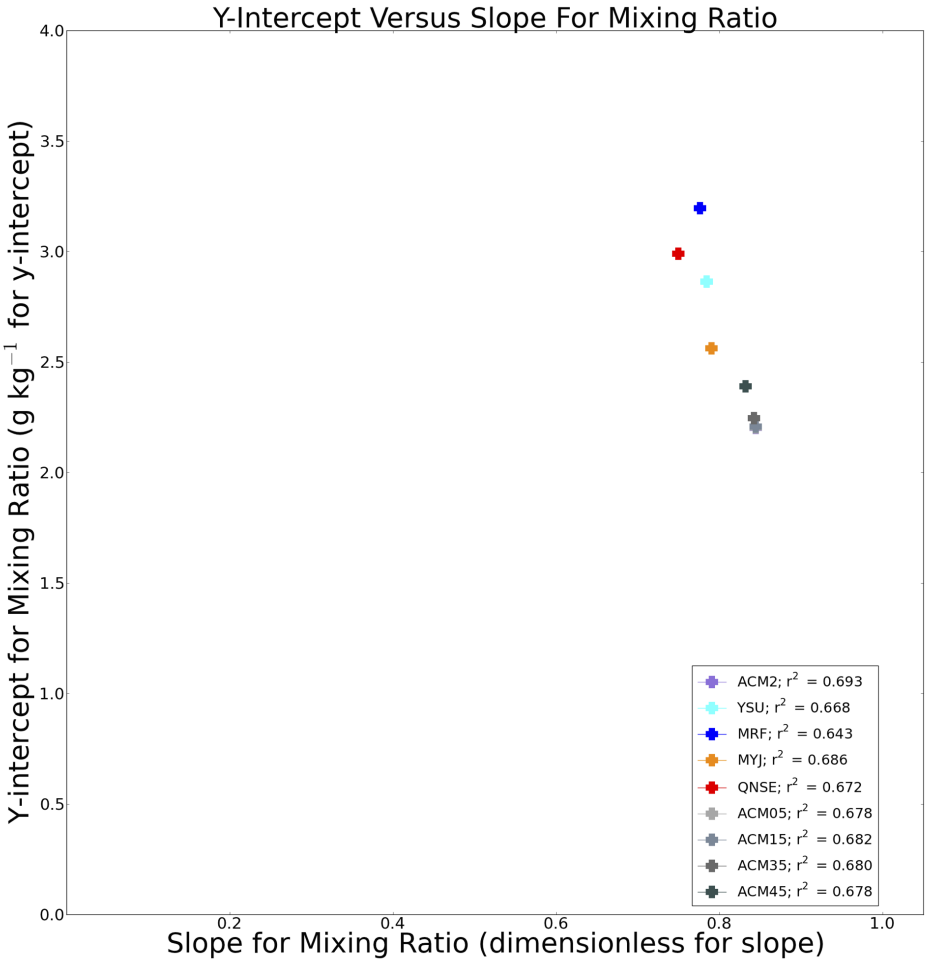

Figure 4.31: As in Fig. 4.26, except for mean mixing ratio in the lowest 100 mb.

Average simulation and average RUC/SFCOA lowest-100-mb mean mixing ratio are relatively similar for each PBL scheme, as shown in Fig. 4.32. This figure illustrates relatively small mean overforecasts for all schemes except local ones.

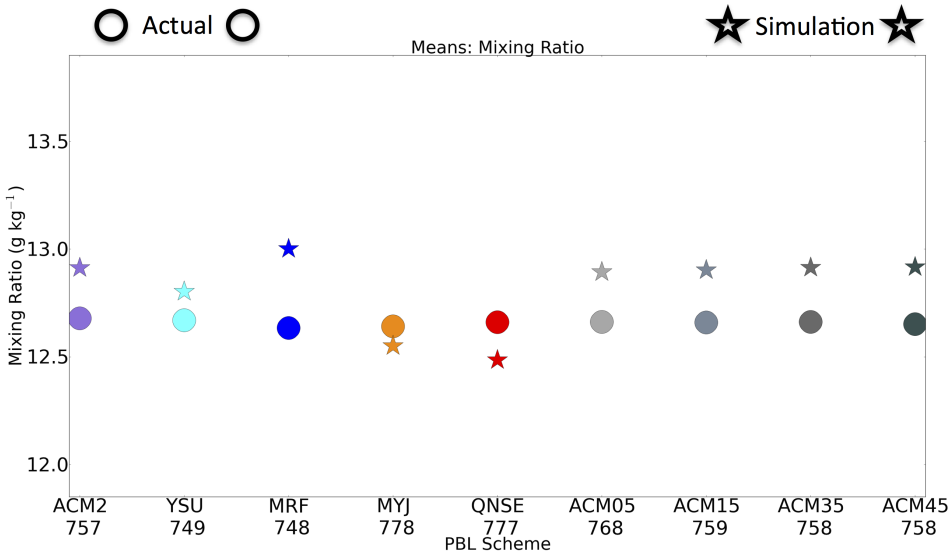

Figure 4.32: As in Fig. 4.27, except for mean mixing ratio in the lowest 100 mb.

With Fig. 4.33 indicating U values that are relatively close to zero and are similar amongst all PBL schemes, lowest-100-mb mean mixing ratio is relatively well forecast by all PBL schemes. The largest U_m bias component is associated with the MRF scheme, and even that value is relatively small, consistent with the limited bias component for all schemes implied by Fig. 4.32.

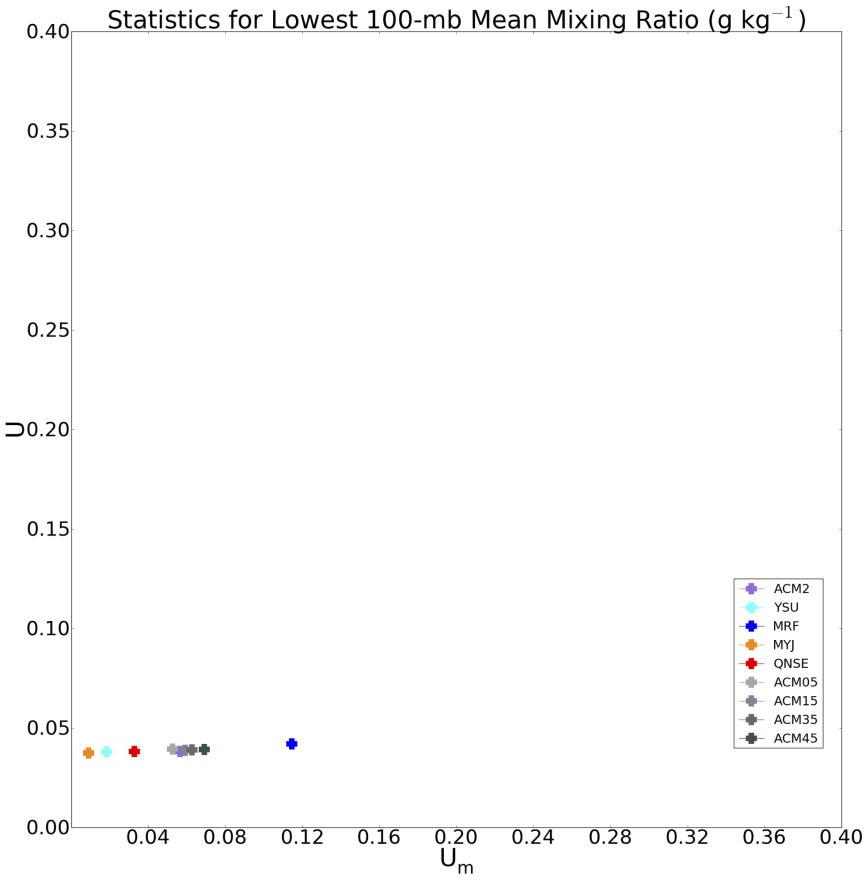

Figure 4.33: As in Fig. 4.28, except for mean mixing ratio in the lowest 100 mb.

4.8 Statistical Analysis of PBL Depth

The next quantity considered is PBL depth, which is a measure of how deep stronger mixing is simulated using the different PBL parameterization schemes. In order to apply a consistent method of determining PBL depths across the wide array of PBL parameterization schemes and the RUC/SFCOA soundings, the methodology of Coniglio et al. (2013) is used in assessing PBL depth, with results displayed in Fig. 4.34. The PBL top is the first level above where the virtual potential temperature exceeds the maximum virtual potential temperature in the lowest 3 levels by more than 0.6 K. This graphic appears similar to Fig. 4.24, highlighting the relationship between lapse rates and vertical mixing depth. However, local PBL schemes more strongly underforecast PBL depth for deeper observed PBLs, and even the nonlocal schemes underforecast the deeper PBLs. The ACM2 (nonlocal/local) scheme and its variants very clearly provide the most accurate forecasts of PBL depth for the various observed PBL-depth regimes. Also, variability in simulated PBL depth is found to increase substantially for actual PBL depths over around 500 m.

Conditional bias for PBL depth is clearly minimized using the ACM2 (nonlocal/local) scheme and its variants, and the ACM45 (nonlocal/local) configuration offers a linear regression slope closest to unity compared to all schemes (Fig. 4.35 and Fig. 4.36). Fig. 4.34 and Fig. 4.35 indicate that this minimization in conditional bias for the ACM2 (nonlocal/local) scheme and its variants is the

result of their reduced underforecast of PBL depth at relatively larger actual PBL depths. This tendency for the ACM2 (nonlocal/local) scheme and its variants to produce deeper PBLs for these regimes could be a topic for further investigation to determine why, physically, the hybrid nonlocal/local schemes produce deeper PBLs than those produced by strictly nonlocal schemes. The differences in conditional bias for PBL depth amongst the variants of the ACM2 (nonlocal/local) scheme are related to different overall mean differences from actual, which is addressed in the subsequent paragraph. Otherwise, conditional bias is markedly greater using strictly nonlocal and local schemes for PBL depth, with the local schemes offering the greatest degree of conditional bias.

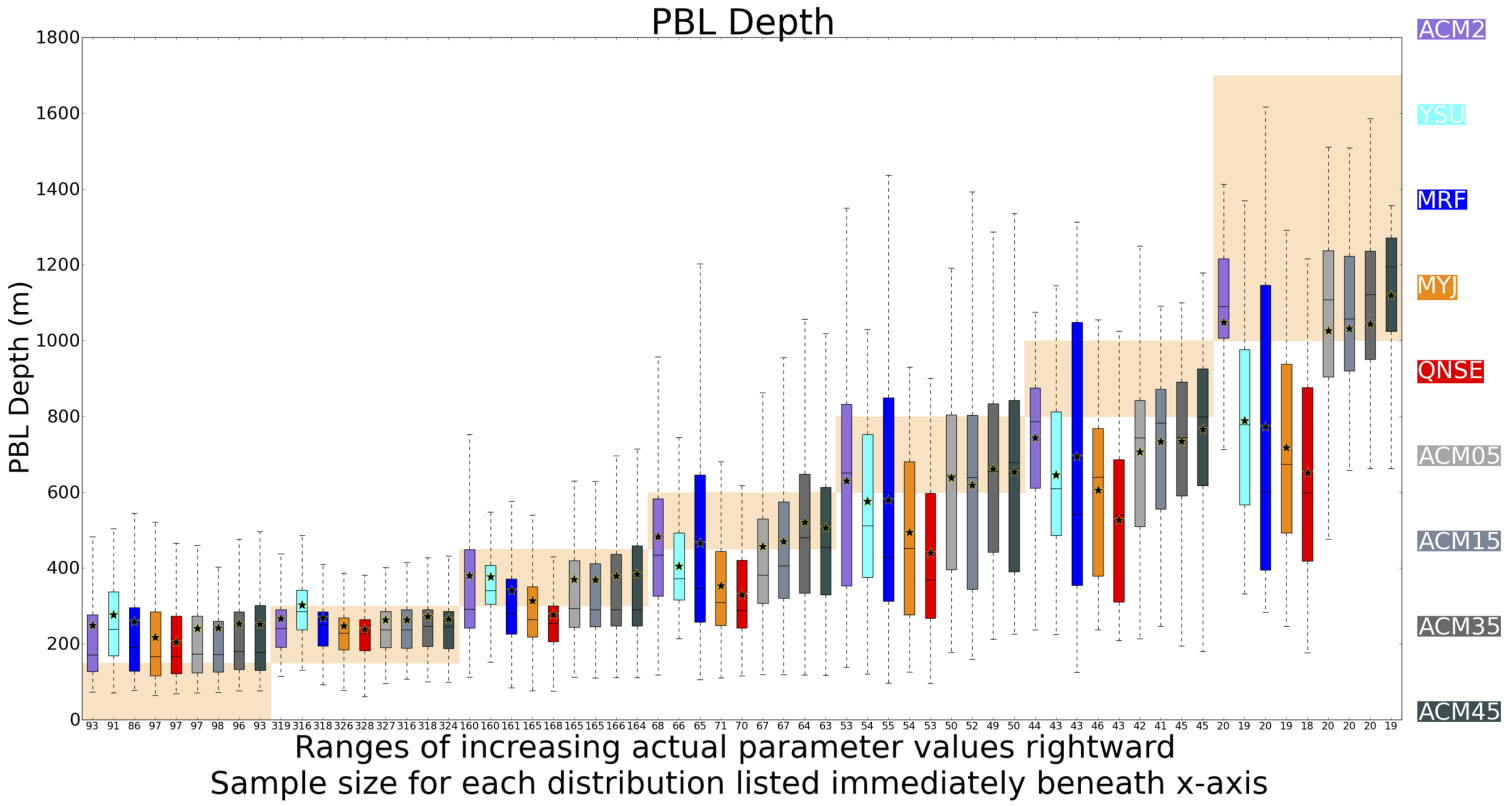

Figure 4.34: As in Fig. 4.24, except for PBL depth.

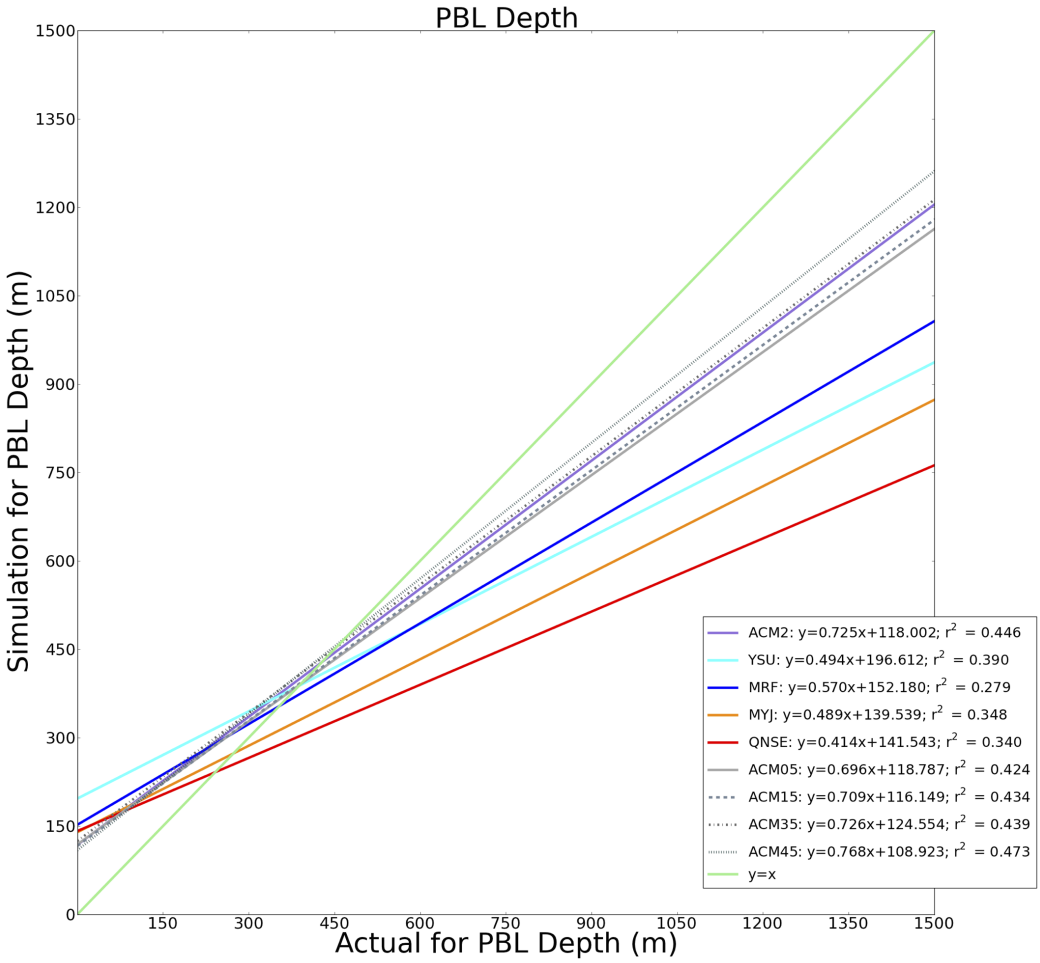

Figure 4.35: As in Fig. 4.25, except for PBL depth.

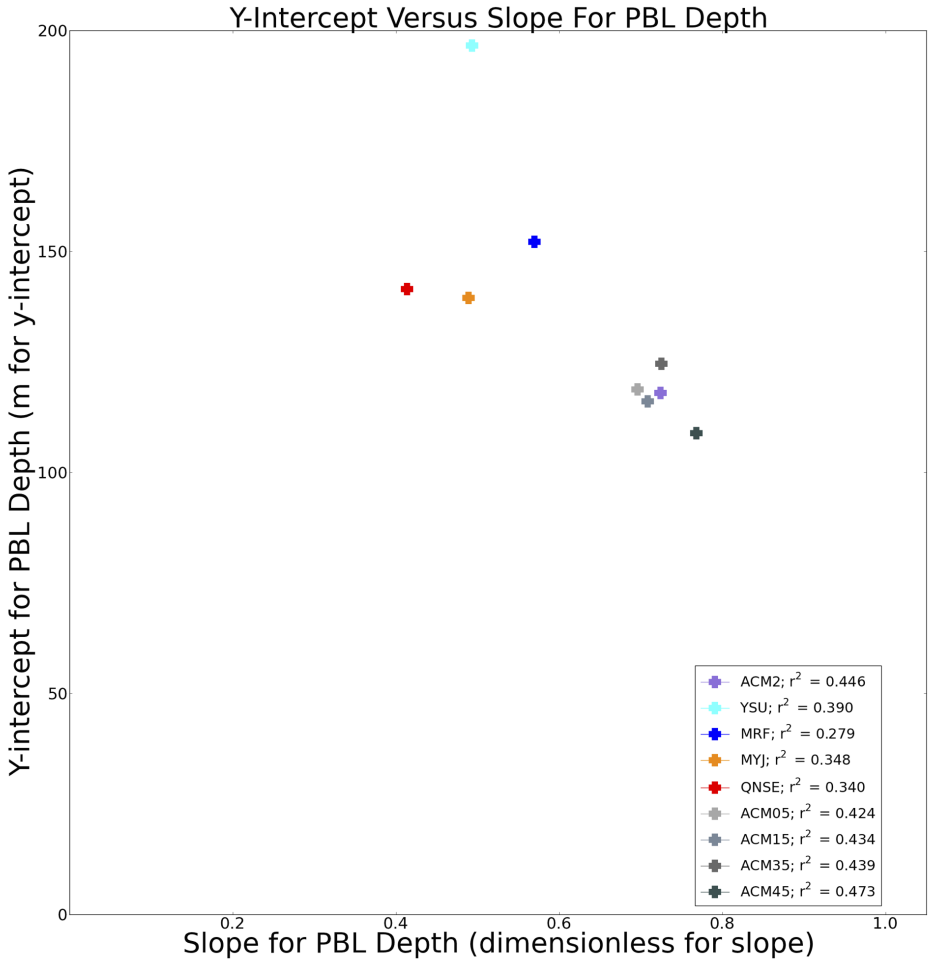

Figure 4.36: As in Fig. 4.26, except for PBL depth.

Differences between mean simulated PBL depth and actual PBL depth are minimized when using nonlocal-influenced schemes, with local schemes indicating markedly shallower PBLs compared to those simulated by nonlocal-influenced schemes (Fig. 4.37). This is consistent with much of the previous literature regarding simulations of the PBL where vertical mixing is enhanced within the convective boundary layer. In the case of the "SECOLD" regime, it is clear that local schemes provide unrealistically shallow PBLs on average across the entire array of simulation results. Furthermore, the increase in average simulated PBL depth with increasing critical Richardson number for the variants of the ACM2 (nonlocal/local) scheme is evident in Fig. 4.37. The notion that the ACM2 (nonlocal/local) variants associated with higher critical Richardson numbers yield the deepest PBLs is consistent with the earlier hypothesis that these higher thresholds would be achieved at a higher level above the ground. This would particularly be the case in an environment characterized by strong vertical shear enhancing turbulence, suppressing the background Richardson number.

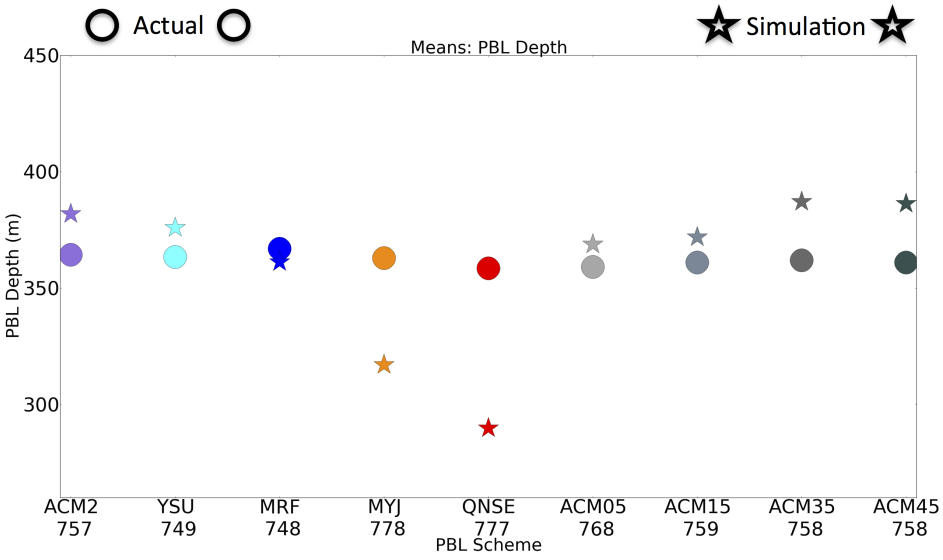

Figure 4.37: As in Fig. 4.27, except for PBL depth.

Figure 4.38 emphasizes the large bias component in PBL depth for the local PBL schemes, and the relatively greater error for the MYJ (local) and QNSE (local) schemes. Minimization of both error and its bias component come from using the ACM2 (nonlocal/local) scheme and its variants, along with the YSU (nonlocal) scheme, with all of these schemes representing nonlocal-influenced mixing.

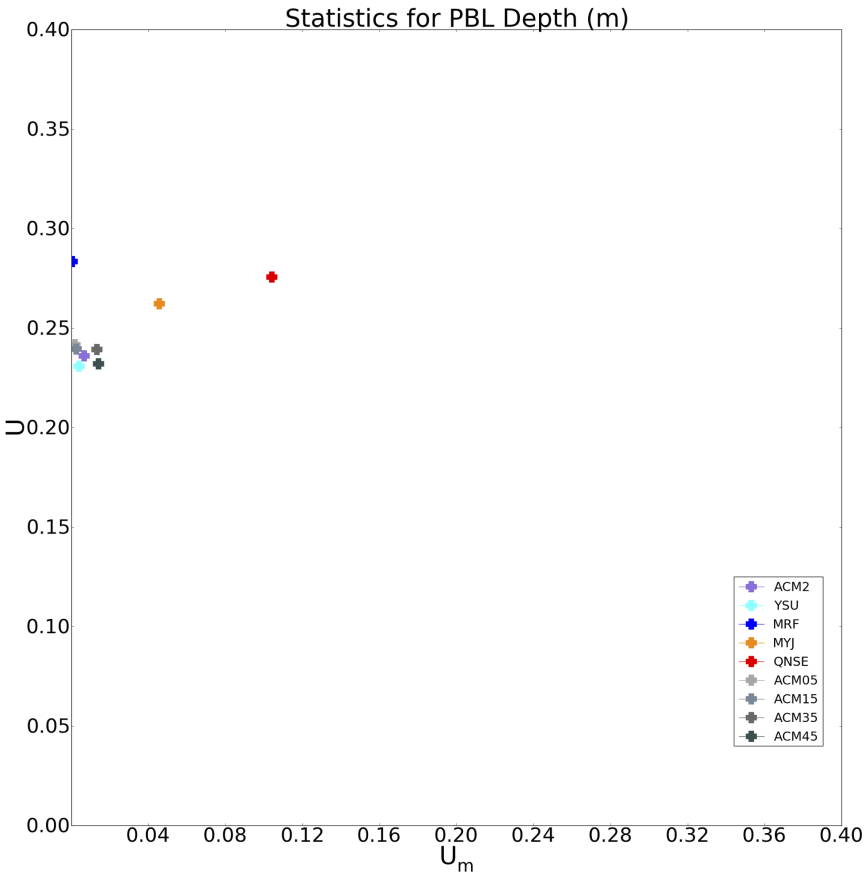

Figure 4.38: As in Fig. 4.28, except for PBL depth.

4.9 Statistical Analysis of MLCAPE

All schemes provide overforecasts of MLCAPE in marginal MLCAPE ranges, and yield closer-to-actual MLCAPE for more moderate MLCAPE ranges, as shown in Fig. 4.39. However, there is a lot of spread amongst simulated values within each of the MLCAPE ranges. Slopes are closest to unity from linear regression for MLCAPE, suggesting the least conditional bias for the ACM2 (nonlocal/local) scheme and its variants, with strictly nonlocal and local schemes both implying greater conditional bias (Fig. 4.40).

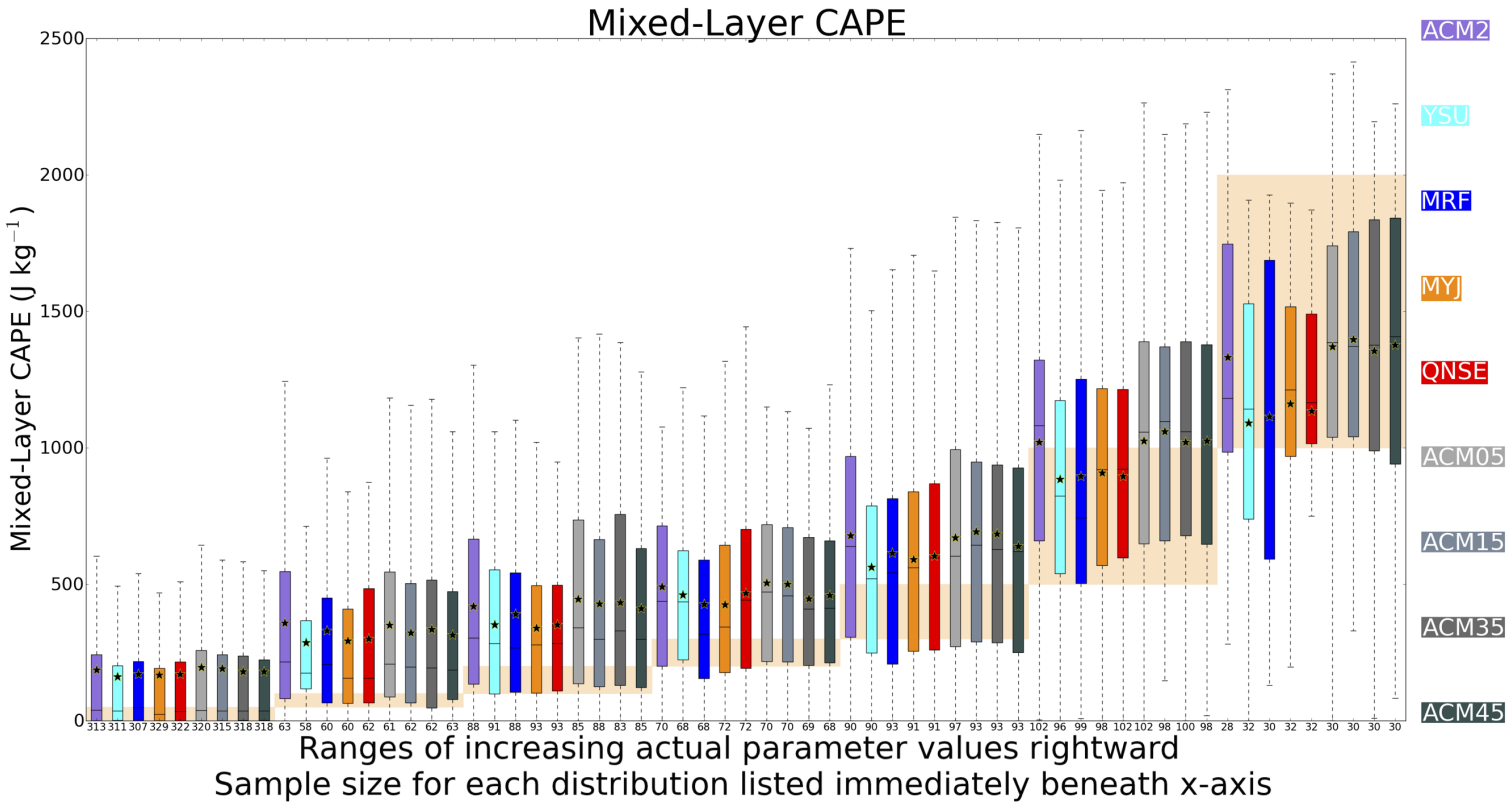

Figure 4.39: As in Fig. 4.24, except for MLCAPE.

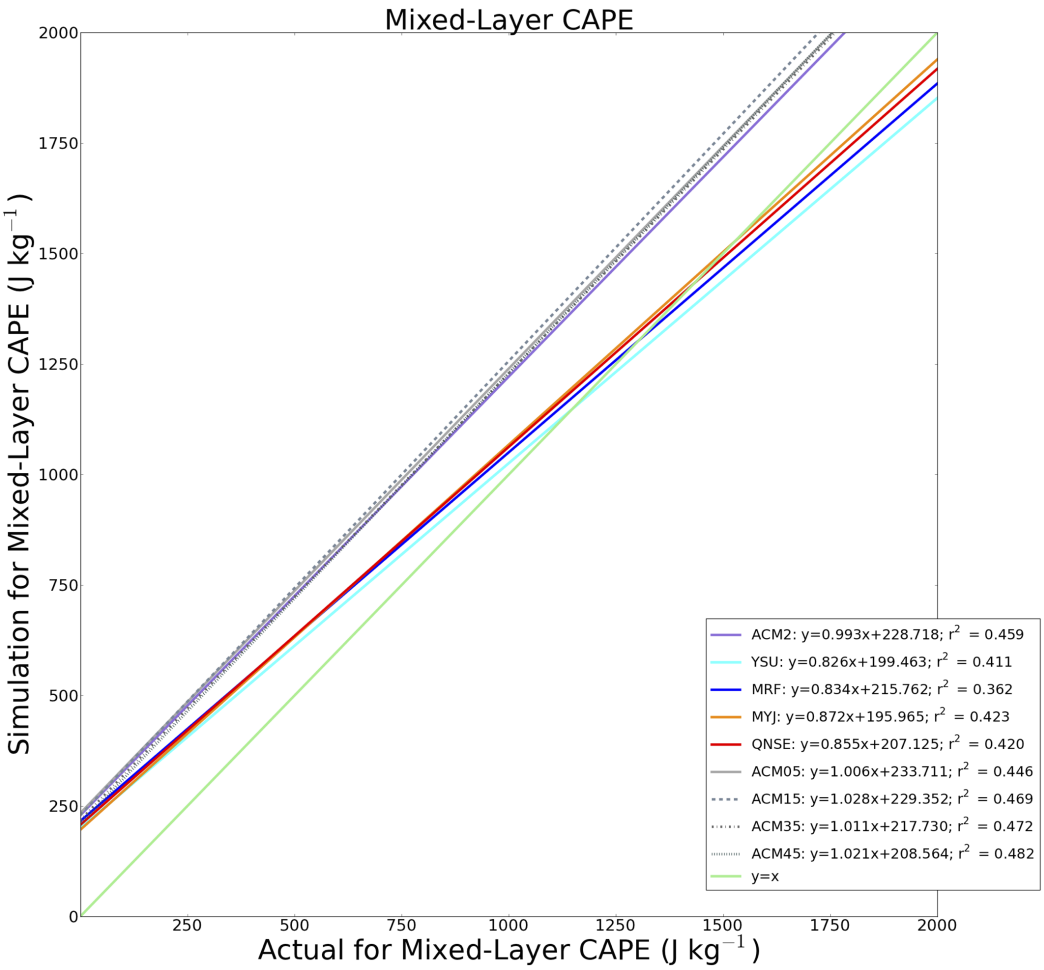

Figure 4.40: As in Fig. 4.25, except for MLCAPE.

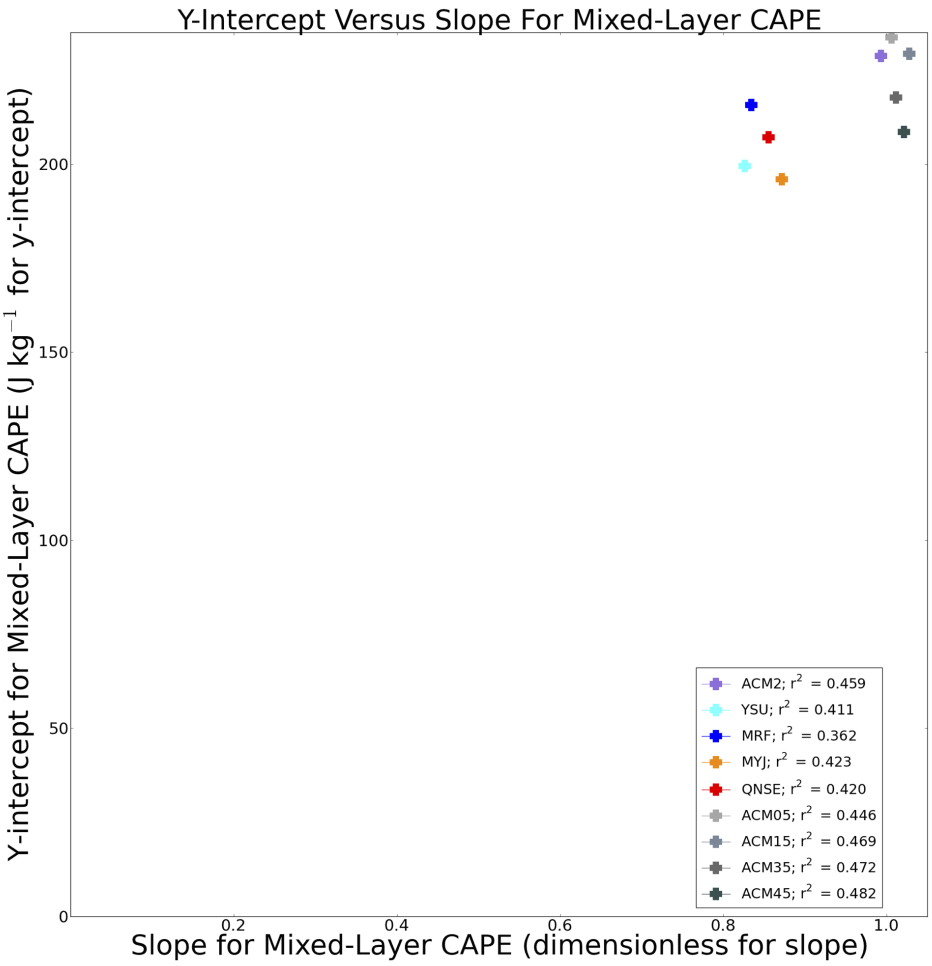

Figure 4.41: As in Fig. 4.26, except for MLCAPE.

Consistent with the net overforecast of MLCAPE depicted in Fig. 4.39, Fig. 4.42 shows the overforecast of MLCAPE associated with all PBL schemes. There is a slight decrease in simulated MLCAPE and decrease in positive bias with increasing critical Richardson number amongst the ACM2 (nonlocal/local) scheme and its variants.

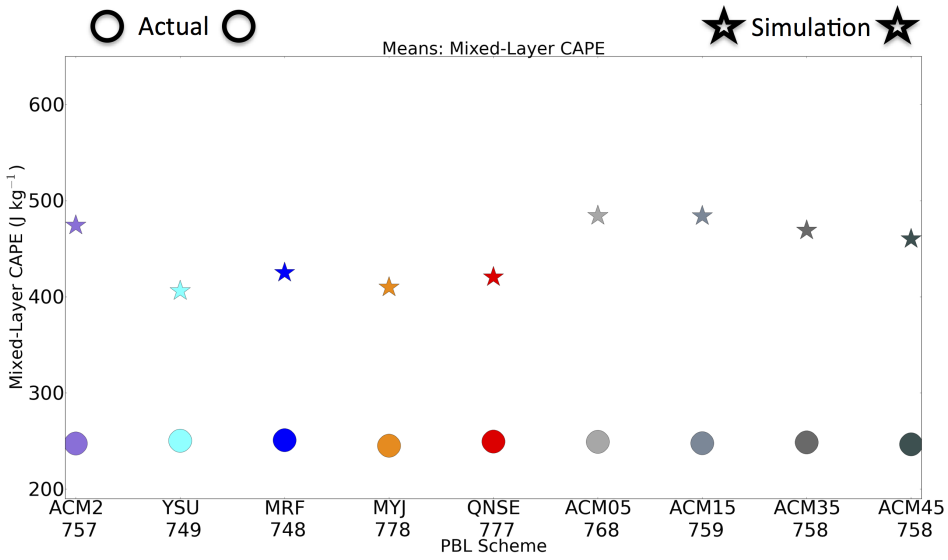

Figure 4.42: As in Fig. 4.27, except for MLCAPE.

The evaluation of MLCAPE using Theil's inequality coefficient suggests that this particular parameter is poorly forecast using all PBL parameterization schemes, when compared to RUC/SFCOA soundings (Fig. 4.43). This calls into question the use of integrated buoyancy in diagnosing the convective parameter space using modern PBL parameterization schemes.

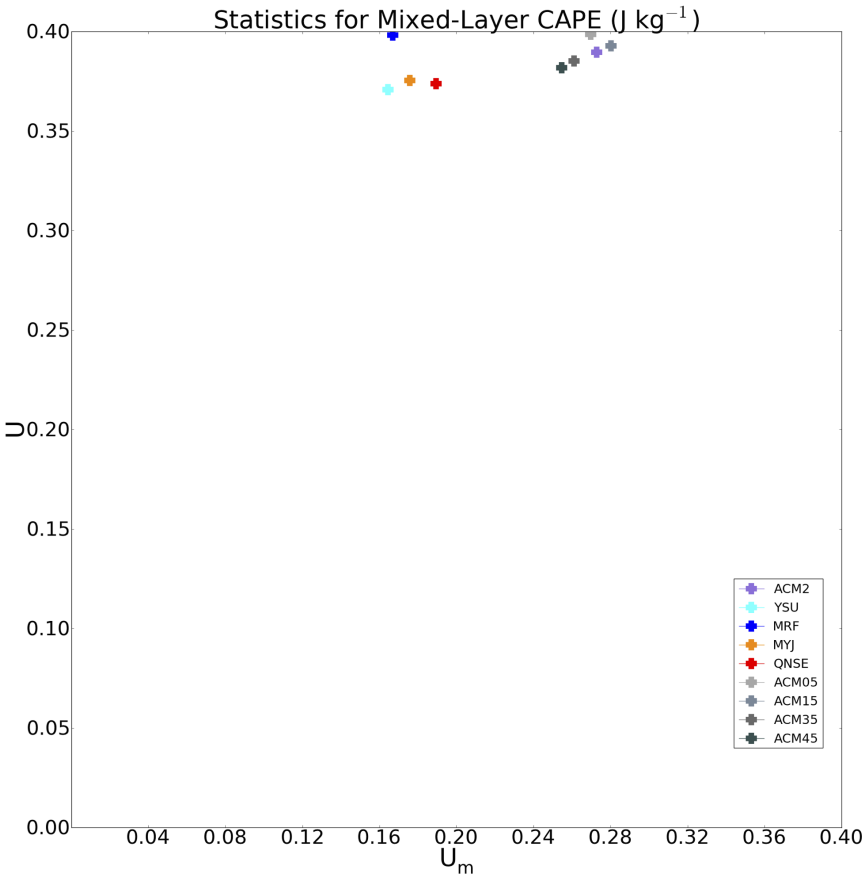

Figure 4.43: As in Fig. 4.28, except for MLCAPE.

4.10 Statistical Analysis of 0-3-km SRH

Similar to the thermodynamic parameters previous discussed, all PBL parameterization schemes result in an underforecast of the variability of 0-3-km SRH, based on Fig. 4.44. In weak-SRH environments, the MYJ (local) and QNSE (local) schemes stand out as providing overforecasts of SRH, whereas in stronger-SRH environments, these local schemes are most accurate. The conditional bias for the various parameterization schemes for 0-3-km SRH is maximized by using nonlocal parameterization schemes and minimized using local parameterization schemes (Fig. 4.45 and Fig. 4.46). Intermediate slopes and conditional bias are evident for the hybrid nonlocal/local ACM2 scheme and its variants.

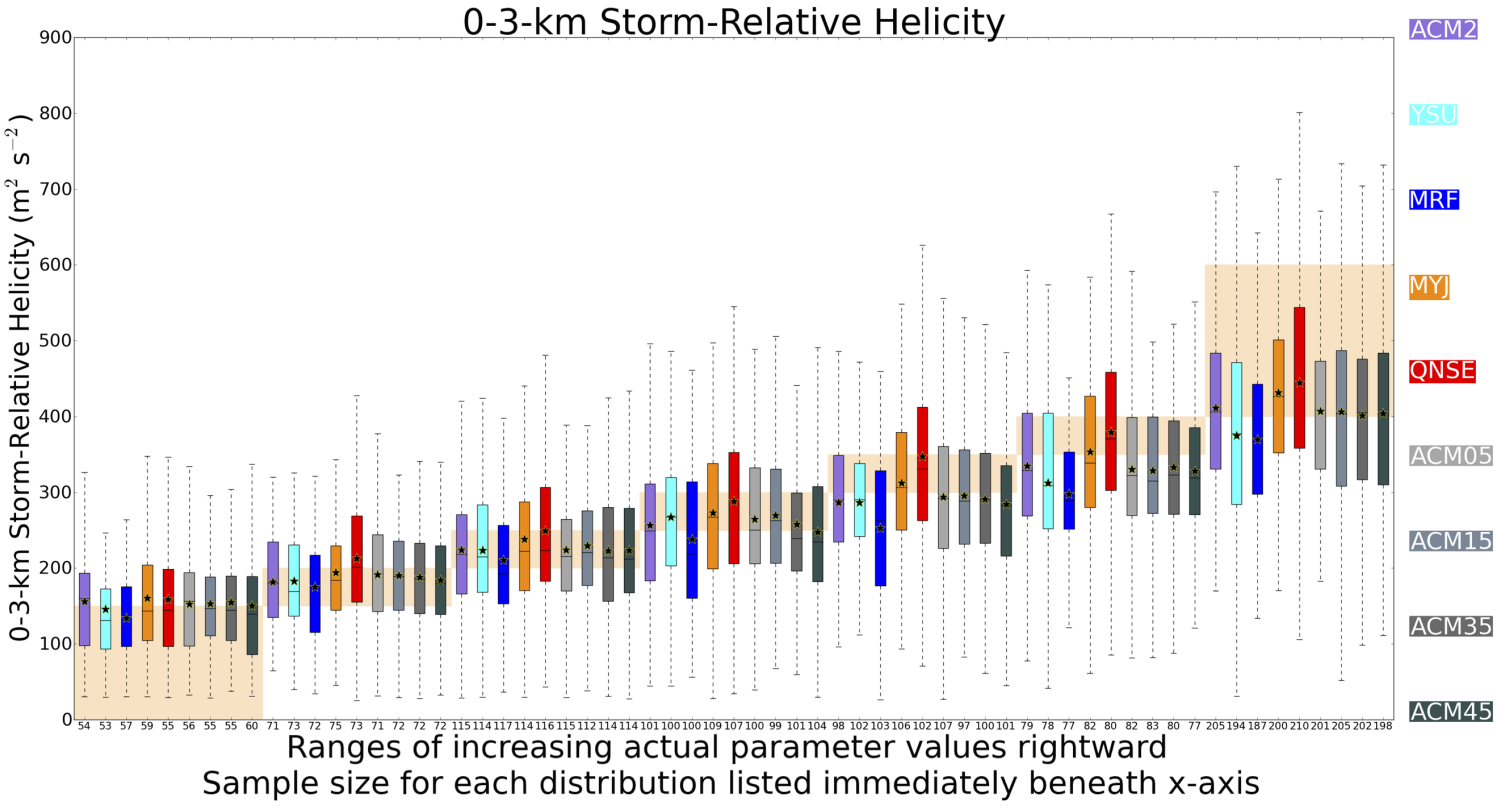

Figure 4.44: As in Fig. 4.24, except for 0-3-km SRH.

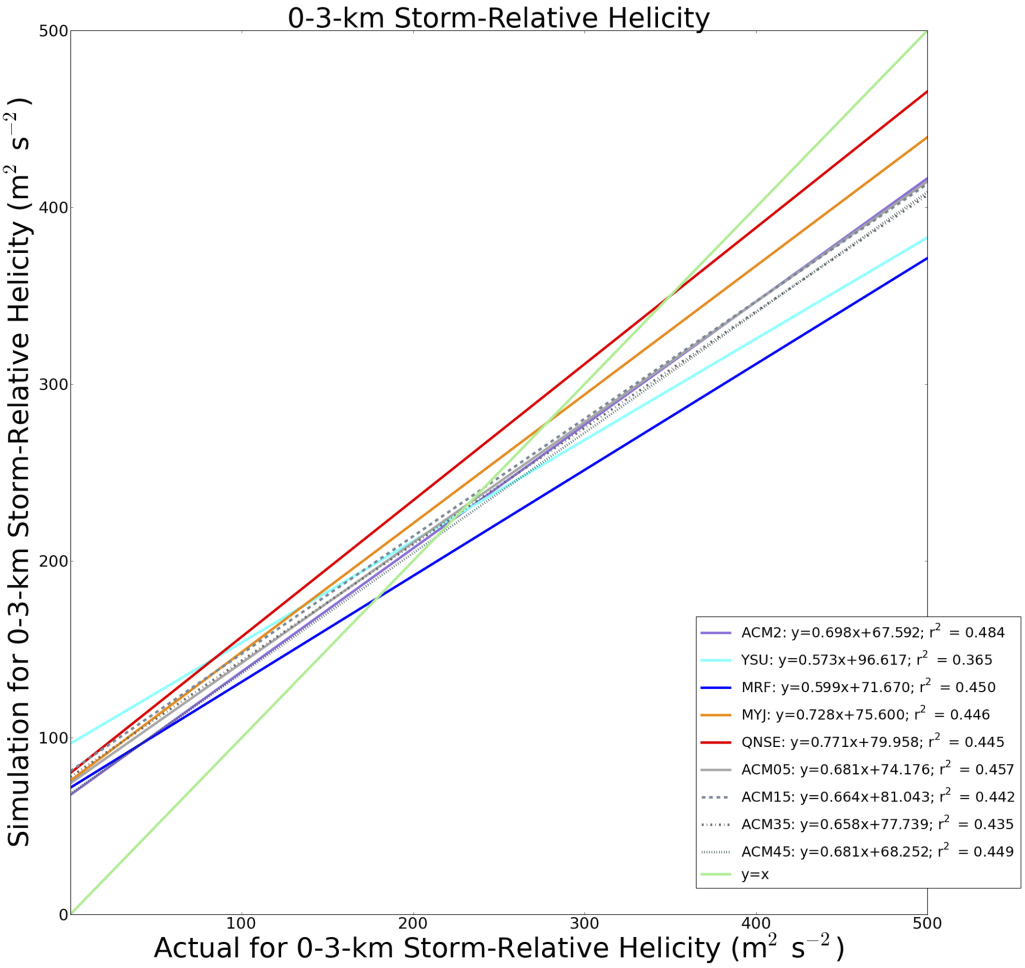

Figure 4.45: As in Fig. 4.25, except for 0-3-km SRH.

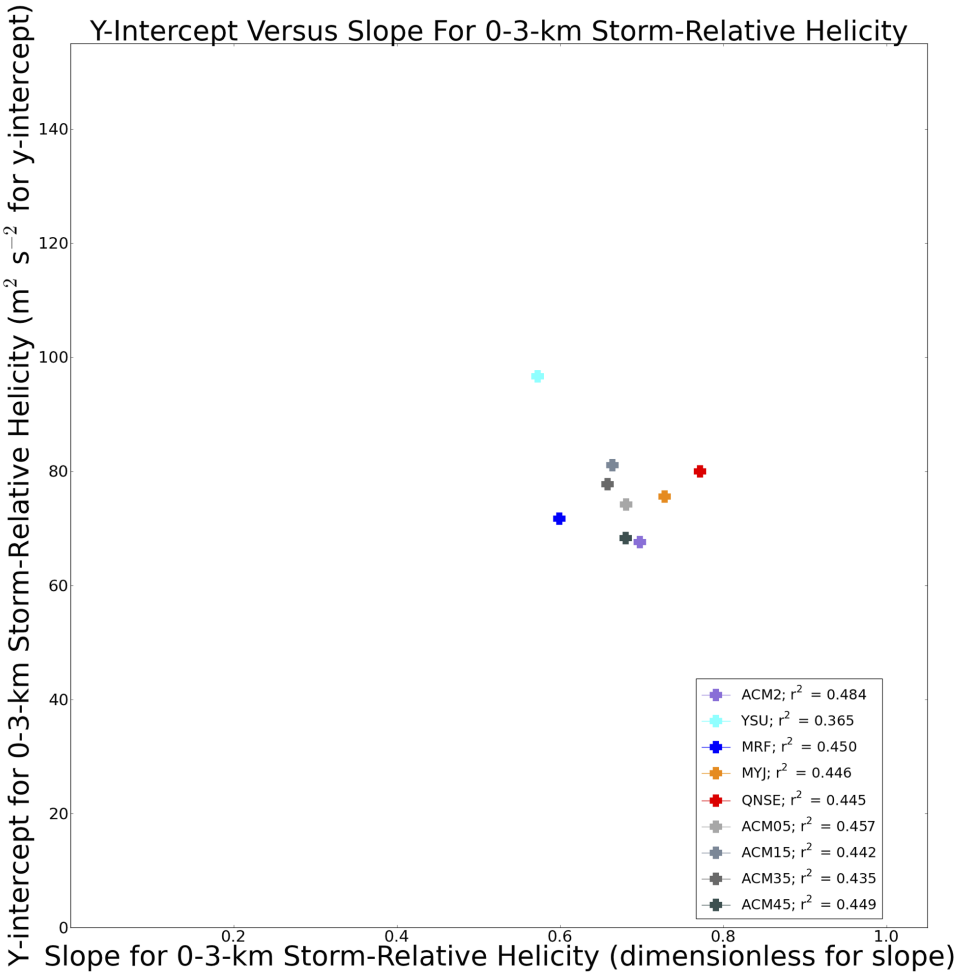

Figure 4.46: As in Fig. 4.26, except for 0-3-km SRH.

Simulation averages of 0-3-km SRH come closest to RUC/SFCOA averages for the MYJ (local) and QNSE (local) schemes, and are lower for the nonlocal-influenced schemes (Fig. 4.47). This is consistent with the notion that nonlocal-influenced schemes yield deeper PBLs with greater smoothing of the vertical wind profile and lower SRH compared to local schemes. The YSU (nonlocal) and MRF (nonlocal) schemes offer the lowest SRH.

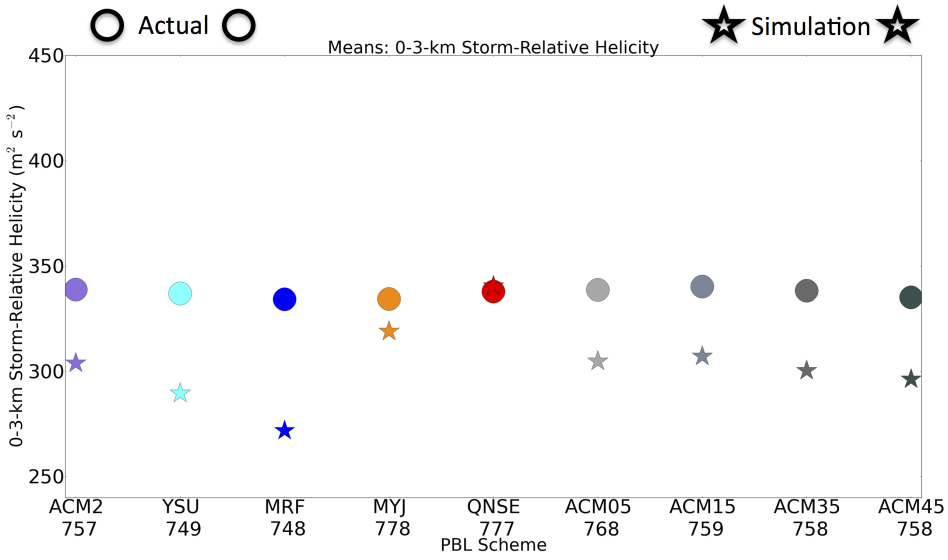

Figure 4.47: As in Fig. 4.27, except for 0-3-km SRH.

Theil's inequality coefficient for 0-3-km SRH (Fig. 4.48) reveals relatively similar error for all PBL schemes for 0-3-km SRH, though slightly lower for the MYJ (local) and QNSE (local) schemes and the ACM2 (nonlocal/local) schemes and its variants. The ACM2 (nonlocal/local) scheme and its variants represent an intermediate zone for the bias component of error, lying between the nonlocal schemes with greater bias component and the local schemes with less bias component. Comparing Fig. 4.48 with Fig. 4.28 and Fig. 4.38 that also display U and U_m statistics except for 0-3-km lapse rate and PBL depth, respectively, it is evident that local schemes offer the greatest bias component for 0-3-km lapse rate and PBL depth, whereas nonlocal schemes offer the greatest bias component for 0-3-km SRH. Meanwhile, the ACM2 (nonlocal/local) and its variants relatively lower the bias component for all of these parameters from the most extreme bias-component magnitudes.

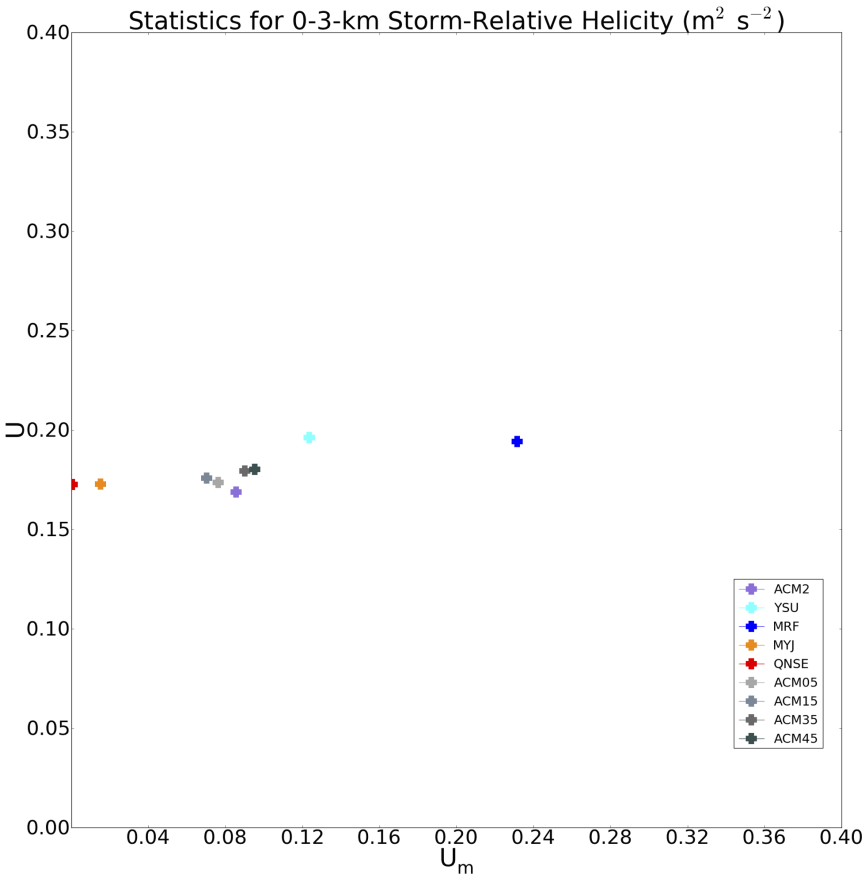

Figure 4.48: As in Fig. 4.28, except for 0-3-km SRH.

4.11 Statistical Analysis of 0-1-km SRH

The statistical metrics corresponding to 0-1-km SRH (Figs. 4.49-4.53) exhibit very similar characteristics to 0-3-km SRH, regarding characteristics of bias including conditional bias and error. One noteworthy difference is that the nonlocal-scheme underforecast of SRH is accentuated at stronger actual SRH in the 0-1-km layer compared to the 0-3-km layer.

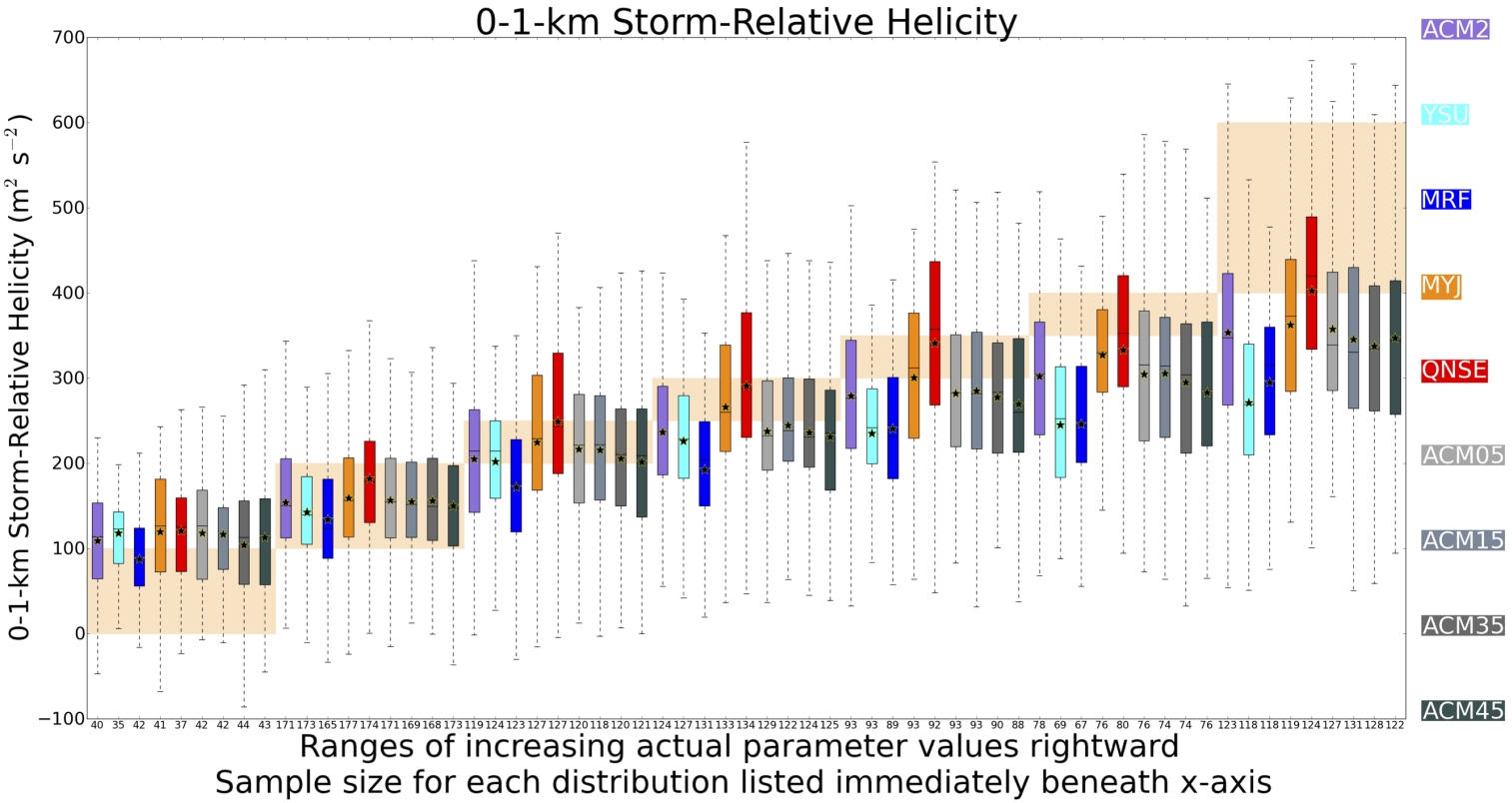

Figure 4.49: As in Fig. 4.24, except for 0-1-km SRH.

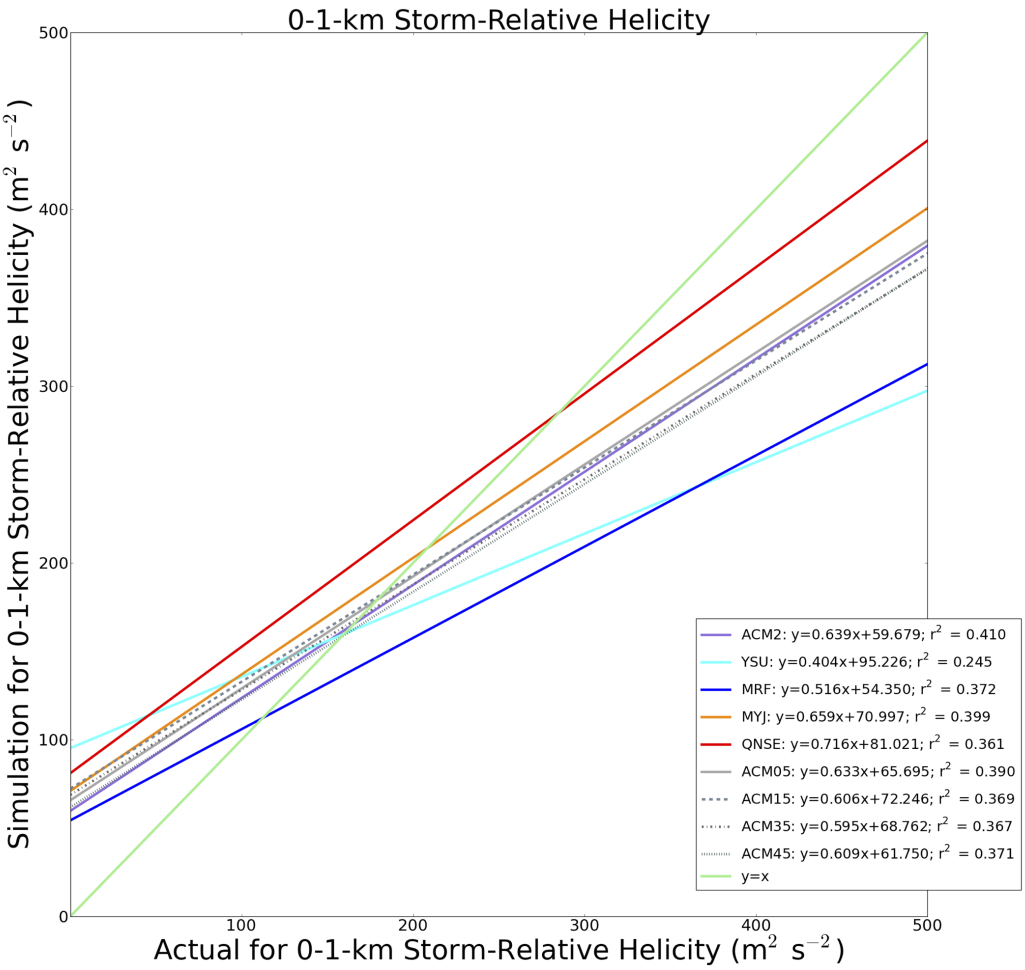

Figure 4.50: As in Fig. 4.25, except for 0-1-km SRH.

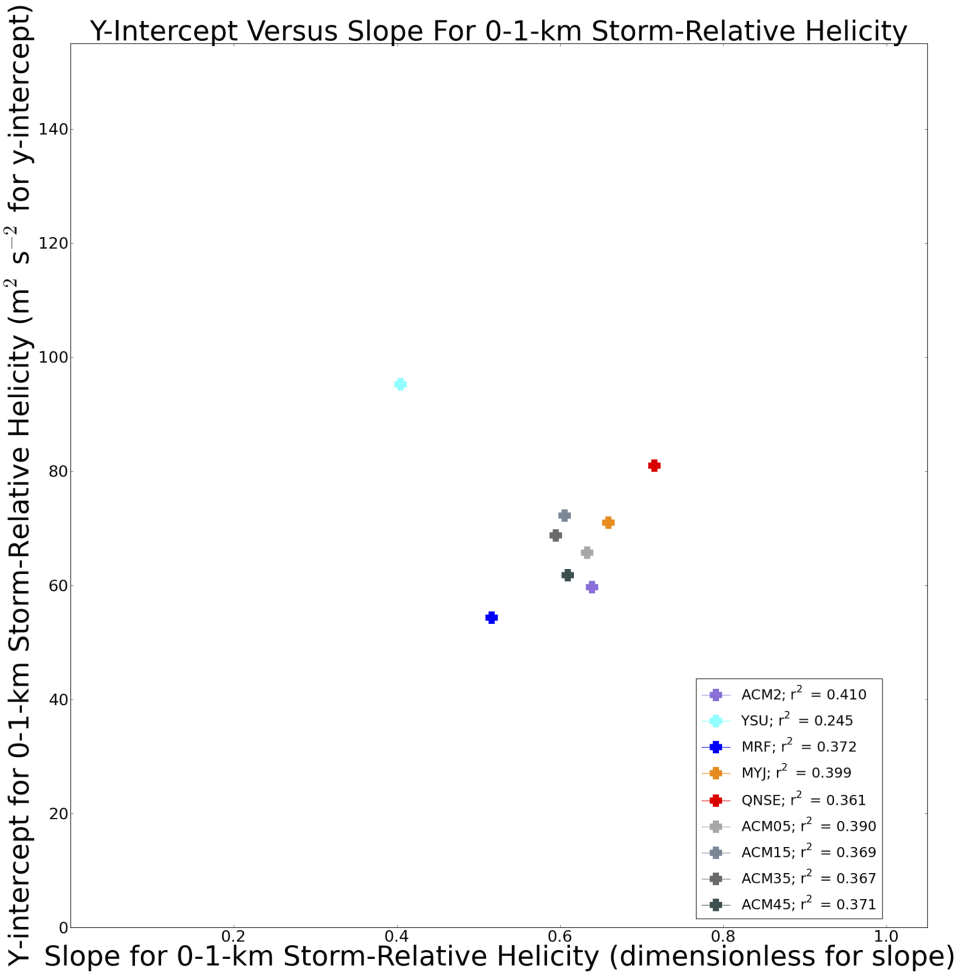

Figure 4.51: As in Fig. 4.26, except for 0-1-km SRH.

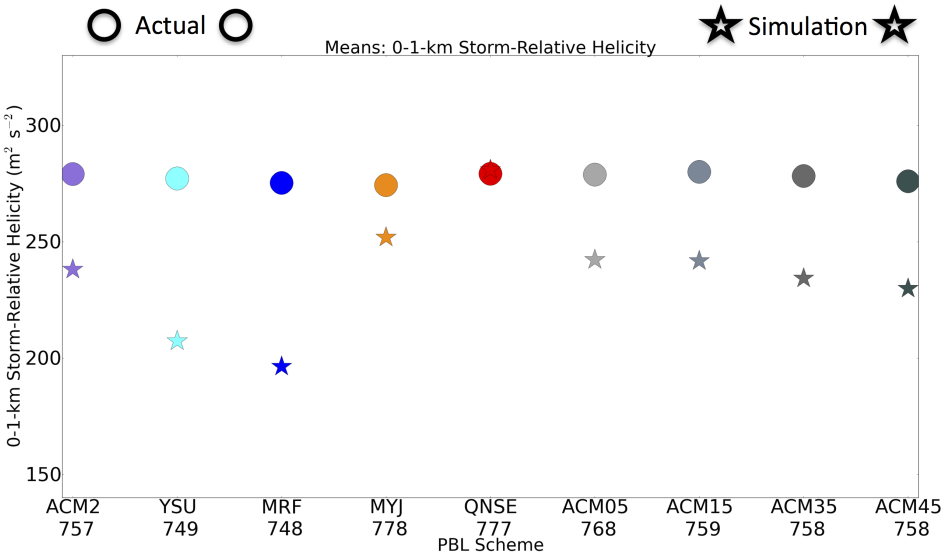

Figure 4.52: As in Fig. 4.27, except for 0-1-km SRH.

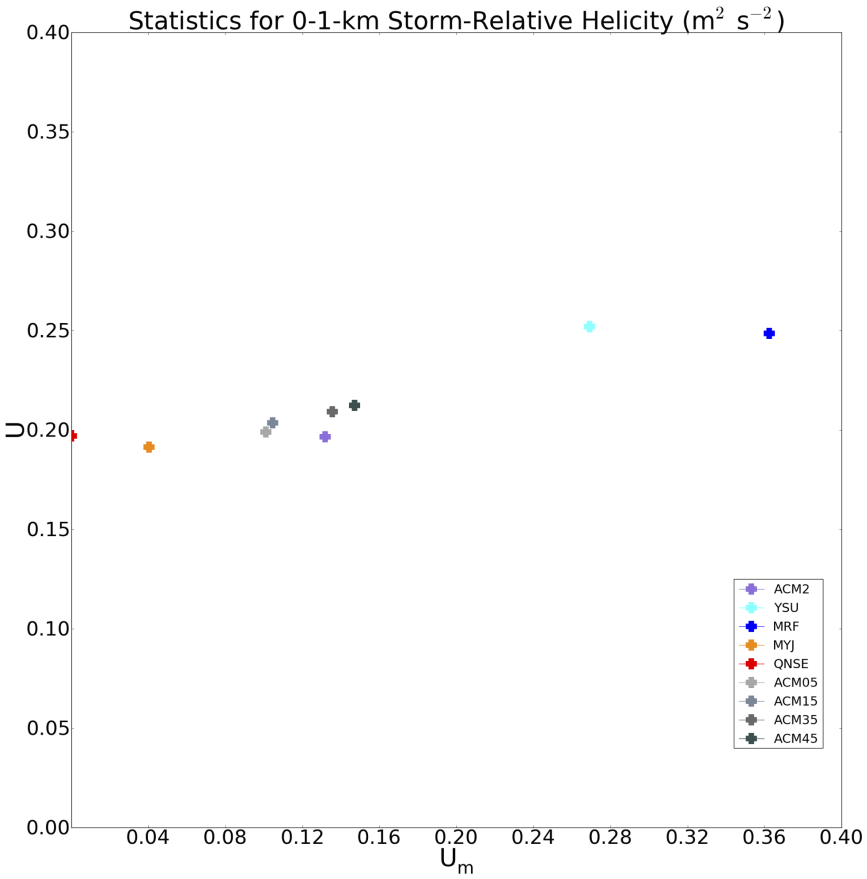

Figure 4.53: As in Fig. 4.28, except for 0-1-km SRH.

Chapter 5

Final Remarks and Future Work

Through a focus on thermodynamic and kinematic parameters explicitly characterizing the near-storm environment of tornadoes across the southeast United States during the cold season, exclusively, it was found that this particular regime is indeed different than other regimes of tornadoes across the country. This is the first near-storm environmental assessment using mesoanalysis data for individual tornado events specifically focused on this particular spatiotemporal regime, which presents distributions of parameter values and statistical tests comparing the "SECOLD" regime with other environments. Relatively smaller buoyancy and stronger vertical wind shear characterize the "SECOLD" regime. Additionally, the notion that, typically, a greater proportion of MLCAPE is concentrated in the lowest 3 km above ground in the "SECOLD" regime compared to other regimes motivates the need to better resolve thermodynamic structures in the lower atmosphere that influence the assessment of this component of buoyancy.

Buoyancy became evident as a discriminator between right-moving supercell and QLCS tornado environments, with greater SBCAPE and MLCAPE associated with right-moving supercell compared to QLCS tornado environments.

Ultimately, this finding helps motivate the need to properly assess the instability component of the forecast problem for severe storms, which is highly influenced by processes within the PBL. Furthermore, investigation of time series of various thermodynamic and kinematic parameters during the "SECOLD" regime reveals behaviors uncharacteristic of those in other regimes, where the parameters of the "SECOLD" regime do not clearly exhibit the strength of typical daytime versus nighttime variability that would be representative of a more quiescent PBL evolution.

Through thorough investigation of the distinguishability of the "SECOLD" environment, the need to study the PBL and its representation in numerical models in this regime became well motivated, as the selected PBL parameterization scheme in a numerical model has an influence on simulated convective environments. The "SECOLD" regime has been one of little focus in the past, and the study of PBL parameterization schemes has been extended to such a challenging forecast problem. As a part of the model evaluation process, work previously introduced by C15 is applied, which invokes a warm-sector-based analysis of forecast soundings compared against a RUC/SFCOA sounding dataset that incorporates observations. This permits a reproducible, relevant-for-operational-meteorology system for evaluation of convection-allowing model guidance.

Through an investigation of 9 different PBL schemes – two nonlocal ones (YSU and MRF), two local ones (MYJ and QNSE), and one hybrid nonlocal/local scheme (ACM2) with four newly constructed variants (ACM05, ACM15,

ACM35, and ACM45) – many distinguishable results became apparent upon comparisons to RUC/SFCOA soundings in the model evaluation process. Firstly, conditional bias is consistently minimized by using the ACM2 (nonlocal/local) scheme and its variants for all evaluated thermodynamic and kinematic variables with two exceptions amongst the studied variables. For 0-1-km and 0-3-km SRH, the ACM2 (nonlocal/local) scheme and its variants do not provide the least conditional bias, but these schemes do produce less conditional bias than that produced by nonlocal schemes. For PBL depth, the smallest error and the smallest bias component correspond to the ACM2 (nonlocal/local) and its variants, along with the YSU (nonlocal) scheme. For 0-3-km lapse rate and PBL depth, local schemes provide the largest mean differences from observations as an underestimation. For 0-1-km SRH and 0-3-km SRH, nonlocal schemes provide the largest mean differences from observations as an underestimation. Mean mixing ratio in the lowest 100 mb is relatively well forecast by all PBL parameterization schemes, though the MRF provides a moister solution in the overall average sense. For all evaluated variables except MLCAPE, the ACM2 (nonlocal/local) scheme and its variants never provide the largest simulation mean difference from observations or error, and sometimes provide the smallest difference and error. MLCAPE is poorly forecast by all schemes, though the ACM2 (nonlocal/local) scheme and its variants provide the least conditional bias. Amongst the variants of the ACM2 (nonlocal/local) scheme, the ACM45 (nonlocal/local) scheme provides the smallest differences from actual for MLCAPE.

This entire set of model evaluation for already-developed PBL parameterization schemes, and modified ones, represents a new area of study through their application in an atmospheric regime not commonly studied. It is clear that simultaneous representation of both nonlocal and local mixing is most appropriate for the "SECOLD" regime. The ACM2 (nonlocal/local) scheme and its variants most consistently reduce extreme forms of bias that making a selection of strictly local or nonlocal PBL parameterization schemes would produce. There is some indication that the ACM45 (nonlocal/local) offering a relatively deeper PBL, on average, would provide the greatest overall reduction of bias component for buoyancy-related parameters amongst the variants of the ACM2 (nonlocal/local) scheme.

These findings can contribute substantially to guiding the numerical modeling and operational meteorology community to the most appropriate PBL parameterization scheme to be used in convection-allowing model guidance in the "SECOLD" regime. Further research can investigate the effects of using such a scheme on morphological characteristics of simulated convection and its attributes in the "SECOLD" regime. Composite reflectivity is a model-derived field that forecasters often reference, and what effect these schemes have on such a field for multiple cases would be an important focus for improving numerical models in this regime. Additionally, comparisons of model forecast soundings with fully observed soundings could provide additional insight on PBL scheme

performance in the "SECOLD" regime. Also, comparisons between fully observed soundings and the soundings from the RUC/SFCOA dataset may assist in identifying errors associated with the RUC/SFCOA dataset for the "SECOLD" regime. Furthermore, the effects of changing domain characteristics such as horizontal grid length, number of vertical levels, and other parameterization schemes such as microphysics could be foci for additional investigation for improving numerical models in this regime. Ultimately, this work sheds light on a severe-weather forecast problem that has had relatively limited treatment in numerical modeling studies. The distinguishability of the "SECOLD" environment and many focused clues to assist with its depiction in numerical modeling identified throughout this work can give rise to additional investigation of this regime in future studies.

Bibliography

Ashley, W. S., 2007: Spatial and temporal analysis of tornado fatalities in the United States: 1880–2005. *Wea. Forecasting*, **22**, 1214–1228.

Benjamin, S. G., and Coauthors, 2004: An hourly assimilation–forecast cycle: The RUC. *Mon. Wea. Review*, **132**, 495–518.

Bothwell, P. D., J. A. Hart, and R. L. Thompson, 2002: An integrated three-dimensional objective analysis scheme in use at the Storm Prediction Center. Preprints, *21st Conf. on Severe Local Storms/19th Conf. on Weather Analysis and Forecasting/15th Conf. on Numerical Weather Prediction*, San Antonio, TX, Amer. Meteor. Soc., JP3.1. [Available online at https://ams.confex.com/ams/pdfpapers/47482.pdf.]

Brooks, H. E., 2009: Proximity soundings for Europe and the United States from reanalysis data. *Atmos. Res.*, **93**, 546–553.

Cavallo, S. M., J. Dudhia, and C. Snyder, 2011: A multilayer upper-boundary condition for longwave radiative flux to correct temperature biases in a mesoscale model. *Mon. Wea. Rev.*, **139**, 1952–1959.

Clements, K. W., and J. A. Frenkel, 1980: Exchange rates, money and relative prices: The dollar–pound in the 1920s. *J. Int. Econ.*, **10**, 249—262.

Cohen, A. E., S. M. Cavallo, M. C. Coniglio, and H. E. Brooks, 2015: A review of planetary boundary layer parameterization schemes and their sensitivity in simulating southeastern U.S. cold season severe weather environments. *Wea. Forecasting*, **30**, 591–612.

Coniglio, M. C., 2012: Verification of RUC 0–1-h forecasts and SPC mesoscale analyses using VORTEX2 soundings. *Wea. Forecasting*, **27**, 667–683.

Coniglio, M. C., J. Correia, P. T. Marsh, and F. Kong, 2013: Verification of convection-allowing WRF model forecasts of the planetary boundary layer using sounding observations. *Wea. Forecasting*, **28**, 842–862.

Craven, J. P., and H. E. Brooks, 2004: Baseline climatology of sounding derived parameters associated with deep, moist convection. *Natl. Wea. Dig.*, **28**, 13–24.

Davies-Jones, R., D. Burgess, and M. Foster, 1990: Test of helicity as a tornado forecast parameter. Preprints, *16th Conf. on Severe Local Storms*, Kananaskis Park, AB, Canada, Amer. Meteor. Soc., 588–592

Edwards, R., A. R. Dean, R. L. Thompson, and B. T. Smith, 2012: Convective modes for significant severe thunderstorms in the contiguous United States. Part III: Tropical cyclone tornadoes. *Wea. Forecasting*, **27**, 1507–1519.

Ek, M. B., K. E. Mitchell, Y. Lin, P. Grunmann, E. Rodgers, G. Gayno, and V. Koren, 2003: Implementation of the upgraded Noah land surface model in the NCEP operational mesoscale Eta model. *J. Geophys. Res.*, **108**, 8851.

Farrell, R. J., and T. N. Carlson, 1989: Evidence for the role of the lid and underrunning in an outbreak of tornadic thunderstorms. *Mon. Wea. Rev.*, **117**, 857–871.

Gallus, W. A., N. A. Snook, and E. V. Johnson, 2008: Spring and summer severe weather reports over the Midwest as a function of convective mode: A preliminary study. *Wea. Forecasting*, **23**, 101–113.

García-Díez, M., J. Fernández, L. Fita, and C. Yagüe, 2013: Seasonal dependence of WRF Model biases and sensitivity to PBL schemes over Europe. *Quart. J. Roy. Meteor. Soc.*, **139**, 501–514.

Gibbs, J. A., E. Fedorovich, and A. M. J. van Eijk, 2011: Evaluating Weather Research and Forecasting (WRF) model predictions of turbulent flow parameters in a dry convective boundary layer. *J. Appl. Meteor. Climatol.*, **50**, 2429–2444.

Glickman, T. S., Ed., 2000: *Glossary of Meteorology*. Amer. Meteor. Soc., 855 pp.

Guyer, J. L., and A. R. Dean, 2010: Tornadoes within weak CAPE environments across the continental United States. Preprints, *25th Conf. on Severe Local Storms*, Denver, CO, Amer. Meteor. Soc., 1.5. [Available online at http://ams.confex.com/ams/pdfpapers/175725.pdf.]

Guyer, J. L., D. A. Imy, A. Kis, and K. Venable, 2006: Cool season significant (F2–F5) tornadoes in the Gulf Coast states. Preprints, *23rd Conf. on Severe Local Storms*, St. Louis, MO, Amer. Meteor. Soc., 4.2. [Available online at https://ams.confex.com/ams/pdfpapers/115320.pdf.]

Hacker, J. P., 2010: Spatial and temporal scales of boundary layer wind predictability in response to small-amplitude land surface uncertainty. *J. Atmos. Sci.*, **67**, 217–233.

Haylock, M. R., N. Hofstra, A. M. G. Klein Tank, E. J. Klok, P. D. Jones, and M. New, 2008: A European daily high-resolution gridded dataset of surface temperature and precipitation. *J. Geophys. Res.*, **113**, D20119.

Holton, J. R., 2004: *Introduction to Dynamic Meteorology*. 4th ed. Elsevier, 535 pp.

Hong, S.-Y., and J. O. J. Lim, 2006: The WRF single-moment 6-class microphysics scheme (WSM6). *J. Korean Meteor. Soc.*, **42**, 129—151.

Hong, S.-Y., Y. Noh, and J. Dudhia, 2006: A new vertical diffusion package with an explicit treatment of entrainment processes. *Mon. Wea. Review*, **134**, 2318–2341.

Hong, S.-Y., and H.-L. Pan, 1996: Nonlocal boundary layer vertical diffusion in a medium-range forecast model. *Mon. Wea. Review*, **124**, 2322–2339.

Hu, X.-M., J. W. Nielsen-Gammon, and F. Zhang, 2010: Evaluation of three planetary boundary layer schemes in the WRF model. *J. Appl. Meteor. Climatol.*, **49**, 1831–1844.

Huang, H.-Y., A. Hall, and J. Teixeira, 2013: Evaluation of the WRF PBL parameterizations for marine boundary layer clouds: Cumulus and stratocumulus. *Mon. Wea. Rev.*, **141**, 2265–2271.

Iacono, M. J., J. S. Delamere, E. J. Mlawer, M. W. Shephard, S. A. Clough, and W. D. Collins, 2008: Radiative forcing by long-lived greenhouse gases: Calculations with the AER radiative transfer models. *J. Geophys. Res.*, **113**, D13103.

Janjić, Z. I., 1990: The step-mountain coordinate: Physical package. *Mon. Wea. Review*, **118**, 1429–1443.

Janjić, Z. I., 1994: The step-mountain eta coordinate model: Further developments of the convection, viscous sublayer, and turbulence closure schemes. *Mon. Wea. Review*, **122**, 927–945.

Jankov, I., W. A. Gallus, M. Segal, B. Shaw, and S. E. Koch, 2005: The impact of different WRF model physical parameterizations and their interactions on warm season MCS rainfall. *Wea. Forecasting*, **20**, 1048–1060.

Kain, J. S., M. E. Baldwin, P. R. Janish, S. J. Weiss, M. P. Kay, and G. W. Carbin, 2003: Subjective verification of numerical models as a component of a broader interaction between research and operations. *Wea. Forecasting*, **18**, 847–860.

Kain, J. S., S. J. Weiss, M. E. Baldwin, G. W. Carbin, D. A. Bright, J. J. Levit, and J. A. Hart, 2005: Evaluating high-resolution configurations of the WRF Model that are used to forecast severe convective weather: The 2005 SPC/NSSL Spring Program. Preprints, *21st Conf. on Weather Analysis and Forecasting/17th Conf. on Numerical Weather Prediction*, Washington, DC, Amer. Meteor. Soc., 2A.5. [Available online at http://ams.confex.com/ams/pdfpapers/94843.pdf.]

Kain, J. S., S. J. Weiss, J. J. Levit, M. E. Baldwin, and D. R. Bright, 2006: Examination of convection-allowing configurations of the WRF model for the prediction of severe convective weather: The SPC/NSSL Spring Program 2004. *Wea. Forecasting*, **21**, 167–181.

Kain, J. S., and Coauthors, 2013: A feasibility study for probabilistic convection initiation forecasts based on explicit numerical guidance. *Bull. Amer. Meteor. Soc.*, **94**, 1213–1225.

Massey, F. J., 1951: The Kolmogorov-Smirnov test for goodness of fit. *J. Amer. Statist. Assoc.*, **46**, 68–77.

Mellor, G. L., and T. Yamada, 1982: Development of a turbulence closure model for geophysical fluid problems. *Rev. Geophys. Space Phys*, **20**, 851–875.

Mesinger, F., and Coauthors, 2006: North American Regional Reanalysis. *Bull. Amer. Meteor. Soc.*, **87**, 343–360.

Miller, D. J., and R. H. Johns, 2000: A detailed look at extreme wind damage in derecho events. Preprints, *20th Conf. on Severe Local Storms*, Orlando, FL, Amer. Meteor. Soc., 4.3

Miller, R. C., 1972: Notes on analysis and severe storms forecasting procedures of the Air Force Global Weather Central. Air Weather Service, Tech. Rep. 200 (rev.), 181 pp. [Available from Air Weather Service, Technical Library, 359 Buchanan St., Scott AFB, IL 62225-5118.]

Moller, A. R., C. A. Doswell III, M. P. Foster, and G. R. Woodall, 1994: The operational recognition of supercell thunderstorm environments and storm structures. *Wea. Forecasting*, **9**, 327–347.

Murphy, A. H., B. G. Brown, and Y.-S. Chen, 1989: Diagnostic verification of temperature forecasts. *Wea. Forecasting*, **4**, 485–501.

Nakanishi, M., and H. Niino, 2009: Development of an improved turbulence closure model for the atmospheric boundary layer. *J. Meteor. Soc. Japan*, **87**, 895–912.

NCAR, cited 2014: NCAR Command Language. [Available online at http://www.ncl.ucar.edu/.]

NCAR, cited 2015: NCEP FNL operational model global tropospheric analyses, continuing from July 1999. Computational and Information Systems Laboratory, National Center for Atmospheric Research. [Available online at http://rda.ucar.edu/datasets/ds083.2/.]

Nielsen-Gammon, J. W., X.-M. Hu, F. Zhang, and J. E. Pleim, 2010: Evaluation of planetary boundary layer scheme sensitivities for the purpose of parameter estimation. *Mon. Wea. Review*, **138**, 3400–3417.

NOAA/NCDC, cited 2014a: Model Data Inventories. NOAA/National Operational Model Archive and Distribution System. [Available online at http://nomads.ncdc.noaa.gov/data.php?name5inventory.]

NOAA/NCDC, cited 2014b: RUC online archive. [Available online at http://nomads.ncdc.noaa.gov/data/ruc/.]

Pindyck, R. S., and D. L. Rubinfeld, 1981: *Econometric Models and Economic Forecasts*. 2nd ed. McGraw-Hill, 630 pp.

Pleim, J. E., 2007a: A combined local and nonlocal closure model for the atmospheric boundary layer. Part I: Model description and testing. *J. of Appl. Meteor. and Climatol.*, **46**, 1383–1395.

Pleim, J. E., 2007b: A combined local and nonlocal closure model for the atmospheric boundary layer. Part II: Application and evaluation in a mesoscale meteorological model. *J. of Appl. Meteor. and Climatol.*, **46**, 1396–1409.

Rasmussen, E. N., and D. O. Blanchard, 1998: A baseline climatology of sounding-derived supercell and tornado forecast parameters. *Wea. Forecasting*, **13**, 1148–1164.

Schaefer, J. T., 1986: Severe thunderstorm forecasting: A historical perspective. *Wea. Forecasting*, **1**, 164–189.

Schneider, R. S., and A. R. Dean, 2008: A comprehensive 5-year severe storm environment climatology for the continental United States. Preprints, *24th Conf. on Severe Local Storms*, Savannah, GA, Amer. Meteor. Soc., 16A.4. [Available online at http://ams.confex.com/ams/pdfpapers/141748.pdf.]

Scott, D. W., 1985: Average shifted histograms: Effective nonparametric density estimation in several dimensions. *Ann. Statist.*, **13**, 1024–1040.

Skamarock, W. C., and Coauthors, 2008: A description of the Advanced Research WRF version 3. NCAR Tech. Note TN-475+STR, 113 pp. [Available online at http://www2.mmm.ucar.edu/wrf/users/docs/arw_v3.pdf.].

Smith, B. T., R. L. Thompson, J. S. Grams, C. Broyles, and H. E. Brooks, 2012: Convective modes for significant severe thunderstorms in the contiguous United States. Part I: Storm classification and climatology. *Wea. Forecasting*, **27**, 1114–1135.

Stensrud, D. J., 2007: *Parameterization Schemes: Keys to Understanding Numerical Weather Prediction Models*. Cambridge University Press, 459 pp.

Storm Prediction Center, cited 2015a: SPC hourly mesoscale analysis. [Available online at http://www.spc.noaa.gov/exper/ma_archive/.]

Storm Prediction Center, cited 2015b: Storm Prediction Center National Severe Weather database browser: Online SeverePlot 3.0. [Available online at http://www.spc.noaa.gov/climo/online/sp3/plot.php.]

Stull, R. B., 1988: *An Introduction to Boundary Layer Meteorology*. Kluwer Academic, 666 pp.

Sukoriansky, S., B. Galperin, and V. Perov, 2005: Application of a new spectral theory of stably stratified turbulence to the atmospheric boundary layer over sea ice. *Bound.-Layer Meteor.*, **117**, 231—257.

Theil, H., 1961: *Economic Forecasts and Policy*. 2nd Ed. North-Holland, 567 pp.

Theil, H., 1966: *Applied Economic Forecasting*. North-Holland, 474 pp.

Thompson, R. L., R. Edwards, J. A. Hart, K. L. Elmore, and P. Markowski, 2003: Close proximity soundings within supercell environments obtained from the Rapid Update Cycle. *Wea. Forecasting*, **18**, 1243–1261.

Thompson, R. L., B. T. Smith, J. S. Grams, A. R. Dean, and C. Broyles, 2012: Convective modes for significant severe thunderstorms in the contiguous United States. Part II: Supercell and QLCS tornado environments. *Wea. Forecasting*, **27**, 1136–1154.

Trapp, R. J., S. A. Tessendorf, E. S. Godfrey, and H. E. Brooks, 2005: Tornadoes from squall lines and bow echoes. Part I: Climatological distribution. *Wea. Forecasting*, **20**, 23–34.

Trnka, M., J. Eitzinger, G. Gruszczynski, K. Buchgraber, R. Resch, and A. Schaumberger, 2006: A simple statistical model for predicting herbage production from permanent grassland. *Grass Forage Sci*, **61**, 253—271.

Weiss, S. J., M. E. Pyle, Z. Janjić, D. R. Bright, and G. J. DiMego, 2008: The operational high resolution window WRF Model runs at NCEP: Advantages of multiple model runs for severe convective weather forecasting. Preprints, *24th Conf. on Severe Local Storms*, Savannah, GA, Amer. Meteor. Soc., P10.8. [Available online at http://ams.confex.com/ams/pdfpapers/142192.pdf.]

Xie, B., J. C.-H. Fung, A. Chan, and A. K.-H. Lau, 2012: Evaluation of nonlocal and local planetary boundary layer schemes in the WRF Model. *J. Geophys. Res.*, **117**, D12103.